ANALYSIS OF PROTEIN-PROTEIN INTERACTION NETWORK FROM LEUKOCYTE

TRANSCRIPTOMIC PROFILES IN SEVERE COVID-19 PATIENTS

Mr. Pakorn Sagulkoo

จุฬาลงกรณ์มหาวิทยาลัย
CHULALONGKORN UNIVERSITY

A Thesis Submitted in Partial Fulfillment of the Requirements

for the Degree of Master of Science in Bioinformatics and Computational Biology

Inter-Department of Bioinformatics and Computational Biology

GRADUATE SCHOOL

Chulalongkorn University

Academic Year 2021

การวิเคราะห์เครือข่ายปฏิสัมพันธ์ระหว่างโปรตีนจากข้อมูลแสดงลักษณะเฉพาะของทรานสคริป
โทมเม็ดเลือดขาวในผู้ป่วยโรคโควิด 19 ที่มีอาการรุนแรง

นายภากร สกุลคู

Thesis Title	ANALYSIS OF PROTEIN-PROTEIN INTERACTION NETWORK
	FROM LEUKOCYTE TRANSCRIPTOMIC PROFILES IN
	SEVERE COVID-19 PATIENTS
By	Mr. Pakorn Sagulkoo
Field of Study	Bioinformatics and Computational Biology
Thesis Advisor	Assistant Professor KITIPORN PLAIMAS, Dr.rer.nat.

Accepted by the GRADUATE SCHOOL, Chulalongkorn University in Partial Fulfillment of the Requirement for the Master of Science

-- Dean of the GRADUATE SCHOOL

(Associate Professor YOOTTHANA CHUPPUNNARAT, Ph.D.)

THESIS COMMITTEE

-- Chairman

(Professor SUPACHITRA CHADCHAWAN, Ph.D.)

-- Thesis Advisor

(Assistant Professor KITIPORN PLAIMAS, Dr.rer.nat.)

-- Examiner

(Sira Sriswasdi, Ph.D.)

-- External Examiner

(Assistant Professor Piyapong Khumrin, Ph.D.)

ภากร สกุลคู : การวิเคราะห์เครือข่ายปฏิสัมพันธ์ระหว่างโปรตีนจากข้อมูลแสดงลักษณะเฉพาะ
ของทรานสคริปโทมเม็ดเลือดขาวในผู้ป่วยโรคโควิด 19 ที่มีอาการรุนแรง . (ANALYSIS OF
PROTEIN-PROTEIN INTERACTION NETWORK FROM LEUKOCYTE TRANSCRIPTOMIC
PROFILES IN SEVERE COVID-19 PATIENTS) อ.ที่ปรึกษาหลัก : ผศ. ดร.กิติพร พลายมาศ

โรคโควิด 19 ยังคงก่อให้เกิดปัญหาด้านสาธารณสุขระดับโลกแม้ว่าจะมีการพัฒนาวัคซีนและยา
ต้านไวรัส ผู้ป่วยบางรายยังมีภาวะเจ็บป่วยที่รุนแรงซึ่งต้องได้รับการดูแลอย่างใกล้ชิด นอกจากนี้บางรายก็
เสียชีวิตเนื่องจากการรักษาที่ล้มเหลว ดังนั้นการค้นหาแยกแยะยีนที่สำคัญและกลไกการเกิดโรคจึงมี
ความสำคัญในการค้นหายาที่รักษาแบบตรงจุดเพื่อรักษาโรคดังกล่าว การวิเคราะห์เครือข่ายปฏิสัมพันธ์
ระหว่างโปรตีนให้ข้อมูลที่ใช้ในการค้นหากลไกการเกิดโรคและยารักษาทางเลือกที่มีประสิทธิภาพ ดังนั้น
การศึกษานี้จึงได้สร้างเครือข่ายปฏิสัมพันธ์ระหว่างโปรตีนจากข้อมูลแสดงลักษณะเฉพาะของทรานสคริปโทม
เม็ดเลือดขาวของผู้ป่วยโรคโควิด 19 ที่มีอาการรุนแรงที่เก็บรวบรวมจาก Gene Expression Omnibus
(GEO) DataSets เพื่อใช้ในการค้นหายีนที่สำคัญและยาที่รักษาแบบตรงจุด วิธีการแพร่ในเครือข่ายโดย
ขั้นตอนวิธีการแพร่ความร้อนแบบลาปลาซถูกนำมาใช้ในการสร้างเครือข่ายปฏิสัมพันธ์ระหว่างโปรตีนที่
เกี่ยวข้องกับระบบภูมิคุ้มกัน นอกจากนี้การวิเคราะห์ค่าความเป็นศูนย์กลางเครือข่ายหลายรูปแบบสามารถ
แยกแยะยีนที่สำคัญ 23 ยีนของเครือข่ายปฏิสัมพันธ์ระหว่างโปรตีนที่เกี่ยวข้องกับระบบภูมิคุ้มกัน ต่อจากนี้
เครือข่ายปฏิสัมพันธ์ระหว่างยากับยีนได้ถูกสร้างจากการค้นหาในฐานข้อมูลโดยอิงจากยีนสำคัญที่พบ ผล
จากการศึกษาพบว่ามียา 5 ตัวที่มีประสิทธิภาพในการปฏิสัมพันธ์กับยีนที่สำคัญ เพื่อที่จะค้นหายีนที่สำคัญ
และยาทางเลือกเพิ่มเติม การผสมผสานข้อมูลแสดงลักษณะเฉพาะของทรานสคริปโทมเม็ดเลือดขาว 2 ข้อมูล
ได้ถูกจัดทำเพื่อสร้างเครือข่ายปฏิสัมพันธ์ระหว่างโปรตีนร่วมกัน การวัดค่าความเป็นศูนย์กลางและการ
วิเคราะห์การรอดชีพถูกนำมาใช้เพื่อค้นหาและตรวจสอบความถูกต้องของยีนที่สำคัญที่พบร่วมกัน จากการ
วิเคราะห์พบว่ามี 4 ยีนที่สำคัญเพิ่มเติม และผลจากเครือข่ายปฏิสัมพันธ์ระหว่างยากับยีนและเทคนิค
molecular docking พบว่ามียาอีก 2 ชนิดที่มีปฏิสัมพันธ์กับยีนสำคัญกลุ่มดังกล่าว นอกจากนี้เครือข่ายการ
ควบคุมการแสดงออกของยีนแบบ miRNA-mRNA ยังพบ 5 ตัวเลือกใหม่ของตัวบ่งชี้ทางชีวภาพเพื่อใช้ในการ
ทำนายความรุนแรงของโรค โดยสรุปแล้วการวิเคราะห์เครือข่ายปฏิสัมพันธ์ระหว่างโปรตีนสามารถค้นพบตัว
บ่งชี้ทางชีวภาพและยาเพื่อใช้สำหรับทำนายและรักษาผู้ป่วยโรคโควิด 19 ที่มีความรุนแรง

สาขาวิชา	ชีวสารสนเทศศาสตร์และชีววิทยา	ลายมือชื่อนิสิต ....
	เชิงคอมพิวเตอร์ (สหสาขาวิชา)	
ปีการศึกษา	2564	ลายมือชื่อ อ.ที่ปรึกษาหลัก ....

6380064520 : MAJOR BIOINFORMATICS AND COMPUTATIONAL BIOLOGY

KEYWORD: Severe COVID-19, Systems biology, PPI network, Drug repurposing

Pakorn Sagulkoo : ANALYSIS OF PROTEIN-PROTEIN INTERACTION NETWORK FROM LEUKOCYTE TRANSCRIPTOMIC PROFILES IN SEVERE COVID-19 PATIENTS . Advisor: Asst. Prof. KITIPORN PLAIMAS, Dr.rer.nat.

Coronavirus disease 2019 (COVID-19) still provides global public health issues although several vaccines and antiviral agents have been developed. Some patients experience severe conditions needed medical intensive care, and some are dead due to the failure of treatments. Therefore, identifying the key genes and underlying molecular mechanisms is necessary to discover precisely targeted drugs. Analysis of protein-protein interaction (PPI) networks provides invaluable information to find disease mechanisms and effective alternative drugs. Hence, PPI network analysis based on leukocyte transcriptomic profiles of severe COVID-19 collected from Gene Expression Omnibus (GEO) DataSets was proposed for this study. A network diffusion method called Laplacian heat diffusion (LHD) algorithm was performed to construct an immune-related PPI network (IPIN). Furthermore, several network centrality measurements can identify 23 key genes from the IPIN. Subsequently, drug-gene interaction networks were constructed using database searching based on the key genes. There were 5 candidate drugs having the potential effect of interacting with the key genes. To find additional key genes and candidate drugs, two different leukocyte transcriptomic datasets were combined for the common PPI network construction. Centrality measurement and survival analysis were used to find and validate the further key genes. The analysis revealed 4 common key genes. The drug-gene interaction and molecular docking technique provided 2 further candidate drugs that interacted with the key genes. Additionally, miRNA-mRNA regulatory networks were built based on the PPI network to recognize 5 novel biomarkers for severe COVID-19 prediction. In conclusion, PPI network analysis can discover candidate biomarkers and drugs to predict and treat severe COVID-19 patients.

| Field of Study: | Bioinformatics and Computational Biology | Student's Signature .... |
| Academic Year: | 2021 | Advisor's Signature .... |

ACKNOWLEDGEMENTS

TABLE OF CONTENTS

LIST OF TABLES

LIST OF FIGURES

PART I

INTRODUCTION

1.1 BACKGROUND AND MOTIVATION

The world has experienced coronavirus disease 2019 (COVID-19), a rapidly spreading infectious disease, although several vaccines and antiviral agents are developed. The infection occurs with the symptoms of unclassified bilateral pneumonia originated in Wuhan, province Hubei, China, in 2019 [1, 2]. COVID-19 is caused by severe acute respiratory coronavirus 2 (SARS-CoV-2). SARS-CoV-2 is positive-sense single-stranded RNA (+ssRNA) β-coronavirus classified in Coronaviridae family [3, 4]. For the global statistics, the number of confirmed cases and death in COVID-19 from WHO data on May 25, 2022, were 524,339,768 and 6,281,260, respectively [5]. In addition, the global fatality rate is 3.4%. The main transmission route is receiving the infectious respiratory droplets from direct person-to-person contact [6, 7]. The infection can spread in all stages of the disease: asymptomatic, presymptomatic, and symptomatic [8]. The most common clinical features of COVID-19 are dry cough, fever, fatigue, and myalgia. Some patients have gastrointestinal symptoms, for instance, nausea, anorexia, and diarrhea [9-12]. About 64% to 80% of patients present with a loss of smell and taste sensation [13-15]. Furthermore, at least 50% of patients will progress to dyspnea [2]. Acute respiratory distress syndrome (ARDS) is a common condition found in severe COVID-19 [16]. Several risk factors contributing to severe illness include older age, chronic lung disease, cardiovascular diseases, diabetes mellitus, obesity, chronic kidney disease, immunocompromised host, and cancer [11, 17]. Nearly 17% to 35% of admitted patients needed intensive care units (ICU) due to respiratory failure [7]. The main causes of death are ARDS, acute respiratory failure, coagulopathy, septic shock, metabolic acidosis, cardiovascular complications, and multiple organ failure [16-19]. Pathogenesis and pathophysiology of COVID-19 are still required for further studies. They can classify the disease into 2 stages, such as early and late stages [7]. In the

early stage, SARS-Co-V 2 infects host cells and initiate proliferation. It enters respiratory epithelial cells and alveolar cells via using spike (S) protein which is primed by type 2 transmembrane serine protease (TMPRSS2) binding to angiotensin-converting enzyme 2 (ACE2) receptor [20, 21]. While viral replication occurs in the host cells, the innate immune system is activated. Hence, mild constitutional symptoms arise during this stage. Type 1 interferons (IFN-I) production is increased by activating JAK-STAT pathway, which promotes the expression of IFN-stimulated genes (ISGs). The activated type 1 IFN will recruit myeloid-lineage leukocytes, such as macrophages, neutrophils, and natural killer (NK) cells, to alveolar tissue [6]. In the late stage, pulmonary tissue damage and hyperinflammation emerge. Infected host respiratory cells (pneumocytes and alveolar endothelial cells) have injury and death, which cause interstitial fluid leakage. Therefore, pulmonary edema will occur and progress to ARDS later [7, 9, 20]. Furthermore, some patients have the clinical progression to hyperinflammation stage or cytokine storm caused by an imbalance between immune hyperactivation and under regulation [22]. Cytokine storm is characterized by cytokine overproduction, causing collateral tissue damage apart from the lungs, such as the heart, liver, kidneys, and brain [20]. Advance and uncontrolled COVID-19-induced cytokine storm can lead to multiple organ failures and death in the last stage [7, 22]. Generally, cytokines promoted in cytokine storm due to infection are IL-1, IL-6, IL-12, IL-17, IL-18, and tumor necrotic factor (TNF). Meanwhile, mitogen-activated protein kinase (MAPK), nuclear factor κB (NF-κB), Janus kinase-signal transducer and activator of transcription 3 (JAK-STAT3), and mammalian target of rapamycin (mTOR) are predominant signaling pathways during hyperinflammation stage [22]. However, COVID-19 associated cytokine storm has still not well understood molecular mechanisms [22]. As a result, the discovery of targeted therapy involving cytokine storm mechanisms could play a crucial role in improving COVID-19 severity.

The gold standard diagnostic testing of COVID-19 is reverse transcriptase-polymerase chain reaction (RT-PCR) from nasal and throat swab samples [7, 11]. The primary treatment of COVID-19 is supportive care and respiratory support [6, 7]. Medical therapies include dexamethasone, remdesivir, and favipiravir [19, 20, 23]. Nonetheless, the current treatments cannot cover all patients with severe conditions, especially patients with the cytokine storm. Therefore, targeted therapy discovery strategies in COVID-19 are still needed. In addition, the role of vaccines in COVID-19 prevention has been studied and needs further investigation.

Bioinformatics, systems biology, and multi-omics data from high throughput technologies allow translational and precision medicine to be effective in clinical practice [24]. For example, *TBX1* mutation disrupts the network function demonstrated by several clinical features in DiGeorge syndrome. High-throughput-based network analysis can predict key proteins that target drug discovery and repurposing [24]. Moreover, integration of structural bioinformatic methods, such as molecular docking and molecular dynamics, with systems biology and drug repurposing has greatly impacted in silico experiments. It is interesting to note that one of the most powerful tools used in bioinformatics and system biology and still popular is network analysis. A network consists of members or units called nodes or vertices and interactions or relationships between nodes called edges or links [24-26]. Networks can be classified into undirected and directed graphs depending on whether edges have directions [24, 25]. There are several measurements used in topological network analysis. Degree is clarified by the number of edges that a node has. Nodes having high degrees are categorized to be hub nodes. Shortest path distance is the lowest number of edges linked between a pair node, and the clustering coefficient measures how many nodes are prone to group together. Moreover, there are measurements of the importance of a node in a network or called centrality. For instance, betweenness centrality is the frequency summation of the shortest path of node pairs that passes through the

interested node, and closeness centrality considers how closed the node is to other nodes. Eigenvector centrality is concerned with node influence by calculating eigenvalues in the adjacency matrix [26]. In biological networks, the essentiality of nodes is measured from degree and betweenness centrality. Nodes with a high degree and betweenness centrality are considered necessary [27]. Topological analysis reveals that biological networks are scale-free, small world, and robust [25, 27]. Protein-protein interaction (PPI) network is one of the most networks used in the study of systems biology. In PPI networks, the nodes represent proteins and edges represent physical interaction between proteins [24, 27, 28].

There are two common methods for disease-related PPI network construction: neighborhood and network diffusion approach. Neighborhood method constructs the network considering nodes adjacent to known disease genes or seed nodes. Network diffusion establishes the network based on the intensity of the signal propagated throughout the network from the seed nodes. The advantages of neighborhood-based PPI network construction are the user-friendly method and less computational time consumption. Several studies in biological network analysis have operated this method for PPI network construction [29-33]. However, the method provides higher false-positive results than the diffusion method. On the other hand, network diffusion can predict disease-associated nodes distant from the seed nodes with low false-positive results, although it requires coding skills and prolonged running time.

There are several previous studies related to biological network analysis in COVID-19. For example, Gordon et al. (2020) generated a viral-host interactome using affinity-purification mass spectrometry from an infected cell line (HK-293T/17) [4]. They also did pathway enrichment analysis. Network and functional enrichment analysis revealed that several viral proteins interact with host proteins involved in innate immune systems. They also found that viral proteins can interact with a Cullin ubiquitin ligase and bromodomain proteins [4]. Prasad et al. (2020) built a transcriptomic-based PPI network

from infected alveolar adenocarcinoma cells (A549). They discovered 15 hub proteins related to IFN pathway. Drug-gene interaction analysis showed that poly I:C, imiquimod, mitomycin C, and vanadium oxide could be potential drugs to improve the disease severity [34]. Zhou et al. (2020) used network-based drug repurposing established from human interactome, viral-host PPI network, and drug-target network. The outcome reveals that many compounds such as melatonin, mercaptopurine, and sirolimus could be potential drugs. Moreover, drug combination identification was conducted based on the complementary exposure pattern. The result shows that combinations between sirolimus and dactinomycin, toremifene and emodin, and mercaptopurine and melatonin could have a role in COVID-19 therapy [35]. Messina et al. (2020) compared viral-host interactome based on S protein by using gene expression data. Random walk with restart (RWR) algorithm was performed to find a proximity network from a seed protein (S protein). The finding indicates that pathway enrichment analysis involves innate immune systems such as Toll-like receptors, TGF-β, and many chemokines [36]. Adhami et al. (2021) used a clustering algorithm called fast agglomerate edge clustering (FAG-EC) to form modules in the PPIs network with data from BioGRID and STRING database. They showed that target drugs are paclitaxel, bortezomib, carboplatin, crizotinib, cytarabine, daunorubicin, and vorinostat. Pathway enrichment analysis was concentrated in the cancer pathway, RNA transport, AMPK signaling pathway, RIG-1-like receptor signaling pathway, and ribosome [37]. More et al. (2021) conducted a PPI network based on SARS-CoV-2 related genes from GeneCards database. Gene Ontology (GO) biological process of hub proteins composed of viral life cycle, C-C chemokine receptor activity, and platelet activation, while Kyoto Encyclopedia of Genes and Genomes (KEGG) pathway enrichment consists of FoxO, GnRH, ErbB, Neurotrophin, Toll-like receptor, IL-17, TNF, insulin, HIF-1, JAK-STAT, estrogen, NF-κ, chemokines, VEGF, and thyroid hormone signaling pathway [38].

Several previous studies applied biological network analysis to discover the key genes, molecular mechanisms, and candidate targeted drugs in COVID-19. However, they mainly focused on the high-throughput data from cell cultures and animal models rather than the clinical data. Furthermore, a small number of network biology research used gene expression data from leukocytes to investigate inflammatory responses in COVID 19. Therefore, biological network analysis and drug repurposing in COVID-19 induced cytokine storm based on severe patients is the primary goal in this study

This study aims to identify the key genes, underlying molecular mechanisms, candidate targeted drugs, and novel biomarkers pertinent to the cytokine storm processes in COVID-19 using PPI network analysis based on leukocytes transcriptomics data of severe COVID-19 patients. The further goals of this study are to reveal candidate biomarkers and target drugs from systems biology approaches.

1.2 RESEARCH OBJECTIVE

1. To identify the key genes and underlying molecular mechanisms of inflammatory processes in severe COVID-19 patients using PPI network analyses

2. To discover the novel biomarkers and candidate drugs via PPI network analysis and network-based drug repurposing

1.3 SCOPES OF THE REASERCH

In this study, the leukocyte transcriptomic profiles of severe COVID-19 patients were downloaded from Gene Expression Omnibus (GEO) DataSets [39] to identify differentially expressed genes (DEGs). In addition, the human interactome data was collected from Search Tool for the Retrieval of Interacting Genes/Proteins (STRING) v11.0 database [40] for human interactome network construction. The DEGs were mapped with the list of the genes in the interactome data for establishing the seed nodes. The immune-related PPI network was constructed using a network diffusion algorithm called Laplacian heat diffusion (LHD). Functional enrichment analysis was performed on the network to find molecular mechanisms. Moreover, the key genes were

identified via several network centrality measurements. The drug-gene interaction networks were built based on the identified key genes using drug-gene or drug-protein interaction databases searching to discover the alternative targeted drugs. The interaction results were confirmed using structural analysis such as molecular docking. Furthermore, the combination of two transcriptomic datasets from different studies was conducted to construct the common PPI network for further discovery of key genes and candidate drugs. MicroRNA (miRNA)-mRNA regulatory networks were also established to find novel candidate biomarkers for severe COVID-19 prediction.

1.4 EXPECTED OUTCOMES

1. This study could reveal underlying molecular mechanisms and key genes in severe COVID-19.
2. This study could discover candidate targeted drugs and novel biomarkers to treat and predict severe COVID-19.
3. The identified candidate drugs and biomarkers can be applied in clinical practice.

1.5 AN OVERVIEW OF THE RESEARCH

Figure 1 shows the overview of this thesis. The thesis contains three parts. Part I describes the background, motivation, research objectives, scopes of the research, and expected outcomes. Part II consists of two research articles relevant to the proposed study. Part III explains discussions, limitations, suggestions, and future works.

Part I
- Background and motivation
- Research objectives
- Scopes of the research
- Expected outcomes

Part II
- Research article 1
- Research article 2

Part III
- Discussions and conclusions
- Limitations
- Future works
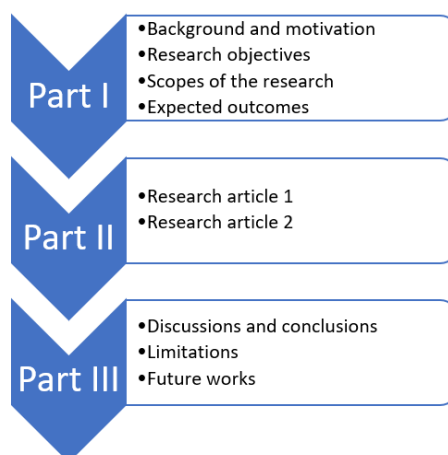
Figure 1. An overflow of the contains in the thesis.

The topic of the first article is "Immune-Related Protein Interaction Network in Severe COVID-19 Patients toward the Identification of Key Proteins and Drug Repurposing". This article proposed a network diffusion method named Laplacian heat diffusion (LHD) algorithm to construct an immune-related PPI network (IPIN) based on leukocyte transcriptomic profiles in severe COVID-19 patients. Functional enrichment analysis was performed to find the underlying molecular mechanisms. Additionally, two network clustering algorithms, such as Markov Clustering (MCL) and Molecular Complex Detection (MCODE), were proceeded to compare the difference between module detection. Numerous centrality measurements, such as degree, betweenness, closeness, and eigenvector, were computed to find the key genes and proteins in the network. Moreover, a ranking scoring was developed by all centrality scores prioritization to identify the key genes in comparison with the conventional centrality measurements. Drug-gene and drug-protein interaction networks were also constructed based on the identified key genes to discover candidate targeted drugs using searching drug interaction databases. The identified key genes and candidate drugs were validated via evidence from literature reviews in computational, experimental, and clinical research.

The topic of the second article is "Multi-level Biological Network Analysis Based on Leukocyte Transcriptomic Profiles in Severe COVID-19: Shed Light on Systems Biology to Precision Medicine". To find further molecular mechanisms, key genes, and candidate drugs, two transcriptomic datasets were combined to find common DEGs. Functional enrichment analysis was conducted based on the common DEGs. This article aims for non-bioinformatician users to understand the workflow of systems biology application in precision medicine. Therefore, the PPI network was constructed in a software tool in the STRING database and was analyzed and visualized in a user-friendly software tool. In addition, the key genes were identified using a combination of between and degree centrality calculation. A survival analysis using the myeloid leukemia model was conducted to validate the key genes. Drug-gene interaction

networks were also established from the searching databases. The interactions were evaluated from a structural biological approach called molecular docking. Furthermore, network community detection was operated using a network clustering algorithm to find specific molecular mechanisms of severe COVID-19. miRNA-mRNA regulatory networks were also built based on the clustered PPI network to identify novel biomarkers, which were miRNAs.

PART II

RESEARCH ARTICLES

2.1 RESEARCH ARTICLE 1

Immune-Related Protein Interaction Network in Severe COVID-19 Patients toward the Identification of Key Proteins and Drug Repurposing

Pakorn Sagulkoo [1,2], Apichat Suratanee [3,4] and Kitiporn Plaimas [5,6,*]

[1]Program in Bioinformatics and Computational Biology, Graduate School, Chulalongkorn University, Bangkok 10330, Thailand; pakorn.sagulkoo@cmu.ac.th

[2]Center of Biomedical Informatics, Department of Family Medicine, Faculty of Medicine, Chiang Mai University, Chiang Mai 50200, Thailand

[3]Department of Mathematics, Faculty of Applied Science, King Mongkut's University of Technology North Bangkok, Bangkok 10800, Thailand; apichat.s@sci.kmutnb.ac.th

[4]Intelligent and Nonlinear Dynamics Innovations Research Center, Science and Technology Research Institute, King Mongkut's University of Technology North Bangkok, Bangkok 10800, Thailand

[5]Advance Virtual and Intelligent Computing (AVIC) Center, Department of Mathematics and Computer Science, Faculty of Science, Chulalongkorn University, Bangkok 10330, Thailand

[6]Omics Science and Bioinformatics Center, Faculty of Science, Chulalongkorn University, Bangkok 10330, Thailand

*Correspondence: kitiporn.p@chula.ac.th

Abstract: Coronavirus disease 2019 (COVID-19) is still an active global public health issue. Although vaccines and therapeutic options are available, some patients experience severe conditions and need critical care support. Hence, identifying key genes or proteins involved in immune-related severe COVID-19 is necessary to find or develop the targeted therapies. This study proposed a novel construction of an immune-related protein interaction network (IPIN) in severe cases with the use of a network diffusion technique on a human interactome network and transcriptomic data. Enrichment analysis revealed that the IPIN was mainly associated with antiviral, innate

immune, apoptosis, cell division, and cell cycle regulation signaling pathways. Twenty-three proteins were identified as key proteins to find associated drugs. Finally, poly (I:C), mitomycin C, decitabine, gemcitabine, hydroxyurea, tamoxifen, and curcumin were the potential drugs interacting with the key proteins to heal severe COVID-19. In conclusion, IPIN can be a good representative network for the immune system that integrates the protein interaction network and transcriptomic data. Thus, the key proteins and target drugs in IPIN help to find a new treatment with the use of existing drugs to treat the disease apart from vaccination and conventional antiviral therapy.

Keywords: severe COVID-19; immune system; network diffusion; protein-protein interaction network; drug repurposing

2.1.1 INTRODUCTION

Coronavirus disease 2019 (COVID-19) has been spreading worldwide, despite several developed vaccines, still causing numerous cases. Moreover, most causes of death are from severe complications from the disease. Currently, the global statistical data from the World Health Organization (WHO) indicate that 476,374,234 and 6,108,976 cases are infected and dead, respectively (26 March 2022) [1]. COVID-19 is an infectious disease caused by severe acute respiratory syndrome *coronavirus-2 (*SARS-CoV-2), a positive-sense single-strand RNA (+ssRNA) virus [2]. SARS-CoV-2 is a betacoronavirus, classified in the Coronaviridae family [3]. Although SARS-CoV-2 incurs a well-known pandemic coronavirus infection in the present, for severe respiratory diseases resulting from the two coronavirus diseases, most known cases emerged before, in the last two decades. For example, SARS-CoV pneumonia occurred from November 2002 to August 2003 from Guangdong, China, spreading to 30 countries worldwide, having 8422 confirmed cases and 916 deaths [4]. Several epidemiolocal studies suggested that palm civets (*Paguma larvata*) in a market in Guangdong were the initial hosts for SAR-CoV infection before the emergence of human-to-human transmission [5]. Middle East Respiratory Syndrome (MERS) was first reported in Jeddah, Saudi Arabia, in June 2012. It then spread to many countries in the Arabian Peninsula and to some countries in North Africa, Western Europe, East Asia, Southeast Asia, and North America [6]. The disease is caused by MERS coronavirus (MERS-CoV),

which has much evidence indicating that its hosts are camels [7]. Various reports show 2578 confirmed cases and 888 deaths from MERS [8,9]. The first case of COVID-19 was reported in Wuhan, China, in December 2019 [10]. The patient was diagnosed with severe pneumonia with an unknown cause [11], while the number of cases in Wuhan increased to 41 in January 2020. In the same month, the first evidence revealed human-human transmission and asymptomatic or pre-symptomatic transmission [12]. Afterwards, COVID-19 spread from China to Thailand, Singapore, Vietnam, Taiwan, Japan, South Korea, Nepal, and the United States [13]. On 11 February 2020, COVID-19 was declared a pandemic by the WHO [12].

As mentioned above, COVID-19 is caused by SARS-CoV-2, a +ssRNA virus classified as a betacoronavirus. SARS-CoV-2 genome sequence shares 79% of genes with SARS-CoV genome compared to MERS-CoV, which has only 53% similarity. Nonetheless, SARS-CoV-2 has a percent identity of more than 96% when compared to bat-SARS-like CoV (SL-CoV), suggesting that bats can be an initial host of COVID-19 [14]. SARS-CoV-2 genome also shares 85.5 to 92.4% of identity with pangolin coronavirus genomes, indicating that pangolins could be an initial host of the infection [15]. The genomic content of SARS-CoV-2 consists of 16 non-structural proteins (NPs), 4 structural proteins, and 9 putative accessory factors [16]. The 16 NPs contain open reading frame (ORF) 1a and 1b. There are three crucial NPs that play a vital role in SARS-CoV-2 replication and pathogenesis. For instance, papain-like protease (PLpro) and 3C-like protease (3CLpro) have functions to cleave the viral polyprotein translated from ORF1a and ORF1b into 16 NPs. RNA dependent RNA polymerase (RdRp) replicates the viral genome in host cells [17,18]. Structural proteins, composed of spike (S), envelope (E), membrane (M), and nucleocapsid (N) protein, play a significant role as a viral genome protector and virulent factors used for virus entry [19]. The putative accessory factors are encoded from ORF3b, ORF6, ORF7a and ORF8. Their roles are not well understood, although some studies revealed that they were involved in interferon antagonism and impaired host immune response [20].

The pathogenesis of COVID-19 occurs when the virus enters a host respiratory epithelial cell using an S protein primed by transmembrane serine protease 2 (TMPRSS2) binding with a host membrane receptor, such as angiotensin-converting

enzyme 2 (ACE2) receptor [21,22]. Meanwhile, SARS-CoV-2 also binds with Toll-like receptors (TLR) 4 and 8, causing innate immune response that will be described in further detail [23]. After entering the host cell, the viral genetic material is replicated to copied viral genomes and translated to essential viral proteins in the host cytoplasm. The copied viral genomes are assembled with the translated structural proteins to form the mature viral particles. Then, the replicated virions are released from the infected host cell and enter other non-infected host cells [24]. During the viral replication, some viral components become pathogen-associated molecular patterns (PAMPs) while the infected host cells express endogenous damage-associated molecular patterns (DAMPs). These molecules are recognized by pattern recognition receptors (PRRs) in the host cells such as TLR-3, 7, and 8, retinoic acid-inducible gene 1 (RIG-1)-like receptors (RLRs)/melanoma differentiation-associated gene 5 (MDA5), and NOD-like receptors (NLRs) [25]. The interaction between PAMPs including DAMPs and PRRs in the infected host cells activates the host innate immune response by promoting the production of antiviral and proinflammatory cytokines; for example, interferon α (IFN-α), IFN-β, IFN-γ, interleukin 1β (IL-1β), IL-6, IL-12, IL-18, IL-33, and tumor necrosis factor α (TNF-α) [26]. Moreover, PAMPs and DAMPs' interaction with PRRs releases nuclear factor κB (NF-κB) [27]. NF-κB from the infected host cell stimulates innate immune cells such as dendritic cells (DCs), monocytes, macrophages, neutrophils, and natural killer (NK) cells to secrete further proinflammatory cytokines [27,28]. As a result, the uncontrolled proinflammatory cytokines are excessively released from both immune and respiratory epithelial cells, leading to collateral tissue damage. This phenomenon is called hyperinflammation or a cytokine storm, the most common fatal complication in COVID-19 [29].

Pathophysiology of severe COVID-19 is initiated when cytokine storm injures lung epithelial and endothelial cell damage and induces apoptosis, resulting in increased pulmonary vascular permeability [30]. The plasma is then leaked from the capillary to the alveolar space. Consequently, the gas exchange defect occurs, leading to acute respiratory distress syndrome (ARDS). Patients with ARDS will have progressive dyspnea, hypoxia and require ventilation support and intensive care [31]. Unfortunately, the excessive proinflammatory cytokines also affect other organs, such as the

gastrointestinal tract, cardiovascular system, brain, liver, and kidney [32]. As a result, the patients will progress the signs and symptoms of multiple organ injuries; for instance, nausea, vomiting, diarrhea, hemodynamic instability, alterative mental status, heart tissue damage, elevated liver enzyme, and creatinine rising [33]. Cytokine storms not only directly injure several organs but also generate organ infarction due to increased thromboembolic phenomena [34]. In addition, disseminated intravascular coagulation (DIC) can arise in severe COVID-19 because of the persistent coagulation factor and platelet consumption, inducing further multiple organ injury [35]. Severe COVID-19 patients usually die from multiple organ dysfunction [36]. Cytokine storms can also provoke other serious conditions, such as secondary hemophagocytic lymphohistiocytosis (sHLH) and macrophage activation syndrome (MAS), characterized by monocytes and macrophages engulfing erythrocytes, platelets, immune cells, and other host cells. Hence, both sHLH and MAS can promote more collateral tissue damage, worsening multiple organ dysfunction [37].

The current treatment trends in COVID-19 are using vaccination to prevent the disease and prescribing antiviral agents to infected people [38-41]. Although COVID-19 susceptibility and severity can be improved by using well-developed vaccines and effective antiviral therapies, some patients still progress the disease to the cytokine storm and other severe complications. COVID-19-associated cytokine storms can be treated with intravenous corticosteroid. Several systemic reviews and meta-analyses have indicated that systemic corticosteroids can improve critically ill COVID-19 patients [42-46]. However, systemic corticosteroid provides many unexpected side effects, such as hyperglycemia, adrenal suppression, and increased secondary bacterial infection [47-49]. Therefore, finding novel target treatments in severe COVID-19 instead of conventional medication is necessary for more effective treatment and fewer side effects. Drug repositioning is another technique to discover an existing drug to treat a disease. Systems biology and network analysis have been directly applied to identify key genes or proteins [50-53], drug–gene or drug–protein interactions [54,55], and drug–disease associations [56,57]. Structural bioinformatics is the main task at the molecular structure level to identify possibilities of compound targeting, such as the study of inverse docking fingerprints in drug repurposing for SAR-CoV-2 [58]. Modern

biopharmaceutical approaches, such as large biomolecules like antibodies (immunoglobulins) and plasma, are of interest to treat COVID-19. However, their roles in clinical trials are currently being studied to treat severe cases.

In the precision medicine and data science era, bioinformatics and systems biology are central in molecular medicine and targeted therapy. Network biology is a powerful tool to identify key genes and targeted drugs involved in many diseases by using topological analysis and network diffusion algorithms. In addition, protein–protein interaction network analysis is usually used to find hub and bottleneck proteins [59-61], to infer protein functions [62-64], find gene–disease [65-67] and disease–disease associations [68,69]. Various centrality calculations, such as degree, betweenness, closeness, and eigenvector, play an important role in biological network analysis. Several systems biological studies have performed these centralities to identify key genes and gene prioritization in the disease-related networks [53,70-72]. Nonetheless, analyses of importance and difference of the centralities in biological roles are still needed for further investigation.

There are two methods for extracting a specific subnetwork: the neighborhood and diffusion approaches. Neighborhood method is a traditional technique performed widely in many biological network studies [73-77]. Furthermore, there are several COVID-19 network studies constructing protein–protein interaction networks and selecting a group of related proteins using this method [50,51,54,55,78-80]. This method extracts subnetworks by considering the nodes with the low shortest path with disease-associated genes or seed nodes [81]. The benefits of neighborhood-based subnetwork construction are that the approach is user-friendly and has fast running time. However, some neighbor nodes in the networks are not disease-associated genes, causing topological changes and missing identification of key nodes. Therefore, the diffusion-based method is preferred to build specific protein–protein interaction subnetworks, such as immune, inflammation, and viral–host interaction network, with lower false-positive disease-related nodes, although it is time consuming and requires coding skills. Network diffusion is the method used to predict novel disease-associated genes based on known disease-associated genes via considering the diffusion or probability scores

from iterative running algorithms at time stable. Nodes with high diffusion scores are inferred as theoretical disease-related genes [82].

Moreover, there have been no COVID-19 studies involved in immune-related biological networks using the network diffusion method. As a result, we proposed this method to construct an immune-related protein interaction network (IPIN). A network diffusion method named Laplacian heat diffusion (LHD) algorithm on a human interactome network was conducted in this study to construct an IPIN in severe COVID-19 patients. Key immune-related proteins in the network were identified using several centralities and ranking score measurement. Additionally, drug repurposing was also performed to find target medication to those key proteins. This study aims to discover candidate target drugs to treat severe COVID-19 at clinical levels.

2.1.2 MATERIALS AND METHODS

The summary of materials and methods used in our study is illustrated as a diagram in Figure 2. First, differentially expressed genes (DEGs) of the transcriptomic data downloaded from GEO DataSets were mapped with the human interactome data from STRING v11.0 database [83] for forming the seed nodes. Second, construction of a human protein interactome network obtained from STRING database [83]. Third, the Laplacian heat diffusion (LHD) algorithm operated network diffusion. Fourth, a permutation test filtered out false-positive high diffusion score nodes. Fifth, significantly high diffuse score nodes were used to construct the IPIN. Metascape [84] was also performed for the functional enrichment analysis of the network. Sixth, Molecular Complex Detection (MCODE) and the Markov Clustering (MCL) algorithm were conducted to find IPIN modules. Next, the centralities and the ranking score were calculated to identify the key immune-related proteins. Finally, candidate drugs targeting the key proteins were discovered by chemical and drug databases searching for drug–gene and drug–protein interactions.
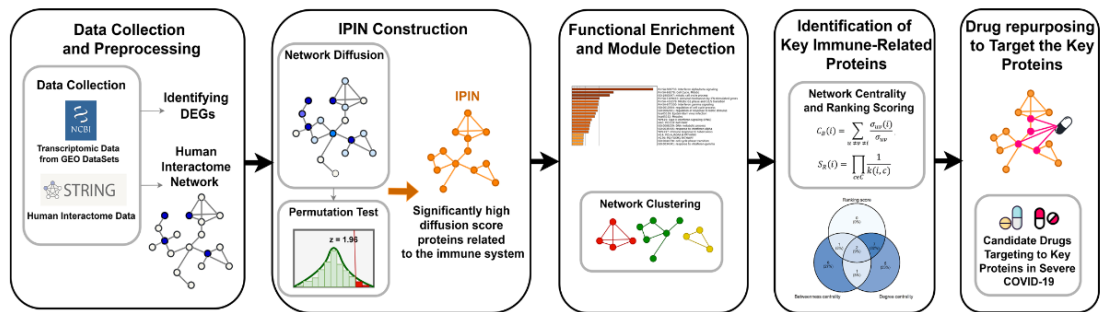
Figure 2. Summary of the process to identify the key proteins and drug repurposing in the severeCOVID-19 based on an immune-related protein interaction network (IPIN). Circles represent protein nodes in a protein-protein interaction network. Dark blue circles are nodes of the DEGs' proteins. Light blue circles are nodes of proteins having diffuse scores. Orange circles represent high diffusion score proteins for IPIN. Red, green, and yellow circles are proteins in different modules. Pink circles are target proteins of an existing drug.

2.1.2.1 DATA COLLECTION AND PREPROCESSING

i. Human Protein Interactome

The human protein interactome data, containing 19,566 proteins (or nodes) and 11,938,498 interactions, was obtained from STRING v11.0 database (https://string-db.org/ accessed on 20 November 2021) [83]. R package 'dplyr' [85] was used to manipulate the data. The interactions with a combined score between 900 and 999 were included. R package 'igraph' [86] was conducted to eliminate isolated nodes and multiple edges. As a result, the rest of the interactome had 11,334 proteins and 123,263 interactions. The combined scores between 900 and 999 were changed to a weighted score by rescaling into the range of [0.01, 1].

ii. Transcriptomic Data

The collected data was from Gill et al.'s study (2020) in GEO DataSets (GSE154998) (https://string-db.org/ accessed on 20 November 2021) [87]. The researchers collected leukocytes samples from COVID-19 cases and controls in an intensive care unit (ICU) to perform transcriptomic profiles by RNA sequencing (RNA-seq) method. The total sample size was 14, with 7 samples being COVID-19 cases and the rest being controls. The SARS-CoV-2-positive cases were confirmed using reverse

transcription-polymerase chain reaction (RT-PCR) method. In addition, genes from RNA-seq data having the false discovery rate (*FDR*) < 0.05 and log2fold change (*log2 FC*) > 1.5 were differentially expressed genes (DEGs). Hence, there were 224 genes meeting the criterion (Table S1 in Supplementary Materials). The DEGs then were mapped with the protein list in the protein–protein interaction network of the STRING v11.0 database by using Ensembl ID joining [83]. Thus, there were 189 Ensembl protein IDs (Table S2 in Supplementary Materials).

With the use of network diffusion, the seed nodes were prepared from mapping between these 189 Ensembl IDs (the immune-related proteins from DEGs) and the human interactome data (in Section 2.1.1). This resulted in 141 seed nodes (Table S3 in Supplementary Materials).

2.1.2.2 IPIN CONSTRUCTION WITH NETWORK DIFFUSION
i. LHD Algorithm

This study used LHD algorithm to operate human interactome network propagation. In many studies, LHD is one of the most common network diffusion algorithms used to infer disease-associated genes or proteins [88,89]. Given a network called *G*, let *W* be a weight adjacency matrix of network *G* calculated from rescaling the combined scores and *D* be a diagonal matrix whose values are a degree of each node arranged diagonally. Laplacian matrix (*L*) was calculated from $D - W$. An initial diffusion vector (H_0) of all nodes is conducted normally by setting the initial heat diffusion score (h_0) to each node. In general, the initial heat scores (h_0) are set as $1/n$ where *n* is the number of seed nodes related to the subject of interest (immune-related proteins as seeds in our case) while the other nodes are set as 0. The diffusion vector at time *t* (H_t) was updated based on the previous diffusion vector at time *t-1* (H_{t-1}) according to this equation:

$$H_t = H_{t-1} \times e^{-Lt} \tag{1}$$

where *e* is defined as Euler's number ($\approx$2.1828). The network diffusion was iterated based on Equation (1) until two consecutive diffusion vectors were relatively similar. In our case, the relative similarity is met if $\left\| H_t - H_{t-1} \right\| < 10^{-6}$, then the diffusion becomes stable. The latest diffusion scores after the stability are used as an indicator of

the relevant scores to the seed nodes. In another word, a node with a high diffusion score was strongly associated with seed nodes.

In our cases, the initial diffusion vector (H_0) contained the initial scores of 11,334 protein nodes in the whole protein–protein interaction network. The initial scores for 141 seed nodes were set as 1/141 while other protein nodes are set as 0. After the network propagation was stable, the final scores were then used for further permutation test analysis. In this study, LHD algorithm was carried out by using R package 'diffusr' [90]. The parameters in the package were well-established using the default setting.

ii. Permutation Test

When LHD algorithm finishes the network propagation, in theory, the nodes with the high diffusion score are strongly associated with the disease-associated proteins. However, some nodes receiving the high diffusion score can be false-positive. This false-positive result can occur because some factors such as the topological structure of network G can provide a high diffusion score apart from the actual association with the seed nodes. Therefore, a permutation test should be conducted to filter out nodes with the false-positive high diffusion score. The permutation test measures whether nodes have a high diffusion score due to statistical significance or chance. The test was operated by assigning 1000 different sets of the initial seeds into the human interactome network for LHD algorithm. Before running the algorithm in each set, 141 seed nodes were randomly assigned, independent of DEGs, from 11,334 nodes. Hence, the sets of seed nodes in the original set and in the 1000 sets were different. The z-score of the diffusion score of node n ($Z(n)$) was calculated according to this equation:

$$Z(n) = \frac{h(n) - \bar{X}(n)}{SD(n)}, \tag{2}$$

where $h(n)$ is defined as the diffusion score of node n in the original set, $\bar{X}(n)$ and $SD(n)$ are the mean and standard deviation, respectively, of diffusion score of node n in the original set and 1000 permutation sets. A node with a z-score more than 1.96 (p-value < 0.05) had the true-positive high diffusion score and was selected for the IPIN construction. Table S4 in Supplementary Materials shows the original diffuse scores including with the mean and standard deviation calculated from the diffusion score in

the original set and 1000 permutation sets in each node in the whole protein–protein interaction network.

iii. IPIN Construction

After the network diffusion by LHD algorithm and the validation of the high diffuse score nodes by permutation testing were performed, 154 nodes with significant diffusion scores were obtained (Table S5 in Supplementary Materials). The filtered significant nodes from the permutation test were mapped with the STRING human interactome network. The largest component of the significantly high diffusion score nodes consisting of 97 nodes and 778 interactions was selected as our immune-related protein interaction network or IPIN for further functional enrichment analysis, topological analysis, and centrality measurement. The construction of the IPIN was based on leukocytes or white blood cells' transcriptome data. Leukocytes are the cells that play an important role in pathogen defense mechanisms or immunity. The gene expression of leukocytes during the infection indicates the host's immune status against the pathogens. Thus, this IPIN was constructed to represent a core host immune system against the severe COVID-19. The edge list information for this IPIN is also provided in Table S14 in Supplementary Materials.

2.1.2.3 TOPOLOGICAL ANALYSIS, NETWORK CENTRALITY, AND RANKING SCORES

R package 'igraph' [86] was performed to calculate global and local topological parameters and network centrality [86]. The global topological parameters such as the number of nodes (N), the number of edges (M), average degree ($<k>$), diameter (D), mean shortest path length ($mspl$), and average clustering coefficient (acc) were computed. Furthermore, degree distribution and a clustering coefficient versus degree curve were plotted to evaluate the scale-free network properties. Several local parameters and centrality measurements such as degree centrality (C_D), betweenness centrality (C_B), closeness centrality (C_C), and eigenvector centrality (C_E) were calculated to find the essential nodes in the network. A node with more than 90th percentile centrality value was listed and its functional importance in the network and the disease

was discussed. These high-value nodes in the four centrality sets were plotted using an upset plot from R package 'UpSetR' [91] to find the node overlapping in each centrality.

Degree centrality is the number of adjacent nodes having the interaction with interested node *i*, according to this equation

$$C_D(i) = \sum_j A_{ij},$$

(3)

where A_{ij} is a value of a non-weight adjacency matrix (*A*) of node *i* and *j*, respectively. In network biology, the high-degree proteins are hub nodes and play an important role in the network function [92]. Therefore, numerous medications are designed for targeting the hub nodes.

Betweenness centrality is the summation of the ratio of the shortest path between node *u* and *v* that passes through node *i*. The betweenness centrality equation is

$$C_B(i) = \sum_{u \neq v \neq i} \frac{\sigma_{uv}(i)}{\sigma_{uv}},$$

(4)

where σ_{uv} is a total number of the shortest path between node *u* and *v* and $\sigma_{uv}(i)$ is the number of the shortest path between node *u* and *v* that pass through node *i*. The high-betweenness proteins indicate the bottleneck property, forming the bridges controlling the flow of information in the network. Interruption of the bottlenecks by several targeted therapies can result in network function destruction in many diseases, improving the disease outcomes [92-95].

Closeness centrality is the inverse of shortest path distance summation between node *i* and all other nodes in the network. The closeness centrality equation is shown as

$$C_C(i) = \frac{N-1}{\sum_{j=1,j\neq i}^{N} d(i,j)},$$

(5)

where *N* is the total number of nodes in the network and $d(i,j)$ is the shortest path length between node *i* and node *j*. Some studies used closeness centrality to find essential genes and proteins in several biological problems [96.97].

Eigenvector centrality is the extended form of degree centrality that focuses on the global high-degree nodes more than the local high-degree nodes. Eigenvector centrality has the assumption that the essential nodes should connect to the other

important nodes. Therefore, nodes with high eigenvector centrality have high degree centrality, and their neighbored nodes also have a high degree value. The equation is demonstrated as

$$C_E(i) = \frac{1}{\lambda} \sum_j A_{ij} C_E(j) \,, \tag{6}$$

where λ is the largest eigenvalue of A. Eigenvector centrality is applied to analyze many connectome studies in neurological diseases [98-101].

As mentioned above, all four centralities play a vital role in discovering essential genes or proteins. Moreover, numerous traditional network biology studies usually use degree and betweenness centrality to find essential genes and proteins. Closeness and eigenvector are occasionally applied to find vital genes and proteins. Therefore, a node with a high value of all centralities was a key protein in the network. The ranking score (S_R) was applied to rank the nodes based on the centralities. Let C be a set of all centralities and c represent a centrality measure in C. A ranking score of any node i ($S_R(i)$) was calculated based on the reciprocal of the product of a ranking position of node i in each centrality c ($k(i,c)$), according to this equation

$$S_R(i) = \prod_{c \epsilon C} \frac{1}{k(i,c)}. \tag{7}$$

Nodes with high ranking scores greater than the 90th percentile were considered as key proteins in the IPIN network. In addition, nodes with degree and betweenness centrality greater than the 90th percentile were used to compare the ranking scoring nodes.

2.1.2.4 FUNCTIONAL ENRICHMENT ANALYSIS AND NETWORK CLUSTERING

Metascape (https://metascape.org/gp/index.html#/main/step1 accessed on 10 December 2021) [84] was conducted for functional enrichment analysis in the largest component network according to the six terms: Gene ontology biological process (GO-BP) [102], Kyoto Encyclopedia of Genes and Genomes (KEGG) pathways [103], Reactome pathways [104], WikiPathways [105], Canonical pathways [106], and CORUM pathway [107]. Moreover, the Molecular Complex Detection (MCODE) algorithm [108] in Metascape was operated to cluster the enrichment terms into large groups to find the

more common biological terms. The Markov Clustering (MCL) algorithm [109] was also used in the STRING v11.0 database to explore the network communities in the IPIN. The inflation parameter of MCL was set to 1.5. Functional enrichment analysis in each module was also conducted in STRING v11.0 database using GO-BP, REACTOME pathways, KEGG pathways, and WikiPathways term. In addition, the clusters were visualized by using STRING v11.0.

2.1.2.5 DETECTION OF POTENTIAL DRUGS FOR DRUG REPURPOSING

The key proteins, having a ranking score, degree, or betweenness centrality above the 90th percentile, were used as the input to find drug–gene and drug–protein interactions from DrugBank database (https://go.drugbank.com/ accessed on 15 December 2021) [110], Therapeutic Target Database (TTD) (http://db.idrblab.net/ttd/ accessed on 15 December 2021) [111], Comparative Toxicogenomics Databases (CTD) (http://ctdbase.org/ accessed on 15 December 2021) [112], and GeneCards (https://www.genecards.org/ accessed on 15 December 2021) [113]. Drugs which have United States Food and Drug Administration (FDA) approval and evidence of interactions with the key genes or proteins were selected. The STITCH v5.0 database (http://stitch.embl.de/ accessed on 18 December 2021) [114], containing drug–protein interaction information, was performed to confirm the chosen drugs. A confidence score of the interaction in the STITCH database was used to find suitable drug–protein interactions. The confidence score is the probability value calculated based on both experimental and computational evidence such as text mining, high-throughput experiments, co-expression and gene fusion data, and information from other databases. A drug with a confidence score of more than 0.9 was considered a candidate drug having efficiency for severe COVID-19 treatment.

2.1.3 RESULTS

2.1.3.1 IPIN CONSTRUCTION AND TOPOLOGICAL PROPERTIES

The immune-related protein interaction network, known as IPIN, was obtained after the network diffusion and the validation of the high diffuse score nodes by

permutation test. This network consisted of 97 nodes and 778 interactions as shown in Figure 3. In addition, the STRING reports showed that the average node degree and the expected edges are 16 and 50, respectively.
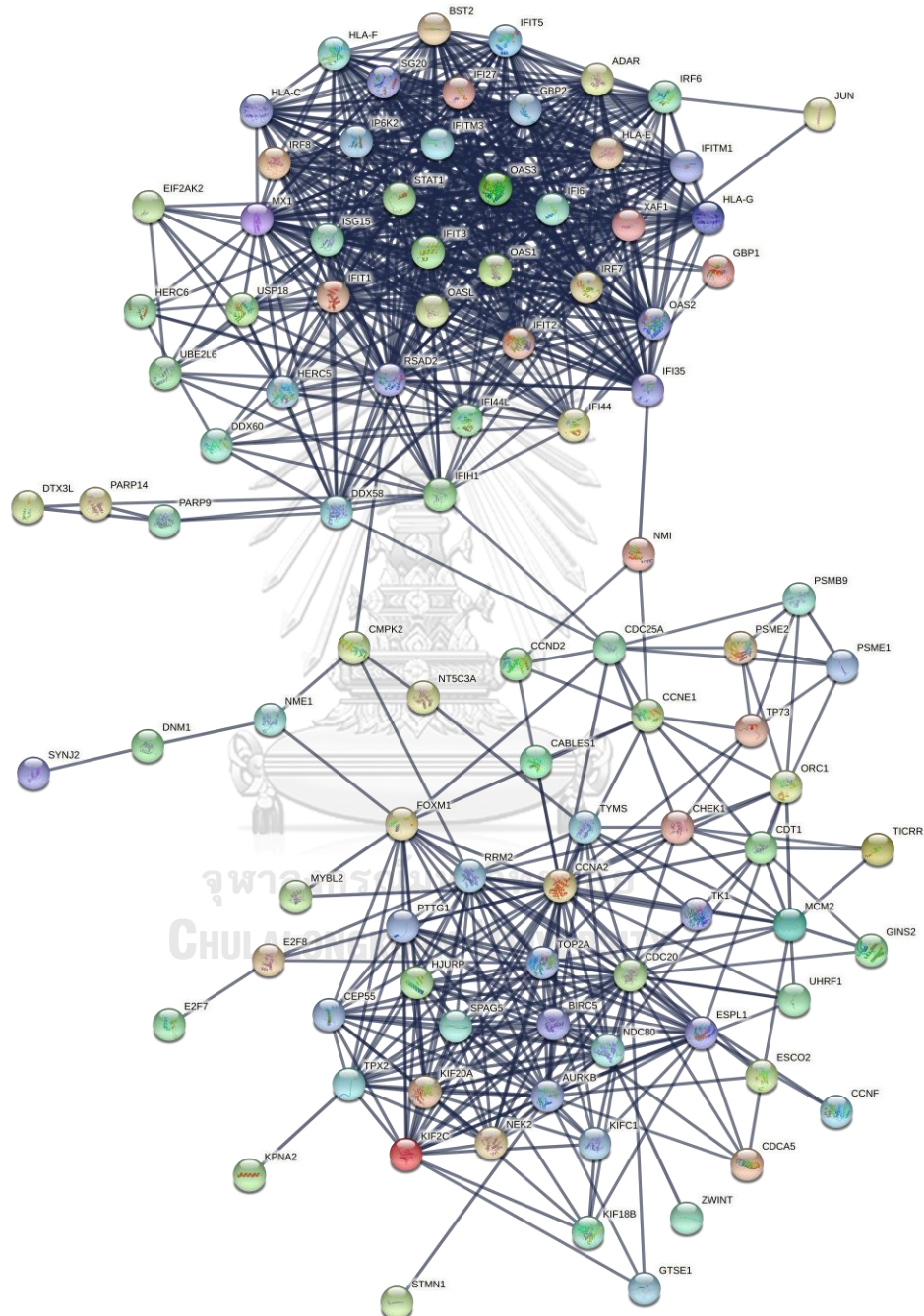
Figure 3. The largest component of the IPIN constructed from the mapping between the nodes with the significant diffusion scores and the human interactome network. The network consists of 97 nodes and 778 interactions.

Table 1 summarizes the global topological parameters of the IPIN. The average degree and diameter of the IPIN are 16.04 and 7, respectively. The network has the small-world effect because it provided the low mean shortest path length ($mspl$ = 3.01) but the high average clustering coefficient (acc = 0.74). These behaviors are concordant with other biological networks. Local topological parameters in each node in the network, for example, clustering coefficient and degree, are summarized in Table S6 in Supplementary Materials. To find the scale-free property, a degree distribution was plotted to prove the power law, as shown in Figure 4a. Furthermore, a clustering coefficient versus degree plot is illustrated in Figure 4b. The degree distribution plot reveals that it does not follow the power-law distribution because it provides a low correlation (R^2 = 0.1). This appearance is explained by the IPIN is a real-world network extracted from the human interactome network. Thus, the power-law properties can be disrupted due to the subnetwork construction. Nevertheless, the clustering coefficient versus degree plot shows the independence between the clustering coefficient and degree (R^2 = 0.061). The independent relation between clustering coefficient and degree is found in random and scale-free networks [115]. Analysis in the STRING revealed that the IPIN's protein–protein interaction (PPI) enrichment p-value is significant (p-value < 10^{-16}), indicating that the proteins have interactions with each other more than by chance. Thus, the interactions in the IPIN were more significant than random interactions. The IPIN was less likely to be a random network even though there is no suitable reason to explain the scale-free properties of the IPIN.

Table 1. Global Topological Parameters of the IPIN.

Symbol	Description	Value
N	Number of nodes	97
M	Number of edges	778
$<k>$	Average degree	16.04
d	Diameter	7
r	Radius	4
$mspl$	Mean shortest path length	3.01
D	Density	0.17
acc	Average clustering coefficient	0.74

(a)   (b)
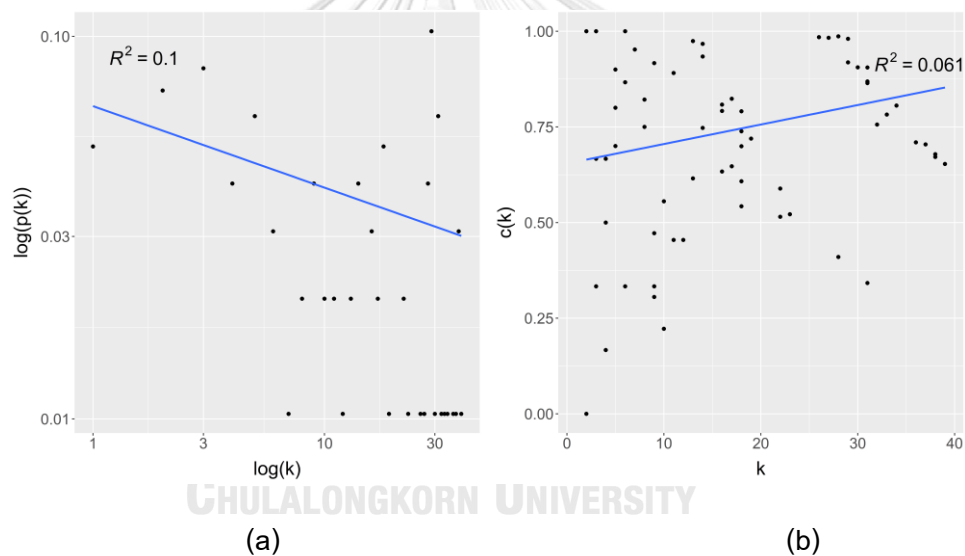
Figure 4. Topological analysis of the IPIN. (a) Degree distribution plot. (b) Clustering coefficient versus degree plot. k denotes the degree; $p(k)$ denotes the probability of degree k; $c(k)$ denotes the clustering coefficient of a node that has degree k.

2.1.3.2 FUNCTIONAL ENRICHMENT AND MODULE IDENTIFICATION IN IPIN

The functional enrichment analysis was performed using a hypergeometric test and Benjamini–Hochberg statistical correction algorithm in Metascape [84], which integrates six biological and pathway enrichment terms: GO-BP [102], KEGG pathways [103], REACTOME pathways [104], WikiPathways [105], Canonical pathways [106], and CORUM pathway [107]. The results revealed that the terms were primarily involved in

immune pathways, cell division, nucleotide metabolisms, and protein processing, as shown in Figure 5. The immune pathways were associated with innate immune response and antiviral signaling pathways such as type I and II IFN (IFN-I and IFN-II) and IFN-stimulated genes (ISGs). IFN-I mainly comprises of IFN-α and IFN-β, while IFN-γ is a component in IFN-II. The cell division terms were relevant to mitotic cell cycle process, mitotic metaphase, regulation of cell cycle, phase transition of cell cycle checkpoint at G1/S and G2/M, cytoskeleton-dependent cytokinesis, and regulation of sister chromatid separation. Moreover, nucleic metabolic pathways, such as pyrimidine metabolism, DNA metabolic process, and regulation of DNA replication, were identified. Apoptosis was also found from the enrichment analysis. Other enrichment terms were protein and enzyme processing, such as protein modification by small protein conjugation, negative regulation of catalytic activity, protein tetramerization, and protein localization to organelle.
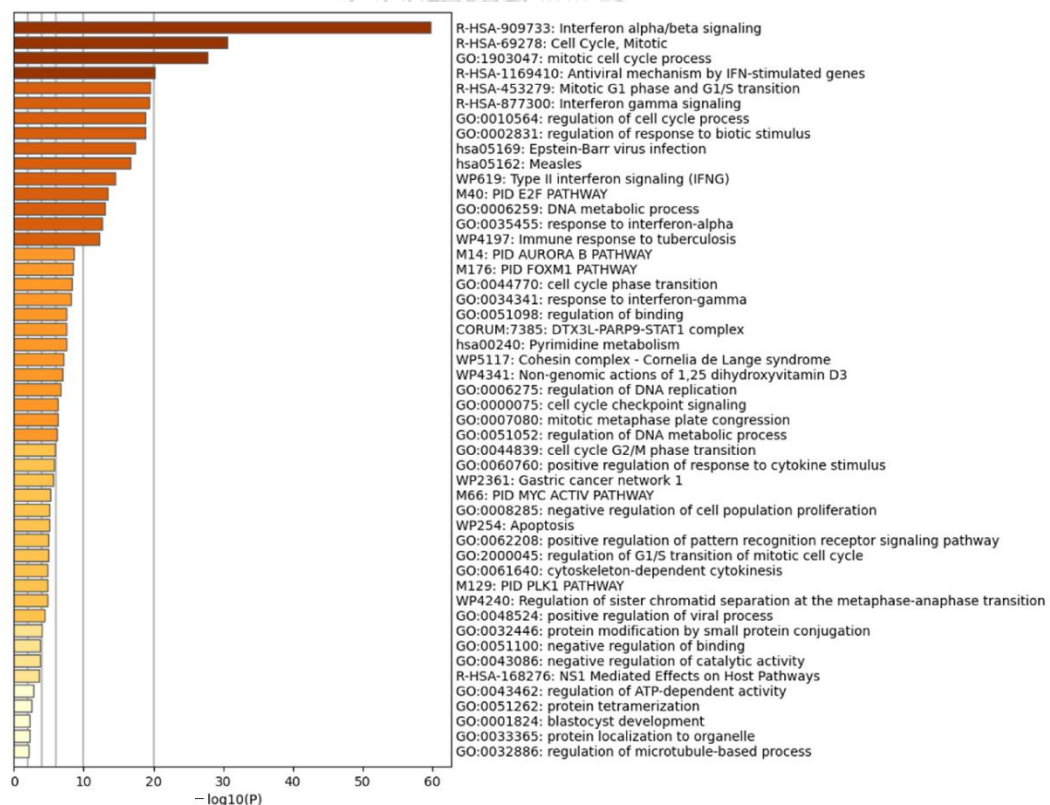
Figure 5. The bar graph represents the enrichment terms analyzed from the IPIN at a significant level (*p*-value < 0.01). Each enrichment term is colored based on the significance level.

In addition, MCODE algorithm clustered the functional enrichment terms into four modules, MCODE1, MCODE2, MCODE3, and MCODE4, as shown in Figure 6. For instance, MCODE1 (Figure 6a) represented the biological term related to innate immune and proinflammatory cytokine signaling pathways: IFN-α and IFN-β. MCODE2 (Figure 6b) was associated with mitotic cell division, cell damage detection, and chromosome segregation. MCODE3 (Figure 6c) was involved in cell cycle checkpoint and cell cycle signaling pathways, and MCODE4 (Figure 6d) was enriched with protein processing and antigen presentation. Table 2 shows the enrichment analysis results from the MCODE algorithm.

(a)   (b)   (c)   (d)
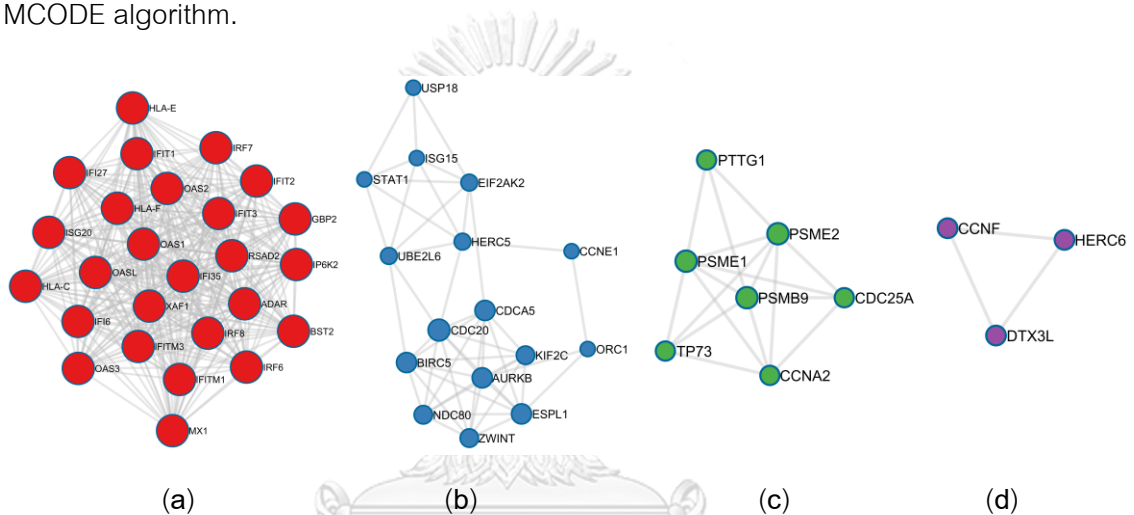
Figure 6. Module detection from the IPIN using MCODE algorithm in Metascape. (**a**) MCODE1 (marked as red nodes) had 26 nodes and 320 edges. (**b**) MCODE2 (marked as blue nodes) had 16 nodes and 49 edges. (**c**) MCODE3 (marked as green nodes) had 7 nodes and 17 edges. (**d**) MCODE4 (marked as purple nodes) had 3 nodes and 3 edges.

Table 2. Clustering of functional enrichment analysis in the IPIN by Molecular Complex Detection (MCODE) algorithm.

Functional Component	Term ID	Biological Term	Log10 (*p*-value)
MCODE1	R-HSA-909733	Interferon alpha/beta signaling	−70.8
	R-HSA-913531	Interferon signaling	−57.5
	R-HSA-1280215	Cytokine signaling in Immune system	−42.5
MCODE2	R-HSA-2467813	Separation of sister chromatids	−13.6
	R-HSA-69278	Cell cycle, mitotic	−13.5
	GO:0098813	Nuclear chromosome segregation	−13.0
MCODE3	R-HSA-69615	G1/S DNA damage checkpoints	−12.0
	R-HSA-176409	APC/C:CDC20 mediated degradation of mitotic proteins	−11.7
	R-HSA-176814	Activation of APC/C and APC/C:CDC20 mediated degradation of mitotic proteins	−11.7
MCODE4	R-HSA-983168	Antigen processing: ubiquitination and proteasome degradation	−6.0
	R-HSA-983169	Class I MHC mediated antigen processing and presentation	−5.7
	GO:0016567	Protein ubiquitination	−5.0

Network clustering of the IPIN by MCL algorithm provided four modules: MCL1, MCL2, MCL3, and MCL4. Figure 6 demonstrates the MCL modules of the IPIN. Further detail about the clusters is described in Table S7 in Supplementary Materials. The result from functional enrichment analysis of the four modules revealed that the MCL1 (Figure 7a) was related to cell cycle regulation functions while MCL2 (Figure 7b) was mainly enriched in innate immune responses. Moreover, MCL3 (Figure 7c) had an association with nucleic acid metabolism. MCL4 (Figure 7d) mixed cell division and immune

response terms. The details of enrichment results in each MCL module are listed in Table S8 in Supplementary Materials. The enrichments result was aggregable with the result from the MCODE analysis.

(a)   (b)   (c)   (d)
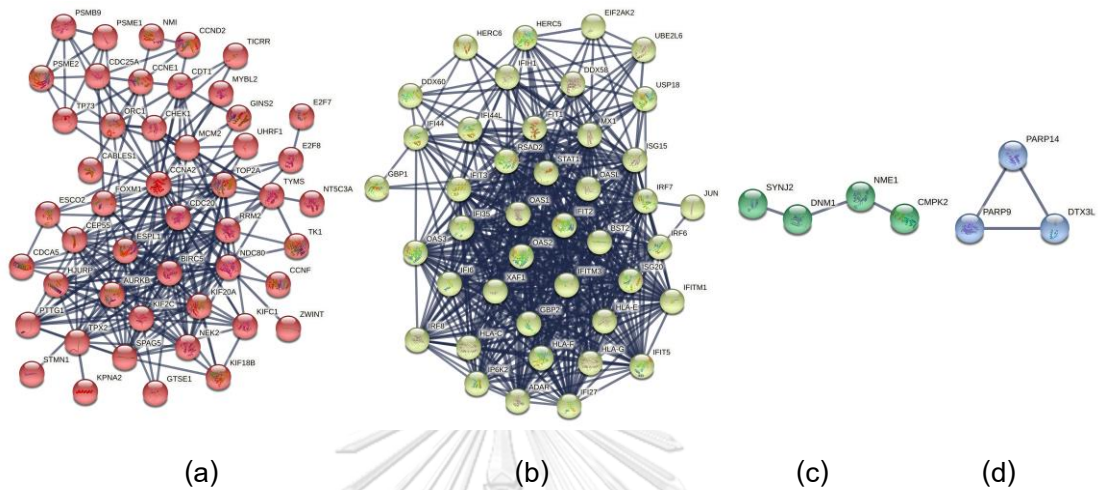
Figure 7. Module detection from the IPIN using MCL algorithm performed in STRING v11.0. (**a**) MCL1 (marked as red) had 48 nodes and 234 edges. (**b**) MCL2 (marked as yellow) had 42 nodes and 528 edges. (**c**) MCL3 (marked as green) had 4 nodes and 3 edges. (**d**) MCL4 (marked as blue) had 3 nodes and 3 edges.

Functional enrichment and network clustering analysis revealed two large biological pathways: antiviral and innate immune response and cell division and cell cycle regulation (as shown in Figures 5–7 and Table 2). The innate immune response found in the study mostly correlated with IFN signaling pathways. IFN can be separated into two groups: type I and II IFN (IFN-I and IFN-II). IFN-I cytokines, such as IFN-α and IFN-β, play an essential role in innate immunity to many viral infections [116]. They are released by the interaction between PAMPs or DAMPs and PRRs. The IFN-I activation controls innate immunity and increases viral clearance by stimulating various antiviral proteins, such as MX1, OASs, and ISGs [117-121]. IFN-I is also involved in NK cells, B lymphocyte, CD4^{+}, and CD8^{+} T lymphocyte stimulation [121]. Nonetheless, IFN-I signaling is suppressed and delayed in coronavirus infections, such as SARS-CoV, MERS-CoV, and SARS-CoV-2, causing viral clearance dysfunction. Persistent viral replication causes the release of uncontrolled proinflammatory cytokines, resulting in the cytokine storm [116,122,123]. This phenomenon is also called paradoxical

hyperinflammation. Although IFN-II, consisting of IFN-γ, has an immune function overlapping with IFN-I to stimulate the antiviral and innate immune response, it causes enhancement predominantly in antigen-presenting cells (APCs) [124]. Several studies have revealed that IFN-II exhaustion is usually found in severe COVID-19 patients, suggesting a vital role of IFN-II in the immunopathology of the disease [125-127]. As a result, IFN signaling enrichment found in the peripheral white blood cells can be from the compensating mechanism of immune cells for IFN suppression and delay in severe cases. However, IFN signaling predominance in this study can indicate the ongoing activation. Persistent IFN stimulation induces apoptosis of $CD4^+$ T lymphocytes and causes lymphopenia. It also increases proinflammatory cytokine production [128-130]. Other evidence supports the notion that increased IFN-I in influenza viral infection can release excessive proinflammatory cytokines, resulting in respiratory epithelial apoptosis and severe pneumonia [131]. Because the IFN function in severe COVID-19 is complicated, the study of IFN roles in the disease should be more investigated.

Leukocyte proliferation is the immune defense mechanism responding to infections. However, cell division and cell cycle regulation can also participate in the pathophysiology of COVID-19-associated cytokine storms. In the RNA-seq study used to construct the IPIN, the patient data revealed that severe COVID-19 cases had elevated neutrophils more than lymphocytes [87]. An excessive number of neutrophils can cause increased production of proinflammatory cytokines. Hence, finding the key immune-related proteins in the cell cycle regulation is necessary to modulate the immune response in severe cases. Nucleic acid metabolism was also found in the enrichment analysis. Increased cell division also stimulates nucleic acid metabolism to produce DNA materials for chromosome segregation. Although cell division is found in leukocytes during the infection, several studies revealed that SARS-CoV could induce cell cycle arrest in host cell lines by using viral proteins interacting with cyclin and the cyclin-dependent kinase (CDK) complex [132-134]. Nevertheless, there is still no research about the relation between SARS-CoV-2 and leukocyte cell cycle regulation. Therefore, studying the cell cycle regulation of host cells in COVID-19 requires further investigation.

Another term found in the enrichment analysis was apoptosis or programmed cell death. Apoptosis in COVID-19 causes deleterious effects, leading to severe complications. For instance, lymphocyte apoptosis results in lymphopenia and delays adaptive immune response, increasing the cytokine storm risk. Many studies have found that B and T lymphocyte apoptosis is associated with severe COVID-19 [135-137]. Apoptosis is also found in respiratory epithelial and endothelial cells, causing the blood-air barrier defect. This event leads to ARDS progression. Therefore, apoptosis regulation in severe COVID-19 is essential to improve adaptive immunity and reduce fatality rates.

Furthermore, there was protein processing found in the IPIN enrichment analysis. Protein processing is post-translational modification occurring in the endoplasmic reticulum (ER) and Golgi apparatus. The immune cells during the infection have more active functions, such as cell proliferation and cytokine production. Hence, protein processing is highly expressed to play a role in these activities.

2.1.3.3 KEY IMMUNE-RELATED PROTEINS IN THE IPIN
2.1.3.3.1 IMPORTANT IMMUNE-RELATED PROTEINS WITH NODE CENTRALITIES

Network centrality aspects such as degree, betweenness, closeness, and eigenvector centralities of each node in the IPIN are illustrated in Table S6 in Supplementary Materials. Nodes with degree, betweenness, closeness, or eigenvector centralities above the 90th percentile are shown in Table S9–S12 in Supplementary Materials, respectively. From the tables, 15 nodes have large degree values, and 10 nodes have high betweenness values. In addition, 11 and 10 nodes have high closeness and eigenvector scores, respectively. These nodes are proteins playing a role in antiviral, innate immune, apoptosis, and cell cycle regulation signaling pathways. The function of each protein including high centrality predominance is displayed in Table 3.

Table 3. Summary of biological function of 23 nodes with high centrality predominance.

Symbol	Description	High Centrality	Biological Function
CCNA2	Cyclin A2	DC, BC, CC	Cell cycle regulation
CCNE1	Cyclin E1	CC	Cell cycle regulation
CDC20	Cell Division Cycle 20	BC	Cell cycle regulation
CDC25A	Cell Division Cycle 25A	BC, CC	Cell cycle regulation
CMPK2	Cytidine/Uridine Monophosphate Kinase 2	BC, CC	Salvage nucleotide synthesis
DDX58	DExD/H-Box Helicase 58	BC, CC	Viral dsRNA recognition
FOXM1	Forkhead Box M1	BC	Transcription activator in cell proliferation
IFI6	IFN-α Inducible Protein 6	DC, EC	Apoptosis regulation and antiviral activity
IFI35	IFN Induced Protein 35	DC, BC	Regulation of innate immune signaling pathway
IFIH1	IFN Induced With Helicase C Domain 1	BC, CC	Intracellular sensor of viral RNA
IFIT1	IFN Induced Protein With Tetratricopeptide Repeats 1	DC, CC, EC	Viral replication inhibition
IFIT2	IFN Induced Protein With Tetratricopeptide Repeats 2	DC, EC	Viral replication inhibition
IFIT3	IFN Induced Protein With Tetratricopeptide Repeats 3	DC, EC	Viral replication inhibition
IRF7	IFN Regulatory Factor 7	DC, EC	Antiviral activity
ISG15	IFN-stimulated gene 15	DC, CC, EC	Antiviral activity

Table 3. *Cont.*

Symbol	Description	High Centrality	Biological Function
MX1	MX Dynamin Like GTPase 1	DC, CC, EC	Viral replication inhibition
OAS1	2′-5′-Oligoadenylate Synthetase 1	DC	Viral replication inhibition
OAS2	2′-5′-Oligoadenylate Synthetase 2	DC	Viral replication inhibition
OASL	2′-5′-Oligoadenylate Synthetase Like	DC	Antiviral activity
RRM2	Ribonucleotide Reductase Regulatory Subunit M2	BC, CC	Cell cycle regulation
RSAD2	Radical S-Adenosyl Methionine Domain Containing 2	DC, BC, CC, EC	Antiviral activity
STAT1	Signal Transducer And Activator Of Transcription 1	DC, EC	Stimulation of proinflammatory cytokines
XAF1	XIAP Associated Factor 1	DC, EC	Antiapoptotic inhibition

IFN, interferon; XIAP, X-linked inhibitor of apoptosis protein; dsRNA, double-strand RNA; DC, degree centrality; BC, betweenness centrality; CC, closeness centrality; EC, eigenvector centrality.

From the tables, we found that nodes with high betweenness values were primarily involved in cell cycle regulation (6 of 10 nodes), while nodes with high degree and eigenvector values were mainly related to antiviral and innate immune signaling pathways (13 of 15 nodes and 9 of 10 nodes with high degree and eigenvector values, respectively). In addition, we discovered that the high closeness nodes had a similar proportion between immune signaling and cell proliferation, explaining that 6 of 11 nodes were involved in the innate immune response. At the same time, the rest of the nodes had a function associated with cell cycle regulation.

The upset plot In Figure 8 shows that all nodes with high eigenvector values are in the high degree nodes. That means the high-eigenvector nodes form a subset of the high-degree nodes. Furthermore, the high-betweenness nodes share the node members mainly with the high-closeness nodes (the intersection size is calculated from 5 + 1 = 6). There is one node shared in all centralities (RSAD2). The degree, betweenness, and closeness centrality provide unique nodes that do not intersect with other centralities. The numbers of unique nodes in degree, betweenness, and closeness centrality are 3, 2, and 1, respectively.
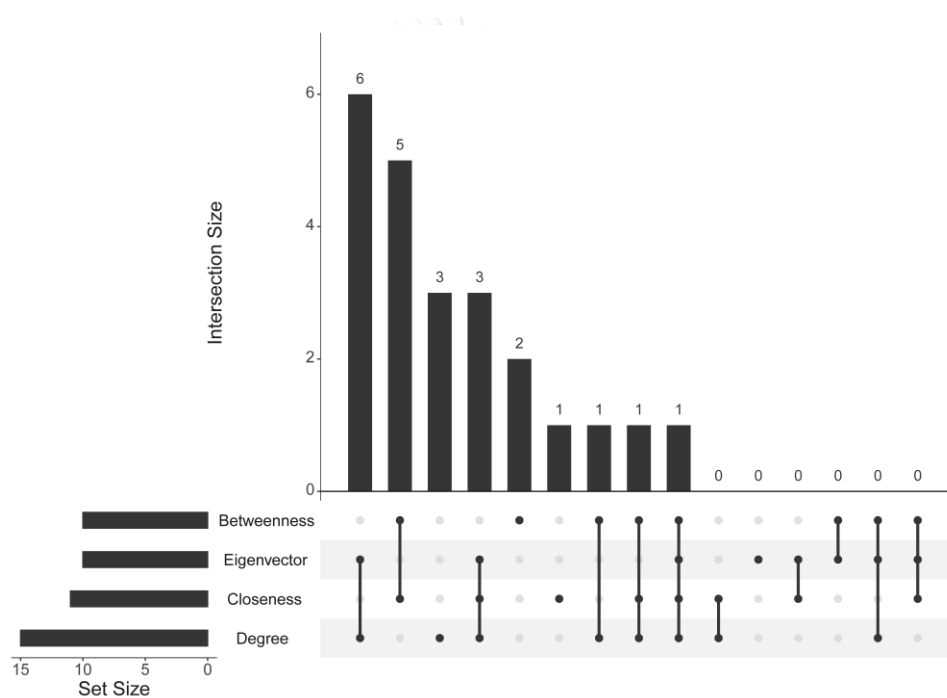
Figure 8. Upset plot of nodes with high values in the four centralities: degree, betweenness, closeness, and eigenvector centrality.

2.1.3.3.2 IMPORTANT IMMUNE-RELATED PROTEINS WITH THE RANKING SCORES

As shown in Table 4, there are 10 nodes with a ranking score above the 90th percentile. Among them, eight nodes have functions relevant to innate immune response and antiviral activity: IFIT1, IFIT2, IFIT3, IRF7, ISG15, MX1, RSAD2, and STAT1. Interestingly, these immune nodes participate in IFN signaling pathways. The signaling pathway is usually activated when viral infections invade the hosts [138]. Stimulated IFNs increase the production of antiviral proteins, for example, ISG15 and MX1

[139,140]. In addition, the rest of the nodes, such as CDC25A and CCNA2, are involved in cell proliferation and cell cycle regulation. During infection, the immune system increases leukocyte proliferation to eradicate pathogens. As a result, cell division regulators can be found in the analysis. Both CDC25A and CCNA2 regulate cell cycle transition in G1/S phase [141]. Cell cycle control during G1/S phase is a critical point for cell division. Hence, drug repurposing targeting these regulators could improve the excessive leukocyte proliferation in the cytokine storm, leading to decreased morbidity and mortality rate in severe COVID-19.

Table 4. List of nodes with high ranking scores.

Ensembl ID	Symbol	Ranking Score
ENSP00000371471	RSAD2	4.166667×10^{-2}
ENSP00000360869	IFIT1	4.629630×10^{-3}
ENSP00000368699	ISG15	6.666667×10^{-4}
ENSP00000381601	MX1	4.370629×10^{-4}
ENSP00000303706	CDC25A	1.940994×10^{-4}
ENSP00000360883	IFIT3	1.449275×10^{-4}
ENSP00000354394	STAT1	1.017501×10^{-4}
ENSP00000274026	CCNA2	6.410256×10^{-5}
ENSP00000360891	IFIT2	4.409171×10^{-5}
ENSP00000380697	IRF7	4.084967×10^{-5}

To compare with the conventional methods usually used for identifying key proteins in IPINs such as degree and betweenness centrality, Figure 9 displays a Venn diagram of nodes found in the ranking score, degree, and betweenness centrality. The figure shows that the score covers mostly proteins in degree centrality (9 of 15 nodes in the degree set). Conversely, the score captured a few nodes in betweenness centrality (3 of 10 nodes in the betweenness set). Noticeably, the nodes merging between degree and betweenness set cover almost the high-value nodes analyzed from the four centralities (22 of 23 nodes). Thus, a combination of degree and betweenness centrality can provide the best result for identifying key proteins in IPINs. Although the ranking

score could not capture other key proteins different from these two centralities, RSAD2 and IFIT1 (the top two genes in Table 4) were detected as the most important immune-related proteins.
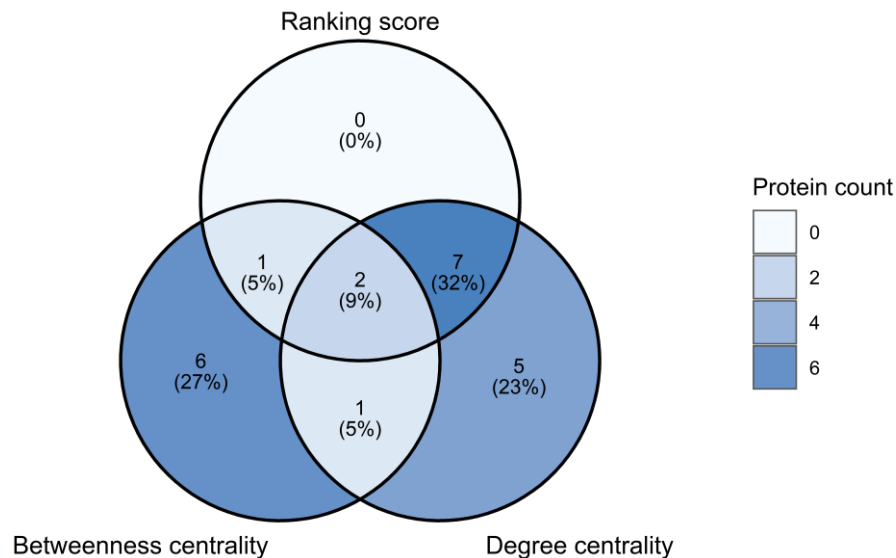
Figure 9. Venn diagram of the key proteins in the ranking score, degree, and betweenness centrality.

RSAD2 or viperin is a broad-spectrum antiviral protein in several viruses such as measles, coxsackievirus A16, and enterovirus A71 [142-144]. Moreover, an animal study revealed that RSAD2 was necessary for dendritic cell development [145]. The DEGs analysis of the overlapping genes in postmortem lung tissue from COVID-19 cases and acute lung injury (ALI) murine model found that RSAD2 had a high degree centrality in a COVID-19-associated regulatory network [146]. Moreover, a lower respiratory tract transcriptomic study revealed that *RSAD2* expression correlated with the viral load in mild and severe COVID-19 [147]. IFIT1 is an antiviral protein interacting with other IFIT family proteins to form an IFN-dependent multiprotein complex. The complex plays an important role to increase innate immunity against RNA viruses via binding between IFIT1 and 5'-triphosphate RNA (PPP-RNA) [148]. Nevertheless, an experimental finding revealed that several SARS-CoV-2 proteins, such as nsp7, nsp15, M, 3CLpro, helicase, and N proteins, suppressed *IFT1* expression in HEK293T cells [149].

Although the ranking score was computed to find the key proteins by considering the four centralities, it captured a few proteins when compared with the

combination between degree and betweenness centrality. Moreover, the score covered the proteins mostly found in degree centrality. The reason to describe the result is that the proteins with high eigenvector centrality were the subset in degree centrality. Meanwhile, some proteins with high closeness centrality were found in both eigenvector and degree centrality. In addition, proteins found in betweenness centrality rarely overlapped with degree centrality. Therefore, the score calculation is weighted to degree centrality more than betweenness centrality. Noticeably, the combination of degree and betweenness centrality covered almost high-value centrality proteins rather than the ranking score, although it lost one protein with a high closeness value (CCNE1).

As described earlier, the 23 key proteins identified using centrality measurement were involved in innate immune response, cell cycle regulation, and apoptosis. IFI35 is an IFN signaling regulator response to viral infections. Many studies have found that IFI35 plays an essential role in cytokine storms and severity in COVID-19 and influenza [150-153]. IFIH1 is an intracellular viral sensing protein that stimulates the IFN signaling pathway when viral particles are detected in the cell [154]. IFIH1 was reported to participate in SARS-CoV-2 sensing and was associated with proinflammatory cytokine overproduction in COVID-19 [155-157]. DDX58 also plays a role as a cytoplasmic viral sensor. High *DDX58* expression in COVID-19 was associated with cytokine responses [158]. IFI6, IFIT1-3, IRF7, ISG15, MX1, OAS1, OAS2, OASL, and RSAD2 have antiviral activity functions. Many studies in IFI6 have revealed that IFI6 plays an essential role against hepatitis B virus (HBV) and flavivirus replication [159,160]. Several systems biological and transcriptomic studies have also shown that IFI6 is a hub gene in the gene co-expression networks and transcriptomic profiles in COVID-19 [52,161-163]. *IFIT1-3*, *OAS1-3*, and *OASL* were upregulated in SARS-CoV-2 and other coronavirus infections [164-167]. Furthermore, the *IRF7* mutation causing loss of function was reported to be associated with severe pneumonia progression in COVID-19 [168,169]. The infected macrophage cell line study showed that extracellular ISG15 stimulated proinflammatory cytokine production, leading to hyperinflammation [170]. The result of a COVID-19 case-control study revealed that *MX1* expression was increased depending on elevated viral load, and the expression was decreased in elderly patients [171]. Older patients have a high risk for COVID-19-associated cytokine storms, suggesting

that low *MX1* expression could play a vital role in the cytokine storm. STAT1 is a signal transduction protein related to various signaling pathways such as IFN, IL-6, epidermal growth factor (EGF), and platelet-derived growth factor (PDGF) pathways [172-174]. Several studies have indicated that phosphorylated STAT1 increases in severe COVID-19 patients, causing STAT1 signaling dysfunction and failed IFN activation [175-177]. XAF1 is a tumor suppressor protein playing as a positive feedback regulator in the p53-induced apoptotic signaling pathway [178]. Numerous studies have reported that XAF1 dysfunction plays a vital role in tumor progression [179-182]. A single-cell transcriptomic study in peripheral blood mononuclear cells showed that COVID-19 caused XAF1-induced T lymphocyte apoptosis, leading to adaptive immune impairment [183]. In addition, IPIN analysis from COVID-19 patient lung tissue revealed that IFIH1, DDX58, ISG15, OASL, and XAF1 were hub genes in the network [184].

CCNA2 and CCNE1 are CDK kinase regulators during G1/S and G2/M phases in the cell cycle. Numerous studies have indicated CCNA2 and CCNE1 play a central role in various types of malignancy such as hepatocellular carcinoma, breast, and colon cancer [185-188]. CDC25A is a protein required in the cell cycle by activating CDKs [189]. *CDC25A* overexpression was found in head and neck, breast, ovarian, and non-small cell lung cancer [190-193]. An immune study revealed that CDC25A had activities decreasing IFN-β transcription and DDX58-mediated antiviral signaling pathway [194]. CDC20 has a function involved in chromosome segregation and is the target for spindle assembly checkpoint (SAC) [195,196]. High-expressed *CDC20* was related to the worst prognosis in lung squamous cell carcinoma [197]. An IPIN analysis in COVID-19-induced thrombocytopenia also reported that *CDC20* was highly expressed in COVID-19 with thrombocytopenia [198]. CMPK2 is an enzyme associated with the nucleotide salvage pathway. Many studies have shown that CMPK2 participates in IFN-I activation and antiviral immune response [199-201]. In COVID-19 studies, *CMPK2* was highly upregulated in severe cases related to ARDS [202,203]. Moreover, FOXM1-dependent tissue regeneration is impaired in severe COVID-19 cases, causing sustained lung injury and a high fatality rate [204]. RRM2, a cell cycle regulator, had an increased expression in lung adenocarcinoma with a poor prognosis [205]. A gene co-expression network and functional enrichment study also showed that RRM2 was a component in a module

involved in p53 signaling pathway, a cell cycle and apoptosis pathway, in COVID-19 [206].

2.1.3.4 POTENTIAL DRUGS TO CURE SEVERE COVID-19 PATIENTS

We used the key immune-related proteins from the ranking score, degree, and betweenness centrality to find the drug–gene or drug–protein interactions from four well-known public databases: DrugBank database [110], TTD [111], CTD [112], and GeneCards [113]. In addition, the protein not found in both degree and betweenness centrality (CCNE1) was used to discover the interaction. The result from database searching revealed 115 FDA-approved drugs interacting with the key genes or proteins. Table S13 in Supplementary Materials shows the drug–gene and drug–protein interactions in detail among the 23 key immune-related proteins.

STITCH v5.0 [114], a drug–protein interaction database, was conducted to confirm the result from the databases by the confidence score cut-off value of 0.9. The STITCH result is demonstrated in Figure 10. The key immune-related proteins are classified into two groups. The former is an antiviral, innate immune response, and apoptosis signaling pathway group, and the latter is a cell division and cell cycle group. Figure 10a displays the drug–protein interaction network in the innate immune response, and Figure 10b illustrates the drug–protein interaction network involved in cell cycle regulation. There are seven candidate drugs interacting with these seven key proteins. Three drugs are associated with the key proteins related to innate immune response and apoptosis. In contrast, the rest interacts with the proteins involved in cell cycle regulation. In the innate immune and apoptosis network, polyinosinic:polycytidylic acid (poly(I:C)) interacts with IFIH1 and DDX58, while mitomycin C interacts with MX1. Decitabine also binds to XAF1 in the network. There are four drug–protein interactions in the cell cycle regulation network. RRM2 is interacted with gemcitabine and hydroxyurea, respectively. Tamoxifen binds to FOXM1, and curcumin has an interaction with CCNE1.
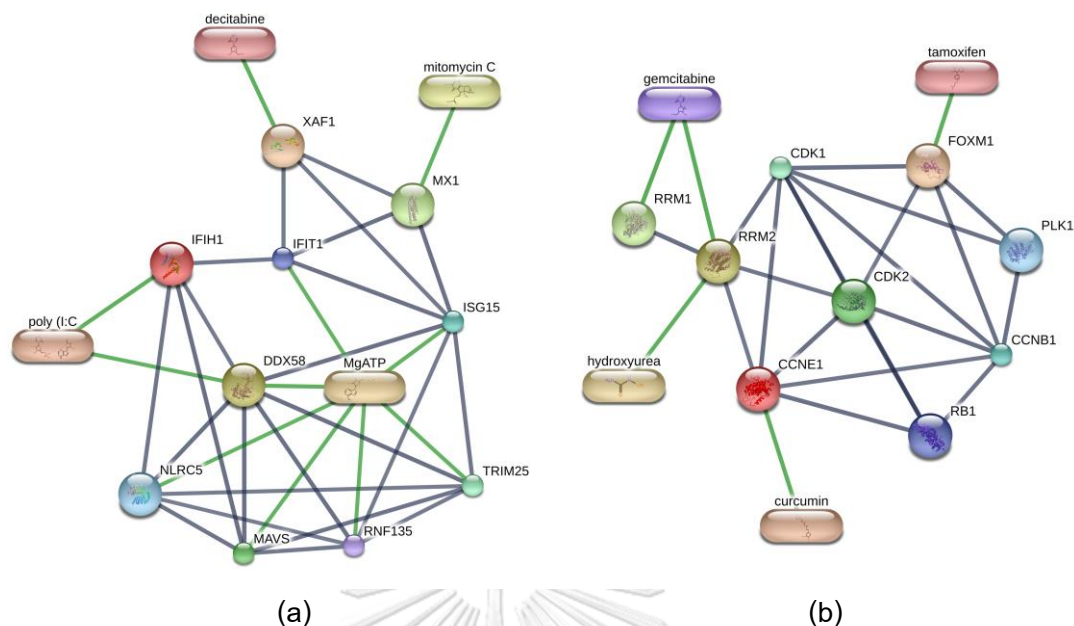
Figure 10. Drug–protein interaction network of candidate drugs targeting the key proteins resulted from STITCH v5.0. (**a**) Drug–proteins interaction network involved in innate immune response and apoptosis. (**b**) Drug–proteins interaction network involved in cell cycle regulation. Grey and green edges represent protein–protein and drug–protein interactions, respectively.

From the STITCH v5.0 result, the seven candidate drugs interacted with the seven key proteins. For instance, Poly(I:C) interacted with IFIH1 and DDX58. Poly(I:C) is an immune stimulant used to activate innate immunity such as IFN by the TL3 agonist effect. It also induces cancer cell apoptosis in various types of malignancy: cervical, prostate, and colon cancer [207-211]. Poly(I:C) also increases cytotoxic activity in CD4$^+$ T lymphocytes in viral infections, promoting adaptive immune response [212]. A study in influenza A virus (IAV) and a SARS-CoV-infected mice model revealed that poly(I:C) had a protective effect in fatal respiratory infections [213]. Interestingly, intranasal poly(I:C) in mice with SARS-CoV-2 infection showed a decreased viral load, suggesting that poly(I:C) can be an effective drug for treating the disease [214]. However, some studies reported that poly(I:C) increased proinflammatory production [215-217]. Therefore, further studies about poly(I:C) in COVID-19 treatment should consider the drug dosage and administration route to prevent the cytokine storm due to the medication. Mitomycin C, a chemotherapeutic agent, interacted with MX1. It is used to treat many cancer types

[218-221]. A systems biological study revealed that mitomycin C interacted with MX1, a key protein in an IPIN, suggesting further studies in the role of the drug in antiviral stimulation [50]. In addition, there was a drug–protein interaction between decitabine and XAF1. Decitabine is a pyrimidine nucleoside antimetabolite used to treat myelodysplastic syndrome (MDS) and acute myeloid leukemia (AML) [222,223]. A study in the mice model showed that decitabine improved FOXM1-dependent endothelial regeneration and vascular repair [204]. As mentioned above, lung tissue degeneration can cause worsening lung injury. Decitabine then could play a role in decreasing lung injury in severe COVID-19. Interestingly, there is a clinical trial that has been studying decitabine treatment in critical ill COVID-19 patients. The estimated research completion date August 2022. Gemcitabine and hydroxyurea also interacted with RRM2. Gemcitabine, a pyrimidine nucleoside analog and chemotherapeutic agent, is used to treat solid tumors such as bladder, pancreatic, breast, and non-small cell lung cancer [224]. Several studies in cell lines have found that decitabine decreases SARS-CoV-2 replication [225-227]. In addition, in a cohort study, gemcitabine reduced SARS-CoV-2 infection in cancer patients [228]. Hydroxyurea, an antimetabolite treating sickle cell anemia, has anti-inflammatory and immunomodulatory effects and was expected to apply well in COVID-19 [229].

A clinical study also revealed that the mortality rate was low in COVID-19 patients receiving hydroxyurea, suggesting a vital role of hydroxyurea in COVID-19 treatment [230]. Tamoxifen, a selective estrogen receptor modulator, had an interaction with CCNE1. The drug is used to treat estrogen receptor-positive breast cancer [231]. Tamoxifen downregulates *TMPRSS2*, preventing SARS-CoV-2 entry into host cells [232]. A preclinical study showed that tamoxifen reduced SARS-CoV-2 in vitro and in vivo [233]. Moreover, a review article in clinical studies found that tamoxifen decreased COVID-19 susceptibility rates in breast cancer patients [234]. Tamoxifen also inhibited viral replication and virus entry in many virus types such as EBOLA, MERS, and SARS-CoV-2 [234]. The drug repurposing result also revealed that curcumin interacted with CCNE1. It is worth noting that curcumin is a promiscuous molecule acting on many receptors. Hence, the effect of curcumin in COVID-19 can be from other mechanisms.

Our study only proposed one of the possible mechanisms of curcumin in severe COVID-19 treatment. Curcumin is a natural product found in turmeric (*Curcuma longa*). Many studies have indicated that curcumin has anti-inflammatory and antioxidant effects [235-237]. Moreover, it provides effects in apoptosis promotion, cell proliferation inhibition, anti-cell adhesion and invasion, decreased angiogenesis, and anti-microbial activity [238]. Therefore, its clinical application is related to numerous diseases, such as rheumatoid arthritis, inflammatory bowel diseases, osteoarthritis, and various types of cancer. In COVID-19, several review articles have revealed that curcumin inhibits viral entry and replication [239-241]. It also promotes IFN and antiviral signaling pathway and decreases proinflammatory cytokine production. Curcumin has protective effects on ARDS by reducing NF-κB, inflammasome, and IL-8 pathway. Furthermore, a randomized control trial study showed that mild, moderate, and severe COVID-19 patients taking oral curcumin with piperine had better clinical outcomes and lower hospitalization duration than the controls [242]. A systematic review reported that curcumin reduced the proinflammatory cytokines, such as IL1β and IL6. It also increased the anti-inflammatory cytokines, for example, IL-10, IL-35 and transforming growth factor α (TGF-α) [243]. Therefore, further study should focus on the effective dose and administration routes of curcumin.

2.1.4. DISCUSSION

This study constructed the immune-related protein interactions network, IPIN, for severe COVID-19 based on the leukocyte transcriptomic profile of critically ill patients using network propagation on the human interactome network. Functional enrichment analysis and network clustering were operated to discover the underlying molecular mechanisms of immune-related severe COVID-19. Topological analysis, centrality, and ranking score measurements were calculated to identify the key immune-related proteins. Finally, the drug–protein interactions were searched to find the candidate drugs to treat the severe COVID-19 patients.

Diffusion-based IPIN construction and permutation testing provided the highly connected immune-related proteins in IPIN. IPIN was a network with a small-world effect in relation to other biological networks. The small-world effect was proved by the low

average shortest path length and high average clustering coefficient. The scale-free property cannot be explained in the network due to a lack of a relationship between degree and its probability. However, the IPIN was less likely to be the random network because it provided the significant PPI enrichment p-value from the STRING database. We performed the four network centralities (degree, betweenness, closeness, and eigenvector) and ranking score to find the key immune-related proteins. The results showed that the combination of degree and betweenness centrality covered a wide range of the key proteins. However, the ranking score can detect the main key proteins: RSAD2 and IFTI1.

We identified 23 key immune-related proteins, such as CCNA2, CCNE1, CDC20, CDC25A, CMPK2, DDX58, FOXM1, IFI6, IFI35, IFIH1, IFIT1, IFIT2, IFIT3, IRF7, ISG15, MX1, OAS1, OAS2, OASL, RRM2, RSAD2, STAT1, and XAF1, using the four centralities and ranking score measurement. These proteins all play an important role in severe COVID-19, validated by several computational, experimental, and clinical studies. The functional enrichment analysis from the whole network and the modules obtained from both MCODE and MCL methods produced similar results. The enrichment terms were divided into four main categories: cell cycle regulation, antiviral and innate immune response, apoptosis, and nucleotide metabolism. These terms were in accordance with leukocytes during viral infections. Furthermore, the main terms were accepted with the functional classification in the key proteins. For instance, the key proteins involved in cell cycle regulation consisted of CCNA2, CCNE1, CDC20, CDC25A, and RRM2, while the others associated with antiviral and innate immune response were DDX58, FOXM1, IFI6, IFI35, IFIH1, IFIT1, IFIT2, IFIT3, IRF7, ISG15, MX1, OAS1, OAS2, OASL, RSAD2, and STAT1. In addition, the remaining key proteins such as CMPK2 and XAF1 play a crucial role in nucleotide metabolism and apoptosis, respectively.

Drug repurposing based on drug–gene and drug–protein interaction database searching provided the seven potential candidate drugs, poly(I:C), mitomycin C, decitabine, gemcitabine, hydroxyurea, tamoxifen, and curcumin. There were three drugs interacting with the key proteins related to antiviral and innate immune response: poly(I:C), mitomycin C, and decitabine. Other drugs interacted with the key proteins involved in cell cycle regulation and apoptosis. Among the candidate drugs, we

recommend that the drugs interacting with proteins involved in IFN and antiviral signaling should be used carefully in clinical application because they promote IFN stimulation. IFN overactivation can result in excessive proinflammatory cytokine production in some studies that we mentioned [41-44]. Moreover, chemotherapeutic agents cause many adverse side effects and should be performed as the second choice. Therefore, we suggest using curcumin and tamoxifen as the first choices for clinical application. They have fewer side effects than other chemotherapeutic agents because curcumin is a natural product and tamoxifen is a targeted drug. In addition, both curcumin and tamoxifen have several clinical studies to support their effectiveness in COVID-19 treatment.

2.1.5. LIMITATIONS AND FUTURE STUDY SUGGESTIONS

Although this study provides novel knowledge and candidate targeted drugs in COVID-19, it has some limitations to be explained. First, the network diffusion method is an algorithm consuming computational time and memory space which depends on the number of nodes, interactions, and permutation tests. We conducted high-performance computing (HPC) for running the LHD algorithm in the original and 1000 random sets to perform the permutation test. Second, many proinflammatory cytokine signaling pathways, such as IL-1β, IL-6, IL-12, IL-18, IL-33, and TNF-α, were rarely detected in this IPIN analysis. Our reason for explaining the issue is that the data came from comparing controls and COVID-19 cases in an intensive care unit. Typically, critically ill patients have stress and inflammatory responses, leading to increased proinflammatory cytokines. Therefore, there was no difference in the proinflammatory cytokine gene expression between cases and controls. Moreover, proinflammatory cytokines are usually released from respiratory epithelial and immune cells in the lung parenchymal tissue. Studies in peripheral white blood cells can lose this proinflammatory cytokine information. Our suggestion for future research is to perform lung transcriptomic profiles comparing severe COVID-19 cases and mild illness or healthy cases for IPIN construction and analysis. Furthermore, a single-cell approach should be conducted to identify an IPIN in each cell type. In COVID-19, there are differences between each cell type such as cell count, behavior, function, and pathogenesis. Therefore, identifying key proteins in these cells can help to treat the disease more precisely.

2.1.6. CONCLUSIONS

This study proposed LHD algorithms to perform network diffusion on the human interactome network to construct the immune-related IPIN in severe COVID-19 based on the transcriptomic data. Functional enrichment analysis found that the network contained the proteins involved in antiviral and innate immune response signaling pathways, cell cycle regulation, apoptosis, and protein processing. The degree and betweenness centrality combination covered almost the key proteins from the four centrality measurements. These key proteins play a significant role in cell proliferation, antiviral activity, and innate immunity responding to the SARS-CoV-2 infection. Moreover, the candidate drugs targeting the key proteins were found from database searching. Most of them have experimental data supporting their effectiveness in COVID-19 treatment. However, other key proteins and candidate drugs were not found in our method and need further investigation. Therefore, a combination of advanced experimental and computational tools should be conducted for further efficient treatment discovery relating to COVID-19.

Supplementary Materials: The following supporting information can be found and downloaded at: https://www.mdpi.com/article/10.3390/biom12050690/s1. Table S1: 224 differentially expressed genes (DEGs) (FDR < 0.05 and log2 FC > 1.5); Table S2: The DEGs in the protein-protein interaction network from STRING with Ensembl protein IDs; Table S3: The immune-related proteins from DEGs in the human interactome data as seed nodes for network diffusion; Table S4: Diffusion scores of the original set and statistic data of each node in the whole PPI network; Table S5: 154 protein nodes with significant diffusion scores by the permutation test; Table S6: Degree, betweenness, closeness, and eigenvector centrality values of each node in the IPIN; Table S7: Network clustering of the IPIN by MCL algorithm provided 4 modules: MCL1, MCL2, MCL3, and MCL4. Table S8: The detail of enrichment results in each MCL module; Table S9: List of nodes with high degree centrality; Table S10: List of nodes with high betweenness centrality; Table S11: List of nodes with high closeness centrality; Table

S12: List of nodes with high eigenvector centrality; Table S13: Drug-gene interactions of the identified key immune-related proteins; Table S14: Edge list of the IPIN.

References

1. World Health Organization (WHO) Coronavirus (COVID-19) Dashboard. 2022. Available online: https://covid19.who.int/ (accessed on 28 March 2022).

2. Lai, C.C.; Shih, T.P.; Ko, W.C.; Tang, H.J.; Hsueh, P.R. Severe acute respiratory syndrome coronavirus 2 (SARS-CoV-2) and coronavirus disease-2019 (COVID-19): The epidemic and the challenges. *Int J. Antimicrob. Agents* **2020**, *55*, 105924–105932. [CrossRef] [PubMed]

3. Gorbalenya, A.E.; Baker, S.C.; Baric, R.S.; de Groot, R.J.; Drosten, C.; Gulyaeva, A.A.; Haagmans, B.L.; Lauber, C.; Leontovich, A.M.; Neuman, B.W.; et al. The species severe acute respiratory syndrome-related coronavirus: Classifying 2019-nCoV and naming it SARS-CoV-2. *Nat. Microbiol.* **2020**, *5*, 536–544. [CrossRef]

4. Hui, D. S. ; Wong, P. C. ; Wang, C. SARS: Clinical features and diagnosis. *Respirology* **2003**, *8* (Suppl. 1), S20–S24. [CrossRef] [PubMed]

5. Vijayanand, P. ; Wilkins, E. ; Woodhead, M. Severe acute respiratory syndrome (SARS): A review. *Clin. Med. (Lond.)* **2004**, *4*, 152–160. [CrossRef] [PubMed]

6. Rasmussen, S. A. ; Watson, A. K. ; Swerdlow, D. L. Middle East Respiratory Syndrome (MERS). *Microbiol. Spectr.* **2016**, *4*, 73–104. [CrossRef]

7. Widagdo, W.; Sooksawasdi Na Ayudhya, S.; Hundie, G.B.; Haagmans, B.L. Host Determinants of MERS-CoV Transmission and Pathogenesis. *Viruses* **2019**, *11*, 280–293. [CrossRef] [PubMed]

8. Azhar, E.I.; Lanini, S.; Ippolito, G.; Zumla, A. The Middle East Respiratory Syndrome Coronavirus—A Continuing Risk to Global Health Security. *Adv. Exp. Med. Biol.* **2017**, *972*, 49–60. [CrossRef]

9. World Health Organization. Middle East Respiratory Syndrome. 2021. Available online: http://www.emro.who.int/healthtopics/mers-cov/mers-outbreaks.html (accessed on 28 March 2022).

10. Wu, F.; Zhao, S.; Yu, B.; Chen, Y.M.; Wang, W.; Song, Z.G.; Hu, Y.; Tao, Z.W.; Tian, J.H.; Pei, Y.Y.; et al. Author Correction: A new coronavirus associated with human respiratory disease in China. *Nature* **2020**, *580*, E7–E26. [CrossRef]

11. Zhou, P.; Yang, X.L.; Wang, X.G.; Hu, B.; Zhang, L.; Zhang, W.; Si, H.R.; Zhu, Y.; Li, B.; Huang, C.L.; et al. Addendum: A pneumonia outbreak associated with a new coronavirus of probable bat origin. *Nature* **2020**, *588*, E6–E25. [CrossRef]

12. Carvalho, T.; Krammer, F.; Iwasaki, A. The first 12 months of COVID-19: A timeline of immunological insights. *Nat. Rev. Immunol.* **2021**, *21*, 245–256. [CrossRef]

13. Tabari, P.; Amini, M.; Moghadami, M.; Moosavi, M. International Public Health Responses to COVID-19 Outbreak: A Rapid Review. *Iran. J. Med. Sci.* **2020**, *45*, 157–169. [CrossRef] [PubMed]

14. Padhan, K.; Parvez, M.K.; Al-Dosari, M.S. Comparative sequence analysis of SARS-CoV-2 suggests its high transmissibility and pathogenicity. *Future Virol.* **2021**, *16*, 245–254. [CrossRef]

15. Wang, H.; Li, X.; Li, T.; Zhang, S.; Wang, L.; Wu, X.; Liu, J. The genetic sequence, origin, and diagnosis of SARS-CoV-2. *Eur. J. Clin. Microbiol. Infect. Dis.* **2020**, *39*, 1629–1635. [CrossRef] [PubMed]

16. Rahimi, A.; Mirzazadeh, A.; Tavakolpour, S. Genetics and genomics of SARS-CoV-2: A review of the literature with the special focus on genetic diversity and SARS-CoV-2 genome detection. *Genomics* **2021**, *113* Pt 2, 1221–1232. [CrossRef]

17. Naqvi, A.A.T.; Fatima, K.; Mohammad, T.; Fatima, U.; Singh, I.K.; Singh, A.; Atif, S.M.; Hariprasad, G.; Hasan, G.M.; Hassan, M.I. Insights into SARS-CoV-2 genome, structure, evolution, pathogenesis and therapies: Structural genomics approach. *Biochim. Biophys. Acta Mol. Basis Dis.* **2020**, *1866*, 165878–165893. [CrossRef]

18. Zhang, Q.; Xiang, R.; Huo, S.; Zhou, Y.; Jiang, S.; Wang, Q.; Yu, F. Molecular mechanism of interaction between SARS-CoV-2 and host cells and interventional therapy. *Signal Transduct. Target.* **2021**, *6*, 233–251. [CrossRef]

19. Yadav, R.; Chaudhary, J.K.; Jain, N.; Chaudhary, P.K.; Khanra, S.; Dhamija, P.; Sharma, A.; Kumar, A.; Handu, S. Role of Structural and Non-Structural Proteins

and Therapeutic Targets of SARS-CoV-2 for COVID-19. *Cells* **2021**, *10*, 821–836. [CrossRef]

20. Redondo, N.; Zaldívar-López, S.; Garrido, J.J.; Montoya, M. SARS-CoV-2 Accessory Proteins in Viral Pathogenesis: Knowns and Unknowns. *Front. Immunol.* **2021**, *12*, 708264–708271. [CrossRef]

21. Senapati, S.; Banerjee, P.; Bhagavatula, S.; Kushwaha, P.P.; Kumar, S. Contributions of human ACE2 and TMPRSS2 in determining host-pathogen interaction of COVID-19. J. *Genet.* **2021**, *100*, 1–16. [CrossRef]

22. Kolarič, A.; Jukič, M.; Bren, U. Novel Small-Molecule Inhibitors of the SARS-CoV-2 Spike Protein Binding to Neuropilin 1. *Pharmaceuticals* **2022**, *15*, 165–178. [CrossRef]

23. Gadanec, L.K.; McSweeney, K.R.; Qaradakhi, T.; Ali, B.; Zulli, A.; Apostolopoulos, V. Can SARS-CoV-2 Virus Use Multiple Receptors to Enter Host Cells? *Int. J. Mol. Sci.* **2021**, *22*, 992–1027. [CrossRef] [PubMed]

24. V'kovski, P.; Kratzel, A.; Steiner, S.; Stalder, H.; Thiel, V. Coronavirus biology and replication: Implications for SARS-CoV-2. *Nat. Rev. Microbiol.* **2021**, *19*, 155–170. [CrossRef] [PubMed]

25. Schultze, J.L.; Aschenbrenner, A.C. COVID-19 and the human innate immune system. *Cell* **2021**, *184*, 1671–1692. [CrossRef] [PubMed]

26. Costela-Ruiz, V.J.; Illescas-Montes, R.; Puerta-Puerta, J.M.; Ruiz, C.; Melguizo-Rodríguez, L. SARS-CoV-2 infection: The role of cytokines in COVID-19 disease. *Cytokine Growth Factor Rev.* **2020**, *54*, 62–75. [CrossRef] [PubMed]

27. Rabaan, A.A.; Al-Ahmed, S.H.; Muhammad, J.; Khan, A.; Sule, A.A.; Tirupathi, R.; Mutair, A.A.; Alhumaid, S.; Al-Omari, A.; Dhawan, M.; et al. Role of Inflammatory Cytokines in COVID-19 Patients: A Review on Molecular Mechanisms, Immune Functions, Immunopathology and Immunomodulatory Drugs to Counter Cytokine Storm. *Vaccines* **2021**, *9*, 436–458. [CrossRef]

28. Attiq, A.; Yao, L.J.; Afzal, S.; Khan, M.A. The triumvirate of NF-_B, inflammation and cytokine storm in COVID-19. *Int. Immunopharmacol.* **2021**, *101* Pt B, 108255–108267. [CrossRef]

29. Fajgenbaum, D.C.; June, C.H. Cytokine Storm. *N. Engl. J. Med.* **2020**, *383*, 2255–2273. [CrossRef]

30. Wiersinga, W.J.; Rhodes, A.; Cheng, A.C.; Peacock, S.J.; Prescott, H.C. Pathophysiology, Transmission, Diagnosis, and Treatment of Coronavirus Disease 2019 (COVID-19): A Review. *JAMA* **2020**, *324*, 782–793. [CrossRef]

31. Pfortmueller, C.A.; Spinetti, T.; Urman, R.D.; Luedi, M.M.; Schefold, J.C. COVID-19-associated acute respiratory distress syndrome (CARDS): Current knowledge on pathophysiology and ICU treatment—A narrative review. *Best Pract. Res. Clin. Anaesthesiol.* **2021**, *35*, 351–368. [CrossRef]

32. Bhaskar, S.; Sinha, A.; Banach, M.; Mittoo, S.; Weissert, R.; Kass, J.S.; Rajagopal, S.; Pai, A.R.; Kutty, S. Cytokine Storm in COVID-19-Immunopathological Mechanisms, Clinical Considerations, and Therapeutic Approaches: The REPROGRAM Consortium Position Paper. *Front. Immunol.* **2020**, *11*, 1648–1663. [CrossRef]

33. Berlin, D.A.; Gulick, R.M.; Martinez, F.J. Severe COVID-19. *N. Engl. J. Med.* **2020**, *383*, 2451–2460. [CrossRef] [PubMed]

34. Rodriguez, J.J.; Munoz, O.C.; Porres-Aguilar, M.; Mukherjee, D. Thromboembolic Complications in Severe COVID-19: Current Antithrombotic Strategies and Future Perspectives. Cardiovasc. *Hematol. Disord. Drug Targets* **2021**, *21*, 23–29. [CrossRef] [PubMed]

35. Asakura, H.; Ogawa, H. COVID-19-associated coagulopathy and disseminated intravascular coagulation. *Int. J. Hematol.* **2021**, *113*, 45–57. [CrossRef] [PubMed]

36. Mokhtari, T.; Hassani, F.; Ghaffari, N.; Ebrahimi, B.; Yarahmadi, A.; Hassanzadeh, G. COVID-19 and multiorgan failure: A narrative review on potential mechanisms. *J. Mol. Histol.* **2020**, *51*, 613–628. [CrossRef]

37. Otsuka, R.; Seino, K.-i. Macrophage activation syndrome and COVID-19. *Inflamm. Regen.* **2020**, *40*, 19–24. [CrossRef]

38. Xing, K.; Tu, X.Y.; Liu, M.; Liang, Z.W.; Chen, J.N.; Li, J.J.; Jiang, L.G.; Xing, F.Q.; Jiang, Y. Efficacy and safety of COVID-19 vaccines: A systematic review. *Zhongguo Dang Dai Er Ke Za Zhi* **2021**, *23*, 221–228. [CrossRef]

39. Rawat, K.; Kumari, P.; Saha, L. COVID-19 vaccine: A recent update in pipeline vaccines, their design and development strategies. *Eur. J. Pharm.* **2021**, *892*, 173751–173763. [CrossRef]

40. Drożdżal, S.; Rosik, J.; Lechowicz, K.; Machaj, F.; Szostak, B.; Przybyciński, J.; Lorzadeh, S.; Kotfis, K.; Ghavami, S.; Łos, M.J. An update on drugs with therapeutic potential for SARS-CoV-2 (COVID-19) treatment. *Drug Resist. Updates* **2021**, *59*, 100794–100821. [CrossRef]

41. Pourkarim, F.; Pourtaghi-Anvarian, S.; Rezaee, H. Molnupiravir: A new candidate for COVID-19 treatment. *Pharm. Res. Perspect.* **2022**, *10*, e00909–e00915. [CrossRef]

42. van Paassen, J.; Vos, J.S.; Hoekstra, E.M.; Neumann, K.M.I.; Boot, P.C.; Arbous, S.M. Corticosteroid use in COVID-19 patients: A systematic review and meta-analysis on clinical outcomes. *Crit. Care* **2020**, *24*, 696–717. [CrossRef]

43. Wagner, C.; Griesel, M.; Mikolajewska, A.; Mueller, A.; Nothacker, M.; Kley, K.; Metzendorf, M.I.; Fischer, A.L.; Kopp, M.; Stegemann, M.; et al. Systemic corticosteroids for the treatment of COVID-19. *Cochrane Database Syst. Rev.* **2021**, *8*, Cd014963–Cd015122. [CrossRef] [PubMed]

44. Pulakurthi, Y.S.; Pederson, J.M.; Saravu, K.; Gupta, N.; Balasubramanian, P.; Kamrowski, S.; Schmidt, M.; Vegivinti, C.T.R.; Dibas, M.; Reierson, N.L.; et al.

Corticosteroid therapy for COVID-19: A systematic review and meta-analysis of randomized controlled trials. *Medicine* **2021**, *100*, e25719–e25725. [CrossRef] [PubMed]

45. Zhan, Y.; Shang, J.; Gu, Y.; Huang, Q.; Xie, J. Efficacy of corticosteroid in patients with COVID-19: A multi-center retrospective study and meta-analysis. *J. Med. Virol.* **2021**, *93*, 4292–4302. [CrossRef] [PubMed]

46. Johns, M.; George, S.; Taburyanskaya, M.; Poon, Y.K. A Review of the Evidence for Corticosteroids in COVID-19. J. Pharm. Pract. **2021**, *897190021998502*, 1–12. [CrossRef]

47. Lester, R.S.; Knowles, S.R.; Shear, N.H. The risks of systemic corticosteroid use. *Derm. Clin.* **1998**, *16*, 277–288. [CrossRef]

48. Poetker, D.M.; Reh, D.D. A comprehensive review of the adverse effects of systemic corticosteroids. *Otolaryngol. Clin. N. Am.* **2010**, *43*, 753–768. [CrossRef]

49. Obata, R.; Maeda, T.; Rizk, D.; Kuno, T. Increased Secondary Infection in COVID-19 Patients Treated with Steroids in New York City. *Jpn. J. Infect. Dis.* **2021**, *74*, 307–315. [CrossRef]

50. Prasad, K.; Khatoon, F.; Rashid, S.; Ali, N.; AlAsmari, A.F.; Ahmed, M.Z.; Alqahtani, A.S.; Alqahtani, M.S.; Kumar, V. Targeting hub genes and pathways of innate immune response in COVID-19: A network biology perspective. *Int. J. Biol. Macromol.* **2020**, *163*, 1–8. [CrossRef]

51. Adhami, M.; Sadeghi, B.; Rezapour, A.; Haghdoost, A.A.; MotieGhader, H. Repurposing novel therapeutic candidate drugs for coronavirus disease-19 based on protein-protein interaction network analysis. *BMC Biotechnol.* **2021**, *21*, 22–32. [CrossRef]

52. Hu, R.W.; Liu, C.; Yan, Y.Y.; Li, D. Identification of hub genes and molecular subtypes in COVID-19 based on WGCNA. *Eur. Rev. Med. Pharm. Sci.* **2021**, *25*, 6411–6424. [CrossRef]

53. Arya, K.R.; Bharath Chand, R.P.; Abhinand, C.S.; Nair, A.S.; Oommen, O.V.; Sudhakaran, P.R. Identification of Hub Genes and Key Pathways Associated with Anti-VEGF Resistant Glioblastoma Using Gene Expression Data Analysis. *Biomolecules* 2021, *11*, 403–422. [CrossRef] [PubMed]

54. Zhou, Y.; Hou, Y.; Shen, J.; Huang, Y.; Martin, W.; Cheng, F. Network-based drug repurposing for novel coronavirus 2019-nCoV/SARS-CoV-2. *Cell Discov.* 2020, *6*, 14–31. [CrossRef] [PubMed]

55. More, S.A.; Patil, A.S.; Sakle, N.S.; Mokale, S.N. Network analysis and molecular mapping for SARS-CoV-2 to reveal drug targets and repurposing of clinically developed drugs. *Virology* 2021, *555*, 10–18. [CrossRef] [PubMed]

56. Kitsiranuwat, S.; Suratanee, A.; Plaimas, K. Multi-Data Aspects of Protein Similarity with a Learning Technique to Identify Drug-Disease Associations. *Appl. Sci.* 2021, *11*, 2914–2931. [CrossRef]

57. Kawichai, T.; Suratanee, A.; Plaimas, K. Meta-Path Based Gene Ontology Profiles for Predicting Drug-Disease Associations. *IEEE Access* 2021, *9*, 41809–41820. [CrossRef]

58. Jukic, M.; Kores, K.; Janezic, D.; Bren, U. Repurposing of Drugs for SARS-CoV-2 Using Inverse Docking Fingerprints. *Front. Chem.* 2021, *9*, 757826–757843. [CrossRef]

59. Suratanee, A.; Plaimas, K. Identification of inflammatory bowel disease-related proteins using a reverse k-nearest neighbor search. *J. Bioinform. Comput. Biol.* 2014, *12*, 1450017–1450035. [CrossRef]

60. Suratanee, A.; Plaimas, K. Hybrid Deep Learning Based on a Heterogeneous Network Profile for Functional Annotations of Plasmodium falciparum Genes. *Int. J. Mol. Sci.* 2021, *22*, 10019–10036. [CrossRef]

61. Kumar, R.; Haider, S. Protein network analysis to prioritize key genes in amyotrophic lateral sclerosis. *IBRO Neurosci. Rep.* 2022, *12*, 25–44. [CrossRef]

62. Suratanee, A.; Plaimas, K. Heterogeneous Network Model to Identify Potential Associations Between Plasmodium vivax and Human Proteins. *Int. J. Mol. Sci.* **2020**, *21*, 1310–1327. [CrossRef]

63. Suratanee, A.; Buaboocha, T.; Plaimas, K. Prediction of Human-Plasmodium vivax Protein Associations From Heterogeneous Network Structures Based on Machine-Learning Approach. *Bioinform. Biol. Insights* **2021**, *15*, 11779322211013350–11779322211013362. [CrossRef] [PubMed]

64. Zhao, B.; Zhang, Z.; Jiang, M.; Hu, S.; Luo, Y.; Wang, L. NPF: network propagation for protein function prediction. *BMC Bioinform.* **2020**, *21*, 355–375. [CrossRef] [PubMed]

65. Suratanee, A.; Plaimas, K. Reverse Nearest Neighbor Search on a Protein-Protein Interaction Network to Infer Protein-Disease Associations. *Bioinform. Biol. Insights* **2017**, *11*, 1177932217720405–1177932217720415. [CrossRef] [PubMed]

66. Suratanee, A.; Plaimas, K. Network-based association analysis to infer new disease-gene relationships using large-scale protein interactions. *PLoS ONE* **2018**, *13*, e0199435– e0199454. [CrossRef] [PubMed]

67. Yang, H.; Ding, Y.; Tang, J.; Guo, F. Identifying potential association on gene-disease network via dual hypergraph regularized least squares. *BMC Genom.* **2021**, *22*, 605–620. [CrossRef]

68. Suratanee, A.; Plaimas, K. DDA: A Novel Network-Based Scoring Method to Identify Disease-Disease Associations. *Bioinform. Biol. Insights* **2015**, *9*, 175–186. [CrossRef]

69. Iida, M.; Iwata, M.; Yamanishi, Y. Network-based characterization of disease-disease relationships in terms of drugs and therapeutic targets. *Bioinformatics* **2020**, *36* (Suppl. 1), i516–i524. [CrossRef]

70. Yang, J.; Li, H.; Wang, F.; Xiao, F.; Yan, W.; Hu, G. Network-Based Target Prioritization and Drug Candidate Identification for Multiple Sclerosis: From

Analyzing "Omics Data" to Druggability Simulations. *ACS Chem. Neurosci.* **2021**, *12*, 917–929. [CrossRef]

71. Oany, A.R.; Mia, M.; Pervin, T.; Alyami, S.A.; Moni, M.A. Integrative Systems Biology Approaches to Identify Potential Biomarkers and Pathways of Cervical Cancer. *J. Pers. Med.* **2021**, *11*, 363–378. [CrossRef]

72. Janyasupab, P.; Suratanee, A.; Plaimas, K. Network diffusion with centrality measures to identify disease-related genes. *Math. Biosci. Eng.* **2021**, *18*, 2909–2929. [CrossRef]

73. Harun, S.; Zulkifle, N. Construction and Analysis of Protein-Protein Interaction Network to Identify the Molecular Mechanism in Laryngeal Cancer. *Sains Malays.* **2018**, *47*, 2933–2940. [CrossRef]

74. Chen, C.; Shen, H.; Zhang, L.G.; Liu, J.; Cao, X.G.; Yao, A.L.; Kang, S.S.; Gao, W.X.; Han, H.; Cao, F.H.; et al. Construction and analysis of protein-protein interaction networks based on proteomics data of prostate cancer. *Int. J. Mol. Med.* **2016**, *37*, 1576–1586. [CrossRef]

75. Hao, T.; Zhao, L.; Wu, D.; Wang, B.; Feng, X.; Wang, E.; Sun, J. The Protein–Protein Interaction Network of Litopenaeus vannamei Haemocytes. *Front. Physiol.* **2019**, *10*, 156–165. [CrossRef]

76. Ran, J.; Li, H.; Fu, J.; Liu, L.; Xing, Y.; Li, X.; Shen, H.; Chen, Y.; Jiang, X.; Li, Y.; et al. Construction and analysis of the protein-protein interaction network related to essential hypertension. *BMC Syst. Biol.* **2013**, *7*, 32–43. [CrossRef]

77. Chen, S.-J.; Liao, D.-L.; Chen, C.-H.; Wang, T.-Y.; Chen, K.-C. Construction and Analysis of Protein-Protein Interaction Network of Heroin Use Disorder. *Sci. Rep.* **2019**, *9*, 4980–4988. [CrossRef]

78. Estrada, E. Cascading from SARS-CoV-2 to Parkinson's Disease through Protein-Protein Interactions. *Viruses* **2021**, *13*, 897–914. [CrossRef]

79. Auwul, M.R.; Zhang, C.; Rahman, M.R.; Shahjaman, M.; Alyami, S.A.; Moni, M.A. Network-based transcriptomic analysis identifies the genetic effect of COVID-19 to chronic kidney disease patients: A bioinformatics approach. *Saudi J. Biol. Sci.* **2021**, *28*, 5647–5656. [CrossRef]

80. Saha, S.; Chatterjee, P.; Nasipuri, M.; Basu, S. Detection of spreader nodes in human-SARS-CoV protein-protein interaction network. *PeerJ* **2021**, *9*, e12117–e12143. [CrossRef]

81. Managbanag, J.R.; Witten, T.M.; Bonchev, D.; Fox, L.A.; Tsuchiya, M.; Kennedy, B.K.; Kaeberlein, M. Shortest-path network analysis is a useful approach toward identifying genetic determinants of longevity. *PLoS ONE* **2008**, *3*, e3802– e3810. [CrossRef]

82. Cowen, L.; Ideker, T.; Raphael, B.J.; Sharan, R. Network propagation: A universal amplifier of genetic associations. *Nat. Rev. Genet.* **2017**, *18*, 551–562. [CrossRef]

83. Szklarczyk, D.; Gable, A.L.; Lyon, D.; Junge, A.; Wyder, S.; Huerta-Cepas, J.; Simonovic, M.; Doncheva, N.T.; Morris, J.H.; Bork, P.; et al. STRING v11: Protein-protein association networks with increased coverage, supporting functional discovery in genome-wide experimental datasets. *Nucleic Acids Res.* **2019**, *47*, D607–D613. [CrossRef]

84. Zhou, Y.; Zhou, B.; Pache, L.; Chang, M.; Khodabakhshi, A.H.; Tanaseichuk, O.; Benner, C.; Chanda, S.K. Metascape provides a biologist-oriented resource for the analysis of systems-level datasets. *Nat. Commun.* **2019**, *10*, 1523–1532. [CrossRef]

85. Wickham, H.; François, R. Dplyr: A Grammar of Data Manipulation. R Package Version 0.4.3. 2015. Available online: http://CRAN.R-project.org/package=dplyr (accessed on 22 November 2021).

86. Csardi, G.; Nepusz, T. The igraph software package for complex network research. *InterJ. Complex. Syst.* **2006**, *1695*, 1–9.

87. Gill, S.E.; Dos Santos, C.C.; O'Gorman, D.B.; Carter, D.E.; Patterson, E.K.; Slessarev, M.; Martin, C.; Daley, M.; Miller, M.R.; Cepinskas, G.; et al. Transcriptional profiling of leukocytes in critically ill COVID-19 patients: Implications for interferon response and coagulation. *Intensive Care Med. Exp.* **2020**, *8*, 75–90. [CrossRef]

88. Lu, S.; Zhao, K.; Wang, X.; Liu, H.; Ainiwaer, X.; Xu, Y.; Ye, M. Use of Laplacian Heat Diffusion Algorithm to Infer Novel Genes With Functions Related to Uveitis. *Front. Genet.* **2018**, *9*, 425–434. [CrossRef]

89. Zhang, J.; Zhang, M.; Zhao, H.; Xu, X. Identification of proliferative diabetic retinopathy-associated genes on the protein-protein interaction network by using heat diffusion algorithm. *Biochim. Biophys. Acta Mol. Basis Dis.* **2020**, *1866*, 165794–165801. [CrossRef]

90. Dirmeier, S. Diffusr: Network Diffusion Algorithms. 2018. Available online: https://cran.rstudio.com/web/packages/diffusr/index.html (accessed on 10 December 2021).

91. Conway, J.R.; Lex, A.; Gehlenborg, N. UpSetR: An R package for the visualization of intersecting sets and their properties. *Bioinformatics* **2017**, *33*, 2938–2940. [CrossRef]

92. Koschützki, D.; Schreiber, F. Centrality analysis methods for biological networks and their application to gene regulatory networks. *Gene Regul. Syst. Biol.* **2008**, *2*, 193–201. [CrossRef]

93. Raman, K.; Damaraju, N.; Joshi, G.K. The organisational structure of protein networks: Revisiting the centrality-lethality hypothesis. *Syst. Synth. Biol.* **2014**, *8*, 73–81. [CrossRef]

94. Grobelny, B.T.; London, D.; Hill, T.C.; North, E.; Dugan, P.; Doyle, W.K. Betweenness centrality of intracranial electroencephalography networks and surgical epilepsy outcome. *Clin. Neurophysiol.* **2018**, *129*, 1804–1812. [CrossRef]

95. Durón, C.; Pan, Y.; Gutmann, D.H.; Hardin, J.; Radunskaya, A. Variability of Betweenness Centrality and Its Effect on Identifying Essential Genes. *Bull. Math. Biol.* **2019**, *81*, 3655–3673. [CrossRef]

96. Wuchty, S.; Stadler, P.F. Centers of complex networks. *J. Biol.* **2003**, *223*, 45–53. [CrossRef]

97. Ma, H.W.; Zeng, A.P. The connectivity structure, giant strong component and centrality of metabolic networks. *Bioinformatics* **2003**, *19*, 1423–1430. [CrossRef]

98. Lohmann, G.; Margulies, D.S.; Horstmann, A.; Pleger, B.; Lepsien, J.; Goldhahn, D.; Schloegl, H.; Stumvoll, M.; Villringer, A.; Turner, R. Eigenvector centrality mapping for analyzing connectivity patterns in fMRI data of the human brain. *PLoS ONE* **2010**, *5*, e10232– e10239. [CrossRef]

99. Binnewijzend, M.A.; Adriaanse, S.M.; Van der Flier, W.M.; Teunissen, C.E.; de Munck, J.C.; Stam, C.J.; Scheltens, P.; van Berckel, B.N.; Barkhof, F.; Wink, A.M. Brain network alterations in Alzheimer's disease measured by eigenvector centrality in fMRI are related to cognition and CSF biomarkers. *Hum. Brain Mapp.* **2014**, *35*, 2383–2393. [CrossRef]

100. Adriaanse, S.M.; Wink, A.M.; Tijms, B.M.; Ossenkoppele, R.; Verfaillie, S.C.; Lammertsma, A.A.; Boellaard, R.; Scheltens, P.; van Berckel, B.N.; Barkhof, F. The Association of Glucose Metabolism and Eigenvector Centrality in Alzheimer's Disease. *Brain Connect.* **2016**, *6*, 1–8. [CrossRef]

101. van Duinkerken, E.; Schoonheim, M.M.; RG, I.J.; Moll, A.C.; Landeira-Fernandez, J.; Klein, M.; Diamant, M.; Snoek, F.J.; Barkhof, F.; Wink, A.M. Altered eigenvector centrality is related to local resting-state network functional connectivity in patients with longstanding type 1 diabetes mellitus. *Hum. Brain Mapp.* **2017**, *38*, 3623–3636. [CrossRef]

102. Harris, M.A.; Clark, J.; Ireland, A.; Lomax, J.; Ashburner, M.; Foulger, R.; Eilbeck, K.; Lewis, S.; Marshall, B.; Mungall, C.; et al. The Gene Ontology (GO) database and informatics resource. *Nucleic Acids Res.* **2004**, *32*, D258–D261. [CrossRef]

103. Kanehisa, M.; Furumichi, M.; Tanabe, M.; Sato, Y.; Morishima, K. KEGG: New perspectives on genomes, pathways, diseases and drugs. *Nucleic Acids Res.* **2017**, *45*, D353–D361. [CrossRef]

104. Jassal, B.; Matthews, L.; Viteri, G.; Gong, C.; Lorente, P.; Fabregat, A.; Sidiropoulos, K.; Cook, J.; Gillespie, M.; Haw, R.; et al. The reactome pathway knowledgebase. *Nucleic Acids Res.* **2020**, *48*, D498–D503. [CrossRef]

105. Martens, M.; Ammar, A.; Riutta, A.; Waagmeester, A.; Slenter, D.N.; Hanspers, K.; Miller, R.A.; Digles, D.; Lopes, E.N.; Ehrhart, F.; et al. WikiPathways: Connecting communities. *Nucleic Acids Res.* **2021**, *49*, D613–D621. [CrossRef]

106. Mvubu, N.E.; Pillay, B.; Gamieldien, J.; Bishai, W.; Pillay, M. Canonical pathways, networks and transcriptional factor regulation by clinical strains of Mycobacterium tuberculosis in pulmonary alveolar epithelial cells. *Tuberculosis* **2016**, *97*, 73–85. [CrossRef]

107. Giurgiu, M.; Reinhard, J.; Brauner, B.; Dunger-Kaltenbach, I.; Fobo, G.; Frishman, G.; Montrone, C.; Ruepp, A. CORUM: The comprehensive resource of mammalian protein complexes-2019. *Nucleic Acids Res.* **2019**, *47*, D559–D563. [CrossRef]

108. Bader, G.D.; Hogue, C.W. An automated method for finding molecular complexes in large protein interaction networks. *BMC Bioinform.* **2003**, *4*, 2–28. [CrossRef]

109. van Dongen, S.; Abreu-Goodger, C. Using MCL to extract clusters from networks. *Methods Mol. Biol.* **2012**, *804*, 281–295. [CrossRef]

110. Wishart, D.S.; Feunang, Y.D.; Guo, A.C.; Lo, E.J.; Marcu, A.; Grant, J.R.; Sajed, T.; Johnson, D.; Li, C.; Sayeeda, Z.; et al. DrugBank 5.0: A major update to the DrugBank database for 2018. *Nucleic Acids Res.* **2018**, *46*, D1074–D1082. [CrossRef]

111. Wang, Y.; Zhang, S.; Li, F.; Zhou, Y.; Zhang, Y.; Wang, Z.; Zhang, R.; Zhu, J.; Ren, Y.; Tan, Y.; et al. Therapeutic target database 2020: Enriched resource for facilitating research and early development of targeted therapeutics. *Nucleic Acids Res*. 2020, *48*, D1031–D1041. [CrossRef]

112. Davis, A.P.; Grondin, C.J.; Johnson, R.J.; Sciaky, D.; Wiegers, J.; Wiegers, T.C.; Mattingly, C.J. Comparative Toxicogenomics Database (CTD): Update 2021. *Nucleic Acids Res*. 2021, *49*, D1138–D1143. [CrossRef]

113. Safran, M.; Dalah, I.; Alexander, J.; Rosen, N.; Iny Stein, T.; Shmoish, M.; Nativ, N.; Bahir, I.; Doniger, T.; Krug, H.; et al. GeneCards Version 3: The human gene integrator. *Database* 2010, *2010*, baq020– baq035. [CrossRef]

114. Szklarczyk, D.; Santos, A.; von Mering, C.; Jensen, L.J.; Bork, P.; Kuhn, M. STITCH 5: Augmenting protein-chemical interaction networks with tissue and affinity data. *Nucleic Acids Res*. 2016, *44*, D380–D384. [CrossRef]

115. Barabási, A.L.; Oltvai, Z.N. Network biology: Understanding the cell's functional organization. *Nat. Rev. Genet*. 2004, *5*, 101–113. [CrossRef]

116. Teijaro, J.R. Type I interferons in viral control and immune regulation. *Curr. Opin. Virol*. 2016, *16*, 31–40. [CrossRef]

117. Doly, J.; Civas, A.; Navarro, S.; Uze, G. Type I interferons: Expression and signalization. *Cell Mol. Life Sci*. 1998, *54*, 1109–1121. [CrossRef]

118. Stetson, D.B.; Medzhitov, R. Type I interferons in host defense. *Immunity* 2006, *25*, 373–381. [CrossRef]

119. Baise, E.; Pire, G.; Leroy, M.; Gérardin, J.; Goris, N.; De Clercq, K.; Kerkhofs, P.; Desmecht, D. Conditional expression of type I interferon-induced bovine Mx1 GTPase in a stable transgenic vero cell line interferes with replication of vesicular stomatitis virus. *J. Interferon. Cytokine Res*. 2004, *24*, 513–521. [CrossRef]

120. Verhelst, J.; Parthoens, E.; Schepens, B.; Fiers, W.; Saelens, X. Interferon-inducible protein Mx1 inhibits influenza virus by interfering with functional viral

ribonucleopr.rotein complex assembly. *J. Virol.* **2012**, *86*, 13445–13455. [CrossRef]

121. McNab, F.; Mayer-Barber, K.; Sher, A.; Wack, A.; O'Garra, A. Type I interferons in infectious disease. *Nat. Rev. Immunol.* **2015**, *15*, 87–103. [CrossRef]

122. Schreiber, G. The Role of Type I Interferons in the Pathogenesis and Treatment of COVID-19. *Front. Immunol.* **2020**, *11*, 595739–595751. [CrossRef]

123. Yang, L.; Xie, X.; Tu, Z.; Fu, J.; Xu, D.; Zhou, Y. The signal pathways and treatment of cytokine storm in COVID-19. *Signal. Transduct. Target. Ther.* **2021**, *6*, 255–274. [CrossRef]

124. Lee, A.J.; Ashkar, A.A. The Dual Nature of Type I and Type II Interferons. *Front. Immunol.* **2018**, *9*, 2061–2070. [CrossRef]

125. Tovo, P.-A.; Garazzino, S.; Daprà, V.; Pruccoli, G.; Calvi, C.; Mignone, F.; Alliaudi, C.; Denina, M.; Scolfaro, C.; Zoppo, M.; et al. COVID-19 in Children: Expressions of Type I/II/III Interferons, TRIM28, SETDB1, and Endogenous Retroviruses in Mild and Severe Cases. *Int. J. Mol. Sci.* **2021**, *22*, 7481–7508. [CrossRef]

126. Kim, M.H.; Salloum, S.; Wang, J.Y.; Wong, L.P.; Regan, J.; Lefteri, K.; Manickas-Hill, Z.; Li, J.Z.; Sadreyev, R.I.; Yu, X.G.; et al. Type I, II, and III interferon signatures correspond to COVID-19 disease severity. *J. Infect. Dis.* **2021**, *224*, 777–782. [CrossRef]

127. Ruetsch, C.; Brglez, V.; Crémoni, M.; Zorzi, K.; Fernandez, C.; Boyer-Suavet, S.; Benzaken, S.; Demonchy, E.; Risso, K.; Courjon, J.; et al. Functional Exhaustion of Type I and II Interferons Production in Severe COVID-19 Patients. *Front. Med.* **2021**, *7*, 603961–603971. [CrossRef]

128. Biron, C.A. Interferons alpha and beta as immune regulators—A new look. *Immunity* **2001**, *14*, 661–664. [CrossRef]

129. Davidson, S.; Crotta, S.; McCabe, T.M.; Wack, A. Pathogenic potential of interferon αβ in acute influenza infection. *Nat. Commun.* **2014**, *5*, 3864–3878. [CrossRef]

130. Le Saout, C.; Hasley, R.B.; Imamichi, H.; Tcheung, L.; Hu, Z.; Luckey, M.A.; Park, J.H.; Durum, S.K.; Smith, M.; Rupert, A.W.; et al. Chronic exposure to type-I IFN under lymphopenic conditions alters CD4 T cell homeostasis. *PLoS Pathog.* **2014**, *10*, e1003976– e1003990. [CrossRef]

131. Herold, S.; Steinmueller, M.; von Wulffen, W.; Cakarova, L.; Pinto, R.; Pleschka, S.; Mack, M.; Kuziel, W.A.; Corazza, N.; Brunner, T.; et al. Lung epithelial apoptosis in influenza virus pneumonia: The role of macrophage-expressed TNF-related apoptosis-inducing ligand. *J. Exp. Med.* **2008**, *205*, 3065–3077. [CrossRef]

132. Yuan, X.; Yao, Z.; Wu, J.; Zhou, Y.; Shan, Y.; Dong, B.; Zhao, Z.; Hua, P.; Chen, J.; Cong, Y. G1 phase cell cycle arrest induced by SARS-CoV 3a protein via the cyclin D3/pRb pathway. *Am. J. Respir. Cell Mol. Biol.* **2007**, *37*, 9–19. [CrossRef]

133. Yuan, X.; Wu, J.; Shan, Y.; Yao, Z.; Dong, B.; Chen, B.; Zhao, Z.; Wang, S.; Chen, J.; Cong, Y. SARS coronavirus 7a protein blocks cell cycle progression at G0/G1 phase via the cyclin D3/pRb pathway. *Virology* **2006**, *346*, 74–85. [CrossRef]

134. Surjit, M.; Liu, B.; Chow, V.T.; Lal, S.K. The nucleocapsid protein of severe acute respiratory syndrome-coronavirus inhibits the activity of cyclin-cyclin-dependent kinase complex and blocks S phase progression in mammalian cells. *J. Biol. Chem.* **2006**, *281*, 10669–10681. [CrossRef]

135. Cizmecioglu, A.; Akay Cizmecioglu, H.; Goktepe, M.H.; Emsen, A.; Korkmaz, C.; Esenkaya Tasbent, F.; Colkesen, F.; Artac, H. Apoptosis-induced T-cell lymphopenia is related to COVID-19 severity. *J. Med. Virol.* **2021**, *93*, 2867–2874. [CrossRef]

136. André, S.; Picard, M.; Cezar, R.; Roux-Dalvai, F.; Alleaume-Butaux, A.; Soundaramourty, C.; Cruz, A.S.; Mendes-Frias, A.; Gotti, C.; Leclercq, M.; et al. T cell apoptosis characterizes severe Covid-19 disease. *Cell Death Differ.* **2022**, 1–14. [CrossRef]

137. Yang, Y.; Kuang, L.; Li, L.; Wu, Y.; Zhong, B.; Huang, X. Distinct Mitochondria-Mediated T-Cell Apoptosis Responses in Children and Adults With Coronavirus Disease 2019. *J. Infect. Dis.* **2021**, *224*, 1333–1344. [CrossRef]

138. Gongora, C.; Mechti, N. Interferon signaling pathways. *Bull. Cancer* **1999**, *86*, 911–919.

139. Perng, Y.-C.; Lenschow, D.J. ISG15 in antiviral immunity and beyond. *Nat. Rev. Microbiol.* **2018**, *16*, 423–439. [CrossRef]

140. Haller, O.; Staeheli, P.; Kochs, G. Interferon-induced Mx proteins in antiviral host defense. *Biochimie* **2007**, *89*, 812–818. [CrossRef]

141. Bertoli, C.; Skotheim, J.M.; de Bruin, R.A. Control of cell cycle transcription during G1 and S phases. *Nat. Rev. Mol. Cell Biol.* **2013**, *14*, 518–528. [CrossRef]

142. Honarmand Ebrahimi, K. A unifying view of the broad-spectrum antiviral activity of RSAD2 (viperin) based on its radical-SAM chemistry. *Metallomics* **2018**, *10*, 539–552. [CrossRef]

143. Kurokawa, C.; Iankov, I.D.; Galanis, E. A key anti-viral protein, RSAD2/VIPERIN, restricts the release of measles virus from infected cells. *Virus Res.* **2019**, *263*, 145–150. [CrossRef]

144. Yogarajah, T.; Ong, K.C.; Perera, D.; Wong, K.T. RSAD2 and AIM2 Modulate Coxsackievirus A16 and Enterovirus A71 Replication in Neuronal Cells in DifferentWays That May Be Associated with Their 5' Nontranslated Regions. *J. Virol.* **2018**, *92*, e01914–e01917. [CrossRef]

145. Jang, J.S.; Lee, J.H.; Jung, N.C.; Choi, S.Y.; Park, S.Y.; Yoo, J.Y.; Song, J.Y.; Seo, H.G.; Lee, H.S.; Lim, D.S. Rsad2 is necessary for mouse dendritic cell maturation via the IRF7-mediated signaling pathway. *Cell Death Dis.* **2018**, *9*, 823–833. [CrossRef]

146. Sen'kova, A.V.; Savin, I.A.; Brenner, E.V.; Zenkova, M.A.; Markov, A.V. Core genes involved in the regulation of acute lung injury and their association with COVID-19

and tumor progression: A bioinformatics and experimental study. *PLoS ONE* 2021, *16*, e0260450– e0260480. [CrossRef]

147. Sarma, A.; Christenson, S.; Mick, E.; Deiss, T.; DeVoe, C.; Pisco, A.; Ghale, R.; Jauregui, A.; Byrne, A.; Moazed, F.; et al. COVID-19 ARDS is characterized by a dysregulated host response that differs from cytokine storm and is modified by dexamethasone. *Res. Sq.* 2021,*1*,1-31. [CrossRef]

148. Pichlmair, A.; Lassnig, C.; Eberle, C.A.; Górna, M.W.; Baumann, C.L.; Burkard, T.R.; Bürckstümmer, T.; Stefanovic, A.; Krieger, S.; Bennett, K.L.; et al. IFIT1 is an antiviral protein that recognizes 5'-triphosphate RNA. *Nat. Immunol.* 2011, *12*, 624–630. [CrossRef]

149. Zhang, Q.; Chen, Z.; Huang, C.; Sun, J.; Xue, M.; Feng, T.; Pan, W.; Wang, K.; Dai, J. Severe Acute Respiratory Syndrome Coronavirus 2 (SARS-CoV-2) Membrane (M) and Spike (S) Proteins Antagonize Host Type I Interferon Response. *Front. Cell. Infect. Microbiol.* 2021, *11*, 766922–766934. [CrossRef]

150. Yu, Y.; Xu, N.; Cheng, Q.; Deng, F.; Liu, M.; Zhu, A.; Min, Y.Q.; Zhu, D.; Huang,W.; Feng, X.; et al. IFP35 as a promising biomarker and therapeutic target for the syndromes induced by SARS-CoV-2 or influenza virus. *Cell Rep.* 2021, *37*, 110126–110143. [CrossRef]

151. Yang, H.; Winkler, W.; Wu, X. Interferon Inducer IFI35 regulates RIG-I-mediated innate antiviral response through mutual antagonism with Influenza protein NS1. *J. Virol.* 2021, *95*, e00283–21. [CrossRef]

152. Ong, E.Z.; Kalimuddin, S.; Chia, W.C.; Ooi, S.H.; Koh, C.W.; Tan, H.C.; Zhang, S.L.; Low, J.G.; Ooi, E.E.; Chan, K.R. Temporal dynamics of the host molecular responses underlying severe COVID-19 progression and disease resolution. *eBioMedicine* 2021, *65*, 103262–103272. [CrossRef]

153. Amado-Rodríguez, L.; Salgado Del Riego, E.; Gomez de Ona, J.; López Alonso, I.; Gil-Pena, H.; López-Martínez, C.; Martín-Vicente, P.; Lopez-Vazquez, A.;

Gonzalez Lopez, A.; Cuesta-Llavona, E.; et al. Effects of IFIH1 rs1990760 variants on systemic inflammation and outcome in critically ill COVID-19 patients in an observational translational study. *eLife* **2022**, *11*, e73012– e73035. [CrossRef]

154. Bouças, A.P.; Oliveira Fdos, S.; Canani, L.H.; Crispim, D. The role of interferon induced with helicase C domain 1 (IFIH1) in the development of type 1 diabetes mellitus. *Arq. Bras. Endocrinol. Metab*. **2013**, *57*, 667–676. [CrossRef]

155. Thorne, L.G.; Reuschl, A.K.; Zuliani-Alvarez, L.; Whelan, M.V.X.; Turner, J.; Noursadeghi, M.; Jolly, C.; Towers, G.J. SARS-CoV-2 sensing by RIG-I and MDA5 links epithelial infection to macrophage inflammation. *EMBO J*. **2021**, *40*, e107826–e107842. [CrossRef]

156. Sampaio, N.G.; Chauveau, L.; Hertzog, J.; Bridgeman, A.; Fowler, G.; Moonen, J.P.; Dupont, M.; Russell, R.A.; Noerenberg, M.; Rehwinkel, J. The RNA sensor MDA5 detects SARS-CoV-2 infection. *Sci. Rep.* **2021**, *11*, 13638–13647. [CrossRef] [PubMed]

157. Yin, X.; Riva, L.; Pu, Y.; Martin-Sancho, L.; Kanamune, J.; Yamamoto, Y.; Sakai, K.; Gotoh, S.; Miorin, L.; De Jesus, P.D.; et al. MDA5 Governs the Innate Immune Response to SARS-CoV-2 in Lung Epithelial Cells. *Cell Rep.* **2021**, *34*, 108628–108644. [CrossRef] [PubMed]

158. Alsamman, A.M.; Zayed, H. The transcriptomic profiling of SARS-CoV-2 compared to SARS, MERS, EBOV, and H1N1. *PLoS ONE* **2020**, *15*, e0243270–e0243286. [CrossRef]

159. Richardson, R.B.; Ohlson, M.B.; Eitson, J.L.; Kumar, A.; McDougal, M.B.; Boys, I.N.; Mar, K.B.; De La Cruz-Rivera, P.C.; Douglas, C.; Konopka, G.; et al. A CRISPR screen identifies IFI6 as an ER-resident interferon effector that blocks flavivirus replication. *Nat. Microbiol*. **2018**, *3*, 1214–1223. [CrossRef]

160. Sajid, M.; Ullah, H.; Yan, K.; He, M.; Feng, J.; Shereen, M.A.; Hao, R.; Li, Q.; Guo, D.; Chen, Y.; et al. The Functional and Antiviral Activity of Interferon Alpha-

Inducible IFI6 Against Hepatitis B Virus Replication and Gene Expression. *Front. Immunol.* **2021**, *12*, 634937–634950. [CrossRef]

161. Loganathan, T.; Ramachandran, S.; Shankaran, P.; Nagarajan, D.; Mohan, S.S. Host transcriptome-guided drug repurposing for COVID-19 treatment: A meta-analysis based approach. *PeerJ* **2020**, *8*, e9357– e9383. [CrossRef]

162. Shaath, H.; Vishnubalaji, R.; Elkord, E.; Alajez, N.M. Single-Cell Transcriptome Analysis Highlights a Role for Neutrophils and Inflammatory Macrophages in the Pathogenesis of Severe COVID-19. *Cells* **2020**, *9*, 2374–2392. [CrossRef]

163. Karami, H.; Derakhshani, A.; Ghasemigol, M.; Fereidouni, M.; Miri-Moghaddam, E.; Baradaran, B.; Tabrizi, N.J.; Najafi, S.; Solimando, A.G.; Marsh, L.M.; et al. Weighted Gene Co-Expression Network Analysis Combined with Machine Learning Validation to Identify Key Modules and Hub Genes Associated with SARS-CoV-2 Infection. *J. Clin. Med.* **2021**, *10*, 3567–3592. [CrossRef]

164. Lieberman, N.A.P.; Peddu, V.; Xie, H.; Shrestha, L.; Huang, M.L.; Mears, M.C.; Cajimat, M.N.; Bente, D.A.; Shi, P.Y.; Bovier, F.; et al. In vivo antiviral host transcriptional response to SARS-CoV-2 by viral load, sex, and age. *PLoS Biol.* **2020**, *18*, e3000849–e3000865. [CrossRef]

165. Prelli Bozzo, C.; Nchioua, R.; Volcic, M.; Koepke, L.; Krüger, J.; Schütz, D.; Heller, S.; Stürzel, C.M.; Kmiec, D.; Conzelmann, C.; et al. IFITM proteins promote SARS-CoV-2 infection and are targets for virus inhibition in vitro. *Nat. Commun.* **2021**, *12*, 4584–4596. [CrossRef] [PubMed]

166. Wauters, E.; Van Mol, P.; Garg, A.D.; Jansen, S.; Van Herck, Y.; Vanderbeke, L.; Bassez, A.; Boeckx, B.; Malengier-Devlies, B.; Timmerman, A.; et al. Discriminating mild from critical COVID-19 by innate and adaptive immune single-cell profiling of bronchoalveolar lavages. *Cell Res.* **2021**, *31*, 272–290. [CrossRef] [PubMed]

167. Park, A.; Harris, L.K. Gene Expression Meta-Analysis Reveals Interferon-Induced Genes Associated With SARS Infection in Lungs. *Front. Immunol.* **2021**, *12*, 694355–694373. [CrossRef] [PubMed]

168. Zhang, Q.; Bastard, P.; Liu, Z.; Le Pen, J.; Moncada-Velez, M.; Chen, J.; Ogishi, M.; Sabli, I.K.D.; Hodeib, S.; Korol, C.; et al. Inborn errors of type I IFN immunity in patients with life-threatening COVID-19. *Science* **2020**, *370*, eabd4570–eabd4583. [CrossRef] [PubMed]

169. Liu, B.M.; Hill, H.R. Role of Host Immune and Inflammatory Responses in COVID-19 Cases with Underlying Primary Immunodeficiency: A Review. *J. Interferon. Cytokine Res.* **2020**, *40*, 549–554. [CrossRef]

170. Munnur, D.; Teo, Q.; Eggermont, D.; Lee, H.H.Y.; Thery, F.; Ho, J.; van Leur, S.W.; Ng, W.W.S.; Siu, L.Y.L.; Beling, A.; et al. Altered ISGylation drives aberrant macrophage-dependent immune responses during SARS-CoV-2 infection. *Nat. Immunol.* **2021**, *22*, 1416–1427. [CrossRef]

171. Bizzotto, J.; Sanchis, P.; Abbate, M.; Lage-Vickers, S.; Lavignolle, R.; Toro, A.; Olszevicki, S.; Sabater, A.; Cascardo, F.; Vazquez, E.; et al. SARS-CoV-2 Infection Boosts MX1 Antiviral Effector in COVID-19 Patients. *iScience* **2020**, *23*, 101585–101605. [CrossRef]

172. Ramana, C.V.; Gil, M.P.; Schreiber, R.D.; Stark, G.R. Stat1-dependent and -independent pathways in IFN-gamma-dependent signaling. *Trends. Immunol.* **2002**, *23*, 96–101. [CrossRef]

173. Adámková, L.; Soucková, K.; Kovarík, J. Transcription protein STAT1: Biology and relation to cancer. Folia Biol. **2007**, *53*, 1–6.

174. Najjar, I.; Fagard, R. STAT1 and pathogens, not a friendly relationship. *Biochimie* **2010**, *92*, 425–444. [CrossRef]

175. Claverie, J.M. A Putative Role of de-Mono-ADP-Ribosylation of STAT1 by the SARS-CoV-2 Nsp3 Protein in the Cytokine Storm Syndrome of COVID-19. *Viruses* **2020**, *12*, 646–653. [CrossRef] [PubMed]

176. Matsuyama, T.; Kubli, S.P.; Yoshinaga, S.K.; Pfeffer, K.; Mak, T.W. An aberrant STAT pathway is central to COVID-19. *Cell Death Differ.* **2020**, *27*, 3209-3225. [CrossRef] [PubMed]

177. Rincon-Arevalo, H.; Aue, A.; Ritter, J.; Szelinski, F.; Khadzhynov, D.; Zickler, D.; Stefanski, L.; Lino, A.C.; Körper, S.; Eckardt, K.U.; et al. Altered increase in STAT1 expression and phosphorylation in severe COVID-19. *Eur. J. Immunol.* **2022**, *52*, 138–148. [CrossRef] [PubMed]

178. Lee, M.G.; Han, J.; Jeong, S.I.; Her, N.G.; Lee, J.H.; Ha, T.K.; Kang, M.J.; Ryu, B.K.; Chi, S.G. XAF1 directs apoptotic switch of p53 signaling through activation of HIPK2 and ZNF313. *Proc. Natl. Acad. Sci.* USA **2014**, *111*, 15532–15537. [CrossRef]

179. Kempkensteffen, C.; Fritzsche, F.R.; Johannsen, M.; Weikert, S.; Hinz, S.; Dietel, M.; Riener, M.-O.; Moch, H.; Jung, K.; Krause, H.; et al. Down-regulation of the pro-apoptotic XIAP associated factor-1 (XAF1) during progression of clear-cell renal cancer. *BMC Cancer* **2009**, *9*, 276–282. [CrossRef]

180. Zhu, L.M.; Shi, D.M.; Dai, Q.; Cheng, X.J.; Yao, W.Y.; Sun, P.H.; Ding, Y.; Qiao, M.M.; Wu, Y.L.; Jiang, S.H.; et al. Tumor suppressor XAF1 induces apoptosis, inhibits angiogenesis and inhibits tumor growth in hepatocellular carcinoma. *Oncotarget* **2014**, *5*, 5403–5415. [CrossRef]

181. Jeong SI; Kim JW; Ko KP; Ryu BK; Lee MG; Kim HJ; et al. XAF1 forms a positive feedback loop with IRF-1 to drive apoptotic stress response and suppress tumorigenesis. *Cell Death Dis.* **2018**, *9*, 806–821. [CrossRef]

182. Zhang, F.; Chen, D.; Yang, W.; Duan, S.; Chen, Y. Combined effects of XAF1 and TRAIL on the apoptosis of lung adenocarcinoma cells. *Exp. Med.* **2019**, *17*, 4663–4669. [CrossRef]

183. Zhu, L.; Yang, P.; Zhao, Y.; Zhuang, Z.; Wang, Z.; Song, R.; Zhang, J.; Liu, C.; Gao, Q.; Xu, Q.; et al. Single-Cell Sequencing of Peripheral Mononuclear Cells Reveals Distinct Immune Response Landscapes of COVID-19 and Influenza Patients. *Immunity* **2020**, *53*, 685–696. [CrossRef]

184. Xie, T.-A.; He, Z.-J.; Liang, C.; Dong, H.-N.; Zhou, J.; Fan, S.-J.; Guo, X.-G. An integrative bioinformatics analysis for identifying hub genes associated with infection of lung samples in patients infected with SARS-CoV-2. *Eur. J. Med. Res.* **2021**, *26*, 146–158. [CrossRef]

185. Huang, Z.; Wang, L.; Chen, L.; Zhang, Y.; Shi, P. Induction of cell cycle arrest via the p21, p27-cyclin E,A/Cdk2 pathway in SMMC-7721 hepatoma cells by clioquinol. *Acta Pharm.* **2015**, *65*, 463–471. [CrossRef] [PubMed]

186. Bayard, Q.; Meunier, L.; Peneau, C.; Renault, V.; Shinde, J.; Nault, J.-C.; Mami, I.; Couchy, G.; Amaddeo, G.; Tubacher, E.; et al. Cyclin A2/E1 activation defines a hepatocellular carcinoma subclass with a rearrangement signature of replication stress. *Nat. Commun.* **2018**, *9*, 5235–5248. [CrossRef] [PubMed]

187. Xing, Z.; Wang, X.; Liu, J.; Zhang, M.; Feng, K.; Wang, X. Expression and prognostic value of CDK1, CCNA2, and CCNB1 gene clusters in human breast cancer. *J. Int. Med. Res.* **2021**, *49*, 300060520980647–300060520980659. [CrossRef] [PubMed]

188. Li, J.; Zhou, L.; Liu, Y.; Yang, L.; Jiang, D.; Li, K.; Xie, S.; Wang, X.; Wang, S. Comprehensive Analysis of Cyclin Family Gene Expression in Colon Cancer. *Front. Oncol.* **2021**, *11*, 1484–1502. [CrossRef]

189. Shen, T.; Huang, S. The role of Cdc25A in the regulation of cell proliferation and apoptosis. *Anticancer Agents Med. Chem.* **2012**, *12*, 631–639. [CrossRef]

190. Gasparotto, D.; Maestro, R.; Piccinin, S.; Vukosavljevic, T.; Barzan, L.; Sulfaro, S.; Boiocchi, M. Overexpression of CDC25A and CDC25B in head and neck cancers. *Cancer Res.* **1997**, *57*, 2366–2368.

191. Wu,W.; Fan, Y.H.; Kemp, B.L.;Walsh, G.; Mao, L. Overexpression of cdc25A and cdc25B is frequent in primary non-small cell lung cancer but is not associated with overexpression of c-myc. *Cancer Res.* **1998**, *58*, 4082–4085.

192. Cangi, M.G.; Cukor, B.; Soung, P.; Signoretti, S.; Moreira, G., Jr.; Ranashinge, M.; Cady, B.; Pagano, M.; Loda, M. Role of the Cdc25A phosphatase in human breast cancer. *J. Clin. Investig.* **2000**, *106*, 753–761. [CrossRef]

193. Broggini, M.; Buraggi, G.; Brenna, A.; Riva, L.; Codegoni, A.M.; Torri, V.; Lissoni, A.A.; Mangioni, C.; D'Incalci, M. Cell cyclerelated phosphatases CDC25A and B expression correlates with survival in ovarian cancer patients. *Anticancer Res.* **2000**, *20*, 4835–4840.

194. Qi, D.; Hu, L.; Jiao, T.; Zhang, T.; Tong, X.; Ye, X. Phosphatase Cdc25A Negatively Regulates the Antiviral Immune Response by Inhibiting TBK1 Activity. *J. Virol.* **2018**, *92*, e01118–18. [CrossRef]

195. Prinz, S.; Hwang, E.S.; Visintin, R.; Amon, A. The regulation of Cdc20 proteolysis reveals a role for APC components Cdc23 and Cdc27 during S phase and early mitosis. *Curr. Biol.* **1998**, *8*, 750–760. [CrossRef]

196. Kapanidou, M.; Curtis, N.L.; Bolanos-Garcia, V.M. Cdc20: At the Crossroads between Chromosome Segregation and Mitotic Exit. *Trends Biochem. Sci.* **2017**, *42*, 193–205. [CrossRef] [PubMed]

197. Deng, H.; Hang, Q.; Shen, D.; Ying, H.; Zhang, Y.; Qian, X.; Chen, M. High Expression Levels of CDK1 and CDC20 in Patients with Lung Squamous Cell Carcinoma are Associated With Worse Prognosis. *Front. Mol. Biosci.* **2021**, *8*, 653805–653819. [CrossRef] [PubMed]

198. Geronikolou, S.A.; Takan, I.; Pavlopoulou, A.; Mantzourani, M.; Chrousos, G.P. Thrombocytopenia in COVID-19 and vaccineinduced thrombotic thrombocytopenia. *Int. J. Mol. Med.* **2022**, *49*, 1–19. [CrossRef] [PubMed]

199. El-Diwany, R.; Soliman, M.; Sugawara, S.; Breitwieser, F.; Skaist, A.; Coggiano, C.; Sangal, N.; Chattergoon, M.; Bailey, J.R.; Siliciano, R.F.; et al. CMPK2 and BCL-G are associated with type 1 interferon-induced HIV restriction in humans. *Sci. Adv.* **2018**, *4*, eaat0843–eaat0853. [CrossRef]

200. Lai, J.H.; Wu, D.W.; Wu, C.H.; Hung, L.F.; Huang, C.Y.; Ka, S.M.; Chen, A.; Chang, Z.F.; Ho, L.J. Mitochondrial CMPK2 mediates immunomodulatory and antiviral activities through IFN-dependent and IFN-independent pathways. *iScience* **2021**, *24*, 102498–102517. [CrossRef]

201. Lai, J.H.; Hung, L.F.; Huang, C.Y.; Wu, D.W.; Wu, C.H.; Ho, L.J. Mitochondrial protein CMPK2 regulates IFN alpha-enhanced foam cell formation, potentially contributing to premature atherosclerosis in SLE. *Arthritis Res. Ther.* **2021**, *23*, 120–131. [CrossRef]

202. Moolamalla, S.T.R.; Balasubramanian, R.; Chauhan, R.; Priyakumar, U.D.; Vinod, P.K. Host metabolic reprogramming in response to SARS-CoV-2 infection: A systems biology approach. *Microb. Pathog.* **2021**, *158*, 105114–105127. [CrossRef]

203. Xian, H.; Liu, Y.; Rundberg Nilsson, A.; Gatchalian, R.; Crother, T.R.; Tourellotte, W.G.; Zhang, Y.; Aleman-Muench, G.R.; Lewis, G.; Chen, W.; et al. Metformin inhibition of mitochondrial ATP and DNA synthesis abrogates NLRP3 inflammasome activation and pulmonary inflammation. *Immunity* **2021**, *54*, 1463–1477.e1411. [CrossRef]

204. Huang, X.; Zhang, X.; Machireddy, N.; Mutlu, G.M.; Fang, Y.; Wu, D.; Zhao, Y.-Y. Decitabine Reactivation of FoxM1-Dependent Endothelial Regeneration and Vascular Repair for Potential Treatment of Elderly ARDS and COVID-19 Patients. *bioRxiv* **2021**, *1*, 1–51. [CrossRef]

205. Jin, C.Y.; Du, L.; Nuerlan, A.H.; Wang, X.L.; Yang, Y.W.; Guo, R. High expression of RRM2 as an independent predictive factor of poor prognosis in patients with lung adenocarcinoma. *Aging* **2020**, *13*, 3518–3535. [CrossRef] [PubMed]

206. Auwul, M.R.; Rahman, M.R.; Gov, E.; Shahjaman, M.; Moni, M.A. Bioinformatics and machine learning approach identifies potential drug targets and pathways in COVID-19. *Brief Bioinform*. **2021**, *22*, bbab120– bbab132. [CrossRef] [PubMed]

207. Chen, H.; Wang, D.L.; Liu, Y.L. Poly (I:C) transfection induces mitochondrial-mediated apoptosis in cervical cancer. *Mol. Med. Rep*. **2016**, *13*, 2689–2695. [CrossRef] [PubMed]

208. Bianchi, F.; Pretto, S.; Tagliabue, E.; Balsari, A.; Sfondrini, L. Exploiting poly(I:C) to induce cancer cell apoptosis. *Cancer Biol*. **2017**, *18*, 747–756. [CrossRef] [PubMed]

209. Kourko, O.; Smyth, R.; Cino, D.; Seaver, K.; Petes, C.; Eo, S.Y.; Basta, S.; Gee, K. Poly(I:C)-Mediated Death of Human Prostate Cancer Cell Lines Is Induced by Interleukin-27 Treatment. *J. Interferon Cytokine Res*. **2019**, *39*, 483–494. [CrossRef] [PubMed]

210. Di, S.; Zhou, M.; Pan, Z.; Sun, R.; Chen, M.; Jiang, H.; Shi, B.; Luo, H.; Li, Z. Combined Adjuvant of Poly I:C Improves Antitumor Effects of CAR-T Cells. *Front. Oncol*. **2019**, *9*, 241–251. [CrossRef] [PubMed]

211. Zhao, J.; Xue, Y.; Pan, Y.; Yao, A.; Wang, G.; Li, D.; Wang, T.; Zhao, S.; Hou, Y. Toll-like receptor 3 agonist poly I:C reinforces the potency of cytotoxic chemotherapy via the TLR3-UNC93B1-IFN-β signaling axis in paclitaxel-resistant colon cancer. *J. Cell Physiol*. **2019**, *234*, 7051–7061. [CrossRef]

212. Meyer, T.; Oberg, H.H.; Peters, C.; Martens, I.; Adam-Klages, S.; Kabelitz, D.; Wesch, D. poly(I:C) costimulation induces a stronger antiviral chemokine and granzyme B release in human CD4 T cells than CD28 costimulation. *J. Leukoc. Biol*. **2012**, *92*, 765–774. [CrossRef]

213. Zhao, J.; Wohlford-Lenane, C.; Zhao, J.; Fleming, E.; Lane, T.E.; McCray, P.B., Jr.; Perlman, S. Intranasal treatment with poly(I:C) protects aged mice from lethal respiratory virus infections. *J. Virol.* **2012**, *86*, 11416–11424. [CrossRef]

214. Tamir, H.; Melamed, S.; Erez, N.; Politi, B.; Yahalom-Ronen, Y.; Achdout, H.; Lazar, S.; Gutman, H.; Avraham, R.; Weiss, S.; et al. Induction of Innate Immune Response by TLR3 Agonist Protects Mice against SARS-CoV-2 Infection. *Viruses* **2022**, *14*, 189–206. [CrossRef]

215. Murray, C.; Griffin, É.W.; O'Loughlin, E.; Lyons, A.; Sherwin, E.; Ahmed, S.; Stevenson, N.J.; Harkin, A.; Cunningham, C. Interdependent and independent roles of type I interferons and IL-6 in innate immune, neuroinflammatory and sickness behaviour responses to systemic poly I:C. *Brain Behav. Immun.* **2015**, *48*, 274–286. [CrossRef] [PubMed]

216. Lever, A.R.; Park, H.; Mulhern, T.J.; Jackson, G.R.; Comolli, J.C.; Borenstein, J.T.; Hayden, P.J.; Prantil-Baun, R. Comprehensive evaluation of poly(I:C) induced inflammatory response in an airway epithelial model. *Physiol. Rep.* **2015**, *3*, e12334– e12344. [CrossRef] [PubMed]

217. Liu, X.; Meng, L.; Chen, L.; Liang, Y.; Wang, B.; Shao, Q.; Wang, H.; Yang, X. IL-6 expression promoted by Poly(I:C) in cervical cancer cells regulates cytokine expression and recruitment of macrophages. *J. Cell Mol. Med.* **2020**, *24*, 2284– 2293. [CrossRef] [PubMed]

218. Verweij, J.; Pinedo, H.M. Mitomycin C: Mechanism of action, usefulness and limitations. *Anticancer Drugs* **1990**, *1*, 5–13. [CrossRef]

219. Bradner, W.T. Mitomycin C: A clinical update. *Cancer Treat. Rev.* **2001**, *27*, 35–50. [CrossRef]

220. Park, S.H.; Kim, Y.S.; Hong, J.; Park, J.; Nam, E.; Cho, E.K.; Shin, D.B.; Lee, J.H.; Lee, W.K.; Chung, M. Mitomycin C plus S-1 as second-line therapy in patients with

advanced gastric cancer: A noncomparative phase II study. *Anticancer Drugs* **2008**, *19*, 303–307. [CrossRef]

221. Ragonese, M.; Racioppi, M.; Bassi, P.F.; Di Gianfrancesco, L.; Lenci, N.; Filianoti, A.; Recupero, S.M. Mitomycin C: New strategies to improve efficacy of a well-known therapy. *Urologia* **2016**, *83* (Suppl. 2), 24–28. [CrossRef]

222. Issa, J.P. Decitabine. Curr. Opin. Oncol. **2003**, 15, 446–451. [CrossRef]

223. Hackanson, B.; Daskalakis, M. Decitabine. *Recent Results Cancer Res*. **2014**, *201*, 269–297. [CrossRef]

224. Toschi, L.; Finocchiaro, G.; Bartolini, S.; Gioia, V.; Cappuzzo, F. Role of gemcitabine in cancer therapy. *Future Oncol*. **2005**, *1*, 7–17. [CrossRef]

225. Zhang, Y.N.; Zhang, Q.Y.; Li, X.D.; Xiong, J.; Xiao, S.Q.; Wang, Z.; Zhang, Z.R.; Deng, C.L.; Yang, X.L.; Wei, H.P.; et al. Gemcitabine, lycorine and oxysophoridine inhibit nov.vel coronavirus (SARS-CoV-2) in cell culture. *Emerg. Microbes Infect*. **2020**, *9*, 1170–1173. [CrossRef] [PubMed]

226. Zheng, Z.; Groaz, E.; Snoeck, R.; De Jonghe, S.; Herdewijn, P.; Andrei, G. Influence of 40-Substitution on the Activity of Gemcitabine and Its ProTide Against VZV and SARS-CoV-2. *ACS Med. Chem. Lett.* **2021**, *12*, 88–92. [CrossRef] [PubMed]

227. Jang, Y.; Shin, J.S.; Lee, M.K.; Jung, E.; An, T.; Kim, U.I.; Kim, K.; Kim, M. Comparison of Antiviral Activity of Gemcitabine with 2′-Fluoro-2′-Deoxycytidine and Combination Therapy with Remdesivir against SARS-CoV-2. *Int. J. Mol. Sci*. **2021**, *22*, 1581–1595. [CrossRef] [PubMed]

228. Foote, M.B.; White, J.R.; Jee, J.; Argilés, G.; Wan, J.C.M.; Rousseau, B.; Pessin, M.S.; Diaz, L.A., Jr. Association of Antineoplastic Therapy With Decreased SARS-CoV-2 Infection Rates in Patients With Cancer. *JAMA Oncol*. **2021**, *7*, 1686–1691. [CrossRef] [PubMed]

229. Ben Moftah, M.; Eswayah, A. Repurposing of Hydroxyurea against COVID-19: A Promising Immunomodulatory Role. *Assay Drug Dev. Technol.* **2022**, *20*, 55–62. [CrossRef]

230. Foster, M.R.B.; Hijazi, A.A.; Opoku, R.; Varghese, P.; Li, C. The Use of Hydroxyurea in the Treatment of COVID-19. *J. Crit. Care Med.* **2021**, *7*, 312–317. [CrossRef]

231. Jordan, V.C. The role of tamoxifen in the treatment and prevention of breast cancer. *Curr. Probl. Cancer* **1992**, *16*, 129–176. [CrossRef]

232. Bravaccini, S.; Fonzi, E.; Tebaldi, M.; Angeli, D.; Martinelli, G.; Nicolini, F.; Parrella, P.; Mazza, M. Estrogen and Androgen Receptor Inhibitors: Unexpected Allies in the Fight Against COVID-19. *Cell Transpl.* **2021**, *30*, 963689721991477–963689721991482. [CrossRef]

233. Zu, S.; Luo, D.; Li, L.; Ye, Q.; Li, R.T.; Wang, Y.; Gao, M.; Yang, H.; Deng, Y.Q.; Cheng, G. Tamoxifen and clomiphene inhibit SARS-CoV-2 infection by suppressing viral entry. *Signal. Transduct. Target.* **2021**, *6*, 435–438. [CrossRef]

234. Abramenko, N.; Vellieux, F.; Tesařová, P.; Kejík, Z.; Kaplánek, R.; Lacina, L.; Dvořánková, B.; Rösel, D.; Brábek, J.; Tesař, A.; et al. Estrogen Receptor Modulators in Viral Infections Such as SARS-CoV-2: Therapeutic Consequences. *Int. J. Mol. Sci.* **2021**, *22*, 6551–6568. [CrossRef]

235. Jurenka, J.S. Anti-inflammatory properties of curcumin, a major constituent of Curcuma longa: A review of preclinical and clinical research. *Altern. Med. Rev.* **2009**, *14*, 141–153. [PubMed]

236. Chainani-Wu, N. Safety and anti-inflammatory activity of curcumin: A component of tumeric (Curcuma longa). *J. Altern. Complement. Med.* **2003**, *9*, 161–168. [CrossRef] [PubMed]

237. Menon, V.P.; Sudheer, A.R. Antioxidant and anti-inflammatory properties of curcumin. *Adv. Exp. Med. Biol.* **2007**, *595*, 105–125. [CrossRef] [PubMed]

238. Fan, X.; Zhang, C.; Liu, D.B.; Yan, J.; Liang, H.P. The clinical applications of curcumin: Current state and the future. *Curr. Pharm. Des*. **2013**, *19*, 2011–2031.

239. Zahedipour, F.; Hosseini, S.A.; Sathyapalan, T.; Majeed, M.; Jamialahmadi, T.; Al-Rasadi, K.; Banach, M.; Sahebkar, A. Potential effects of curcumin in the treatment of COVID-19 infection. *Phytother. Res*. **2020**, *34*, 2911–2920. [CrossRef]

240. Thimmulappa, R.K.; Mudnakudu-Nagaraju, K.K.; Shivamallu, C.; Subramaniam, K.J.T.; Radhakrishnan, A.; Bhojraj, S.; Kuppusamy, G. Antiviral and immunomodulatory activity of curcumin: A case for prophylactic therapy for COVID-19. *Heliyon* **2021**, *7*, e06350–e06361. [CrossRef]

241. Rattis, B.A.C.; Ramos, S.G.; Celes, M.R.N. Curcumin as a Potential Treatment for COVID-19. *Front. Pharm*. **2021**, *12*, 675287–675300. [CrossRef]

242. Pawar, K.S.; Mastud, R.N.; Pawar, S.K.; Pawar, S.S.; Bhoite, R.R.; Bhoite, R.R.; Kulkarni, M.V.; Deshpande, A.R. Oral Curcumin With Piperine as Adjuvant Therapy for the Treatment of COVID-19: A Randomized Clinical Trial. *Front. Pharm*. **2021**, *12*, 669362–669368. [CrossRef]

243. Vahedian-Azimi, A.; Abbasifard, M.; Rahimi-Bashar, F.; Guest, P.C.; Majeed, M.; Mohammadi, A.; Banach, M.; Jamialahmadi, T.; Sahebkar, A. Effectiveness of Curcumin on Outcomes of Hospitalized COVID-19 Patients: A Systematic Review of Clinical Trials. *Nutrients* **2022**, *14*, 256–269. [CrossRef]

2.2 RESEARCH ARTICLE 2

Multi-Level Biological Network Analysis and Drug Repurposing Based on Leukocyte Transcriptomics in Severe COVID-19: In Silico Systems Biology to Precision Medicine

Pakorn Sagulkoo [1,2], Hathaichanok Chuntakaruk [1,3], Thanyada Rungrotmongkol [1,3], Apichat Suratanee [4,5] and Kitiporn Plaimas [1,6,7,*]

[1] Program in Bioinformatics and Computational Biology, Graduate School, Chulalongkorn University, Bangkok 10330, Thailand; pakorn.sagulkoo@cmu.ac.th (P.S.); hathaichanok.chuntakaruk@gmail.com (H.C.); t.rungrotmongkol@gmail.com (T.R.)

[2] Center of Biomedical Informatics, Department of Family Medicine, Faculty of Medicine, Chiang Mai University, Chiang Mai 50200, Thailand

[3] Center of Excellence in Biocatalyst and Sustainable Biotechnology Research Unit, Department of Biochemistry, Faculty of Science, Chulalongkorn University, Bangkok 10330, Thailand

[4] Department of Mathematics, Faculty of Applied Science, King Mongkut's University of Technology North Bangkok, Bangkok 10800, Thailand; apichat.s@sci.kmutnb.ac.th

[5] Intelligent and Nonlinear Dynamics Innovations Research Center, Science and Technology Research Institute, King Mongkut's University of Technology North Bangkok, Bangkok 10800, Thailand

[6] Advance Virtual and Intelligent Computing (AVIC) Center, Department of Mathematics and Computer Science, Faculty of Science, Chulalongkorn University, Bangkok 10330, Thailand

[7] Omics Science and Bioinformatics Center, Faculty of Science, Chulalongkorn University, Bangkok 10330, Thailand

* Correspondence: kitiporn.p@chula.ac.th

Abstract: The coronavirus disease 2019 (COVID-19) pandemic causes many morbidity and mortality cases. Despite several developed vaccines and antiviral therapies, some patients experience severe conditions that need intensive care units (ICU); therefore, precision medicine is necessary to predict and treat these patients using novel biomarkers and targeted drugs. In this study, we proposed a multi-level biological network analysis framework to identify key genes via protein–protein interaction (PPI) network analysis as well as survival analysis based on differentially expressed genes (DEGs) in leukocyte transcriptomic profiles, discover novel biomarkers using microRNAs

(miRNA) from regulatory network analysis, and provide candidate drugs targeting the key genes using drug–gene interaction network and structural analysis. The results show that upregulated DEGs were mainly enriched in cell division, cell cycle, and innate immune signaling pathways. Downregulated DEGs were primarily concentrated in the cellular response to stress, lysosome, glycosaminoglycan catabolic process, and mature B cell differentiation. Regulatory network analysis revealed that hsa-miR-6792-5p, hsa-let-7b-5p, hsa-miR-34a-5p, hsa-miR-92a-3p, and hsa-miR-146a-5p were predicted biomarkers. *CDC25A*, *GUSB*, *MYBL2*, and *SDAD1* were identified as key genes in severe COVID-19. In addition, drug repurposing from drug–gene and drug–protein database searching and molecular docking showed that camptothecin and doxorubicin were candidate drugs interacting with the key genes. In conclusion, multi-level systems biology analysis plays an important role in precision medicine by finding novel biomarkers and targeted drugs based on key gene identification.

Keywords: severe COVID-19; systems biology; key genes; novel biomarkers; drug repurposing

2.2.1 INTRODUCTION

Nowadays, our world has experienced the coronavirus disease 2019 (COVID-19) pandemic, causing numerous morbid and mortal cases. The disease is caused by severe infection of acute respiratory syndrome coronavirus-2 (SARS-CoV-2). The virus is a positive-sense single-strand RNA β-coronavirus classified in the Coronaviridae family, which also consists of SARS-CoV and middle east respiratory syndrome coronavirus (MERS-CoV) [1]. These viruses all emerged within the first 20 years of the 21st century and caused numerous public health and economic issues. Comparative genomics studies have revealed that the SARS-CoV-2 genome resembles the SARS-CoV sequence, with 79% identity. In contrast, the MERS-CoV sequence shares only 50% identity with SARS-CoV-2's sequence [2]. Moreover, phylogenetic analysis using whole-genome sequences and phylogenetic tree construction by the neighbor-joining method reveals that SARS-CoV-2 is clustered in the sarbecovirus group and the virus is close to coronaviruses in bats and pangolins [2].

For the global statistics, the number of confirmed cases and deaths of COVID-19 from World Health Organization (WHO) data on 21 June 2022 were 537,591,764 and 6,319,395, respectively [3]. In addition, the global fatality rate is 3.4%. The rate is higher than seasonal flu but lower than SARS-CoV and MERS-CoV infections [4,5]. Despite the assumption that bats were hosts in this zoonotic infection, several studies have indicated that the disease occurred via an intermediate host such as pangolins [6,7]. The disease's main transmission route is receiving infectious respiratory droplets from direct person-to-person contact [8,9]. SARS-CoV-2 can spread in all stages of the disease: asymptomatic, presymptomatic, and symptomatic stages [6]. The median incubation period is approximately 5.1 days, and most people (97.5%) have symptoms within 11.5 days. Only 1% of patients develop symptoms after 14 days of quarantine [10]. The most common clinical features of COVID-19 are dry cough, fever, fatigue, and myalgia. Some patients have gastrointestinal symptoms, for instance, nausea, anorexia, and diarrhea [11–13]. Less common clinical presentations include sputum production, headache, and hemoptysis [11,12]. About 64% to 80% of patients present with anosmia or ageusia [14–16]. Furthermore, at least 50% of patients will progress to dyspnea [17]. Progressive dyspnea and hypoxemia usually develop approximately one week after the clinical onset [18]. Acute respiratory distress syndrome (ARDS), characterized by severe hypoxemia, and bilateral pulmonary edema that cannot be explained by cardiac causes or volume overload, is a condition mainly found in severe COVID-19 [18]. Several risk factors contributing to severe illness include older age, chronic lung diseases, cardiovascular diseases, diabetes mellitus, obesity, chronic kidney diseases, immunocompromised host, and cancers [12,18]. Nearly 17% to 35% of admitted patients needed intensive care units (ICU) due to respiratory failure. Approximately 29% to 91% of patients in ICU obtain mechanical ventilation [19–22]. The main causes of death are ARDS, acute respiratory failure, coagulopathy, septic shock, metabolic acidosis, cardiovascular complications, and multiple organ failure [23].

Pathogenesis and pathophysiology of COVID-19 are required for further studies. The disease is classified into two stages: early and late stages [9]. In the early stage, SARS-CoV-2 infects host cells and initiates proliferation. It enters respiratory epithelial cells and alveolar cells via using spike (S) protein, primed by host transmembrane

serine protease 2 (TMPRSS2), binding to host membrane receptors, for example, angiotensin-converting enzyme 2 (ACE2) [24,25]. While viral replication occurs, the immune system will proceed. Hence, mild constitutional symptoms arise in this stage. The innate immunity will recruit myeloid-lineage leukocytes such as macrophages, neutrophils, and natural killer (NK) cells to alveolar tissue [8]. In the late stage, pulmonary tissue damage and hyperinflammation emerge from excessive proinflammatory cytokine secreted from these leukocytes. Pneumocytes and alveolar endothelial cells are injured and dead, resulting in interstitial fluid leakage; therefore, pulmonary edema will occur and progress to ARDS later [24]. Accumulation of fluid in alveolar space and pneumocyte damage leads to impaired gas exchange, causing hypoxia and hypercapnia [24]. Furthermore, some patients will develop to hyperinflammation stage or cytokine storm caused by excessive proinflammatory cytokines such *as* interferon α (IFN-α), IFN- β, IFN-γ, interleukin 1β (IL-1β), IL-6, IL-12, IL-18, IL-33, and tumor necrosis factor α (TNF-α) [26]. Cytokine storm is characterized by cytokine overproduction causing collateral tissue damage [27]. Uncontrolled cytokine storms can lead to multiple organ dysfunction and failure in the last stage [27]. Severe COVID-19 cases usually die due to cytokine storms with multiple organ failures [28].

The gold standard diagnostic testing of COVID-19 is the reverse transcriptase-polymerase chain reaction (RT-PCR) from nasal and throat swab samples [29]. The specificity of PCR is nearly 100% if there are no contaminations. Antigen tests have benefits over PCR as they have lower costs and are used in the point-of-care setting, though they have sensitivity less than PCR [30,31]. Nevertheless, there are still no effective diagnostic testing or biomarkers used to predict the possibility of severe illness progression precisely. The primary treatment for COVID-19 is the best supportive care and respiratory support [23,24]. Medical therapies include anti-inflammatory agents using corticosteroids and antiviral treatments such as ritonavir and favipiravir [32–34]. In addition, the role of vaccines in COVID-19 prevention has been studied and needs further investigation. Although the current treatments improve the disease, they cannot cover all patients with severe conditions. As a result, discovering novel biomarkers and targeted drugs based on cytokine storm and impaired immune-associated key genes and proteins could play a crucial role in predicting and improving COVID-19 severity.

In the bioinformatics and precision medicine era, systems biology and multi-omics studies allow translational medicine to be effective in clinical practices [35]. Several combined wet and dry experimental studies have provided invaluable information in molecular biology and medicine [36–38]. Moreover, a combination of knowledge between biology, computer science, statistics, and mathematics explores the underlying molecular mechanisms of numerous diseases such as cancer, degenerative diseases, genetic diseases, etc. Structural information on protein-related SARS-CoV-2 such as S protein, main protease (M^{pro}), and papain-like protease (PL^{pro}), obtained from the Protein Data Bank (PDB), has also provided the details on physical protein interactions and benefits for identifying drug–protein interaction in COVID-19 via protein binding site analyses [39–45]. One of the most powerful tools used in bioinformatics is network analysis. With the use of network analysis, central node identification using various centrality measurements and community detection by several network clustering algorithms [46,47] have been widely used in much research. These approaches were successfully applied in several applications to identify key disease-related genes, disease–disease associations, disease–protein associations, and drug–disease associations [48–57]. Additionally, the benefit of the network analysis is drug repositioning or drug repurposing, characterized by discovering a new role of treatment from existing drugs based on the key disease-related genes identified from the biological network [58]. Structural bioinformatics also plays a vital role in drug repurposing via finding physical interactions between targeted proteins from PDB structures and drugs using molecular docking [59–61]. In addition, novel biomarkers can be recognized from the network analysis [62].

In this study, we proposed multi-level biological networks analysis, such as regulatory and protein–protein interaction (PPI) network, based on leukocyte transcriptomic profiles to identify novel biomarkers and key genes in severe COVID-19. Furthermore, drug repurposing was performed based on drug–gene and drug–protein interaction database searching and molecular docking. This study aims to discover

novel biomarkers and candidate targeted drugs to predict and treat severe COVID-19 at clinical levels by applying various biological data and networks.

2.2.2 MATERIALS AND METHODS

The overall process of identifying key genes, novel biomarkers, and candidate drugs using several levels of the biological network is summarized in Figure 11. All our proposed methods were dry experiments or in silico studies based on wet experimental data acquisition from databases. First, the leukocyte transcriptomic profiles from Gene Expression Omnibus (GEO) datasets [50] were downloaded to indicate an overall immune status in severe COVID-19 patients compared to controls. Common differentially expressed genes (DEGs) were identified by considering statistical criteria described in Section 2.1 Data Collection and Preprocessing. The functional enrichment analysis of upregulated and downregulated DEGs were conducted using Metascape [63]. Second, STRING v11.0 [64] was used to construct the PPI network based on the common DEGs. Network clustering was conducted using the Molecular Complex Detection (MCODE) plugin in Cytoscape [65]. The degree and betweenness centrality were calculated using Network Analyzer in Cytoscape to find hub and bottleneck genes in the PPI network. Additionally, the survival analysis from Gene Expression Profiling Interactive Analysis (GEPIA2) [66], using acute myeloid leukemia (LAML) as a cell type model, was operated to identify key genes from the hub and bottleneck genes. Third, MicroRNA Enrichment Turned Network (MIENTURNET) [67,68] was used to construct regulatory networks and identify novel biomarkers. Finally, drugs resulting from drug–gene and drug–protein interaction databases were studied by molecular docking.
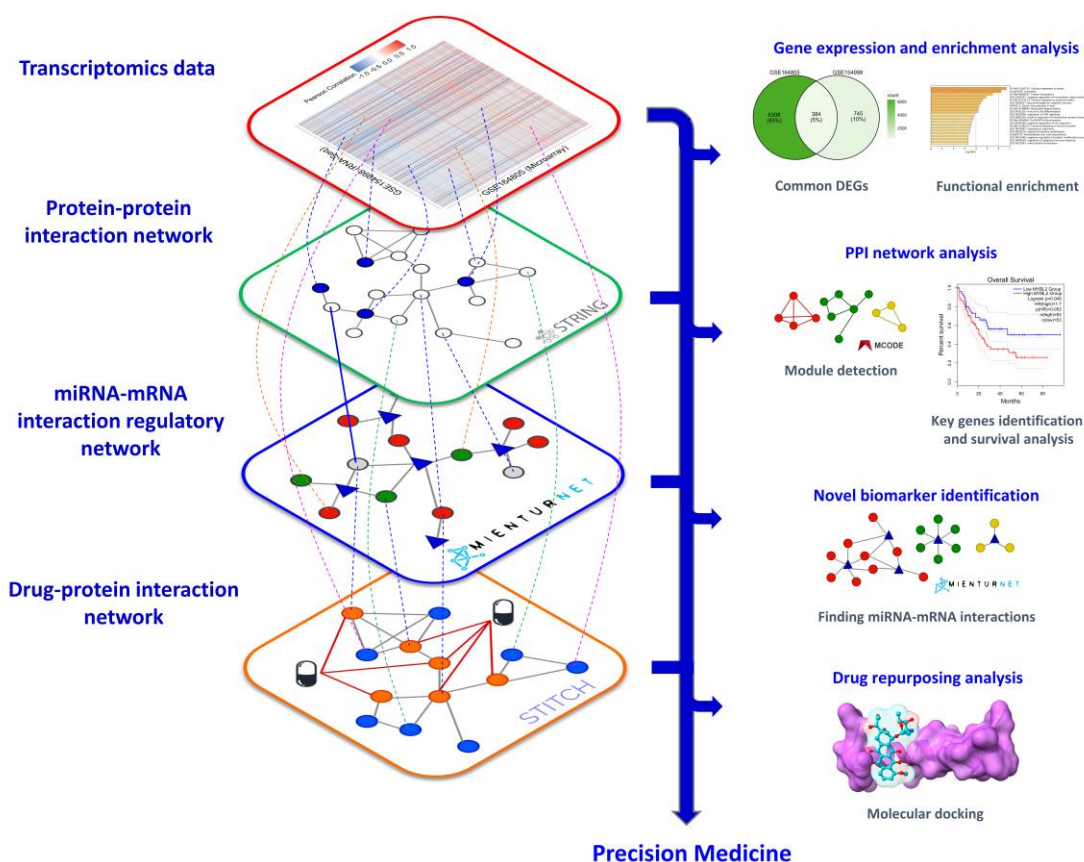
Figure 11. Diagram summarizes the process of identifying key genes, novel biomarkers, and candidate drugs using multi-levels of biological network analyses. There are four principal data and networks, including transcriptomics data, protein–protein interaction network, miRNA–mRNA interaction regulatory network, and drug–protein interaction network towards precision medicine.

2.2.2.1 DATA COLLECTION AND PREPROCESSING

Two gene expression datasets (GSE164805 and GSE154998) were downloaded from GEO DataSets (https://www.ncbi.nlm.nih.gov/geo/, accessed on 14 January 2022) [69]. Both datasets are leukocyte transcriptomic profiles collected from peripheral blood samples in severe COVID-19 patients compared to non-COVID-19 controls. The gene expression method in GSE164805 was conducted based on the microarray technique, while GSE154998 measured the transcriptomic profiles via the RNA sequencing (RNA-Seq) method [70,71]. The complete data sets, consisting of false discovery rate (FDR) *q*-value and log2fold change (log2 FC), were manipulated using R package 'dplyr' [72]. The DEGs were filtered based on genes expression having the FDR < 0.05 and absolute

log2 FC (|log2 FC|) > 1. DEGs that met the criteria in both data sets were common DEGs that were used for further analysis. Moreover, common DEGs with log2 FC > 1 and log2 FC < −1 were considered upregulated and downregulated DEGs, respectively.

2.2.2.2 FUNCTIONAL ENRICHMENT ANALYSIS BASED ON UP- AND DOWNREGULATED DEGs

Metascape (https://metascape.org/gp/index.html#/main/step1, accessed on 20 January 2022) [63] was performed for functional enrichment analysis of the upregulated and downregulated DEGs. Metascape is a web-based portal integrating functional enrichment, interactome analysis, gene annotation, and membership search from over 40 knowledgebases [63]. Functional and pathway terms used in the software include Gene ontology biological process (GO-BP) [73], Kyoto Encyclopedia of Genes and Genomes (KEGG) pathways [74], Reactome pathways [75], WikiPathways [76], Canonical [77], and CORUM pathway [78]. The functional enrichment analysis in the software was performed using a hypergeometric test and Benjamini–Hochberg statistical correction algorithm [63]. Enrichment terms with a significant level (FDR q-value < 0.01) were selected.

2.2.2.3 PPI NETWORK CONSTRUCTION FROM THE COMMON DEGs

STRING v11.0 (https://string-db.org/, accessed on 20 January 2022) [64], a protein interactome online database collecting a human interactome consisting of 19,556 proteins and 11,938,498 interactions, was performed to construct the PPI network without adjacent node expansion using the common DEGs as the input. The PPI network was built with an interaction confidence score greater than 0.400 (medium confidence). The confidence score of the interaction is the probability value calculated based on both experimental and computational evidence such as text mining, high-throughput experiments, co-expression and gene fusion data, and information from other databases. Furthermore, the PPI network was downloaded and exported to Cytoscape 3.9.0 (https://cytoscape.org/, accessed on 20 January 2022) [65], a biological network visualizing software.

2.2.2.4 TOPOLOGICAL AND NETWORK CLUSTERING ANALYSIS OF THE PPI NETWORK

In Cytoscape, the Network Analyzer plugin was performed to calculate global topological parameters, for instance, average degree, diameter, radius, average clustering coefficient, average shortest path length, and network density. Local topological parameters, such as degree, closeness, betweenness, and clustering coefficient, were also computed. Moreover, network clustering was conducted using MCODE plugin [79] in Cytoscape. The plugin was used by default settings, for example, a degree cut-off: 2, node score cut-off: 0.2, k-core: 2, and max depth: 100. An MCODE score cut-off for cluster selection was greater than 5.

2.2.2.5 REGULATORY NETWORK CONSTRUCTION AND NOVEL BIOMARKERS IDENTIFICATION

The gene sets in each MCODE cluster were inputted in MIENTURNET (http://userver.bio.uniroma1.it/apps/mienturnet/, accessed on 22 January 2022) [67], an online-based software, to construct microRNA (miRNA)–mRNA regulatory networks. The software was used to find miRNA–mRNA interactions based on miRTarBase, a miRNA-target database validated from experimental data [68]. miRNAs with interaction FDR q-value less than 0.05 were considered novel biomarkers in severe COVID-19.

2.2.2.6 IDENTIFICATION OF HUB AND BOTTLENECK GENES

Degree and betweenness centrality were measured using the Network Analyzer plugin in the Cytoscape to find the hub and bottleneck genes in the PPI network. Given a network called G, let A be a non-weight adjacency matrix of network G. Degree centrality (C_D) is the number of adjacent nodes interacting with interested node i, according to this equation

$$C_D(i) = \sum_j A_{ij} \, ,$$

(1)

where A_{ij} is a value of matrix A of node i and j, respectively. In biological networks, the high-degree nodes are hub genes playing a crucial role in the network function due to numerous interactions. Nodes in the PPI network having degree centrality greater than the 95th percentile were considered hub genes.

Betweenness centrality (C_B) is the summation of the ratio between the shortest path of node *u* and *v* that pass through node *i*. The betweenness centrality is calculated based on this equation

$$C_B(i) = \sum_{u \neq v \neq i} \frac{\sigma_{uv}(i)}{\sigma_{uv}}, \tag{2}$$

where σ_{uv} is a total number of the shortest path between node *u* and *v* and $\sigma_{uv}(i)$ is the number of the shortest path between node *u* and *v* that pass through node *i*. Nodes with betweenness more than 95th percentile were bottleneck genes in the PPI network. The bottleneck nodes play an important function in forming the bridges controlling the flow of information in the network.

2.2.2.7 FINDING KEY GENES USING SURVIVAL ANALYSIS

Because there is no powerful tool to validate and predict the gene essentiality in severe COVID-19 recently, we applied the cancer survival analysis to find key genes from the PPI network. The key genes in severe COVID-19 were identified based on the hub and bottleneck genes by using GEPIA2 (http://gepia2.cancer-pku.cn/#index, accessed on 25 January 2022) [66]. GEPIA2 provides the single gene essentiality in several cancer types by using survival and gene expression analysis based on The Cancer Genome Atlas (TCGA) [80] and Genotype-Tissue Expression (GTEx) data [81]. As earlier described, the myeloid-lineage leukocytes such as macrophages, neutrophils, and NK cells play a vital role in COVID-19-associated cytokine storm by releasing the excessive proinflammatory cytokines. Hence, LAML was used as a cell type model to find the key genes related to immune-induced severe COVID-19. The survival analysis was performed by the Kaplan–Meier method, which considers these parameters such as log-rank *p*-value and hazard ratio (HR) with 95% confidence interval.

2.2.2.8 DRUG REPURPOSING BASED ON THE KEY GENES

i. Drug–Gene and Drug–Protein Interaction Database Searching

The key genes were inputted to find targeted drugs in these drug–gene interaction databases, for example, DrugBank database (https://go.drugbank.com/, accessed on 30 January 2022) [82], Therapeutic Target Database (TTD) (http://db.idrblab.net/ttd/, accessed on 30 January 2022) [83], Comparative

Toxicogenomics Databases (CTD) (http://ctdbase.org/, accessed on 30 January 2022) [84], and GeneCards (https://www.genecards.org/, accessed on 30 January 2022) [85]. The selected drugs were confirmed the interaction significance using the STITCH v5.0 database (http://stitch.embl.de/, accessed on 30 January 2022) [86], a drug–protein interaction database, by considering a confidence score greater than 0.400 (medium confidence). The confidence score is calculated based on both experimental and computational evidence, similar to the STRING database. Drugs that met the criteria were considered candidate-targeted drugs.

ii. Molecular Docking of Potential Drugs against B-Myb

Molecular docking was performed to elucidate the interaction between drug candidates and a target protein named B-Myb. This protein is encoded from *MYBL2*, an essential gene in the network analysis. The crystal structure of B-Myb was received from PDB (https://www.rcsb.org/, accessed on 12 June 2022) [87] using PDB ID: 6C48 from the study [88]. The function of B-Myb is activated via binding between the LXXLL motif located in the B-Myb transactivation domain and the KIX domain of coactivator p300 to form a transcriptional module [89–92]. Thus, the motif containing L688, R687, G686, L685, and L684 residues was set as the binding site. Several studies have shown that plumbagin, a natural naphthoquinone binding at this motif, can cause B-Myb/p300 interaction interference [93–95]*;* therefore, plumbagin was used as a reference ligand in the docking study to compare with candidate drugs such as doxorubicin and camptothecin. The three compounds were individually docked into B-Myb using HDOCK server (http://hdock.phys.hust.edu.cn/, accessed on 12 June 2022) [96] and AutoDock VinaXB, a docking program using a genetic algorithm [97]. The ionized states of B-Myb were configured at pH 7.4 using PROPKA3.1 [98], while ChemAxon [99] was used to check the pKa value of the compounds. The binding affinity of the candidate drugs was calculated and compared to plumbagin. The 3D and 2D structures demonstrating the drug–protein interactions were visualized using the UCSF Chimera package [100] and the LigPlot [101].

2.2.3 RESULTS

2.2.3.1 IDENTIFICATION OF COMMON DEGs

The common DEGs were filtered from the transcriptomics data based on microarray and RNA-Seq dataset (see Material and Methods) by considering FDR q-value < 0.05 and |log2 FC| > 1. There were 6692 and 1129 DEGs found by microarray technique and RNA-Seq technology, respectively. Figure 12a displays the Venn diagram representing the common DEGs from both datasets. In total, 384 common DEGs were identified, having 39 upregulated and 221 downregulated DEGs; however, the remaining common DEGs (124 genes) had both upregulation and downregulation because their expression pattern was contradictory between the two datasets. Figure 12b shows the correlation heatmap of the common DEGs between the two datasets. The gene list of the common DEGs is shown in Table S1 in Supplementary Materials.
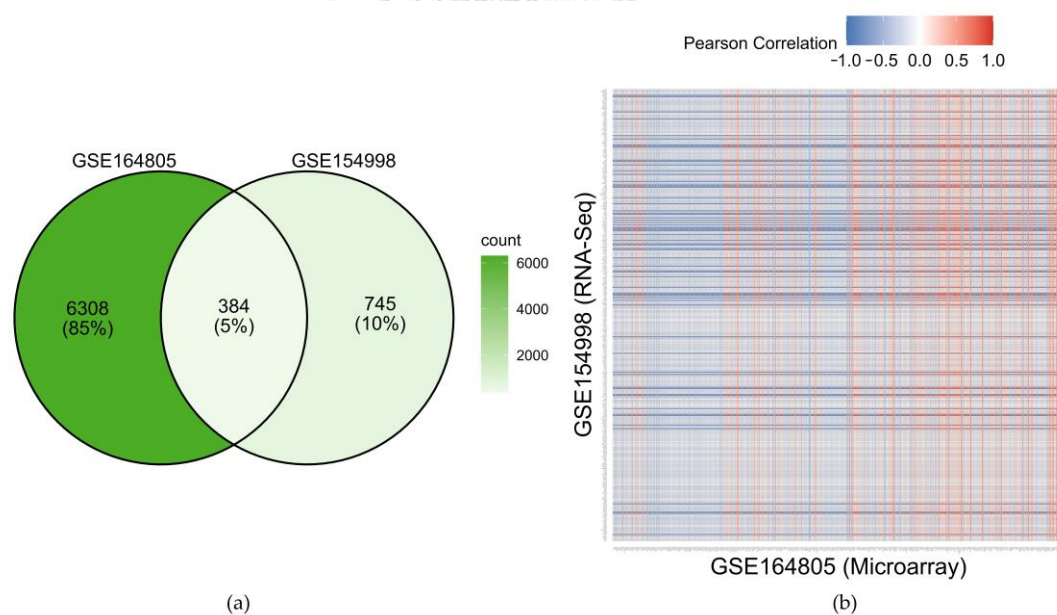
Figure 12. Identifying the common DEGs between the two transcriptomic GEO datasets (GSE164805 and GSE154998). (**a**) Venn diagram of the DEGs found in the datasets. (**b**) Correlation heatmap of the common DEGs between the two datasets.

2.2.3.2 FUNCTIONAL ENRICHMENT ANALYSIS OF UP- AND DOWNREGULATED DEGs

The functional enrichment analysis using Metascape of the DEGs is shown in Figure 13. In the upregulated DEGs, the terms were primarily enriched relevantly to viral

innate immune response and cell cycle regulation (Figure 13a). For instance, IFN-α and IFN-β were type I IFN (IFN-I) predominant in the viral innate immune response. In addition, anaphase-promoting complex/cyclosome (APC/C), a cell cycle regulator complex, and chromosome segregation were enhanced in leukocytes during severe COVID-19. Other increased functional terms, such as regulation of binding and endopeptidase activity, were also found in the upregulated DEGs. Moreover, the functional enrichment in the downregulated DEGs was mainly associated with cellular response to stress, lysosome, protein localization (the processes establishing and maintaining proteins at specific locations), glycosaminoglycan catabolic pathway, mature lymphocyte differentiation, positive regulation of intracellular protein transportation, negative regulation of protein modification, response to hyperoxia, and adaptive immune response (Figure 13b).
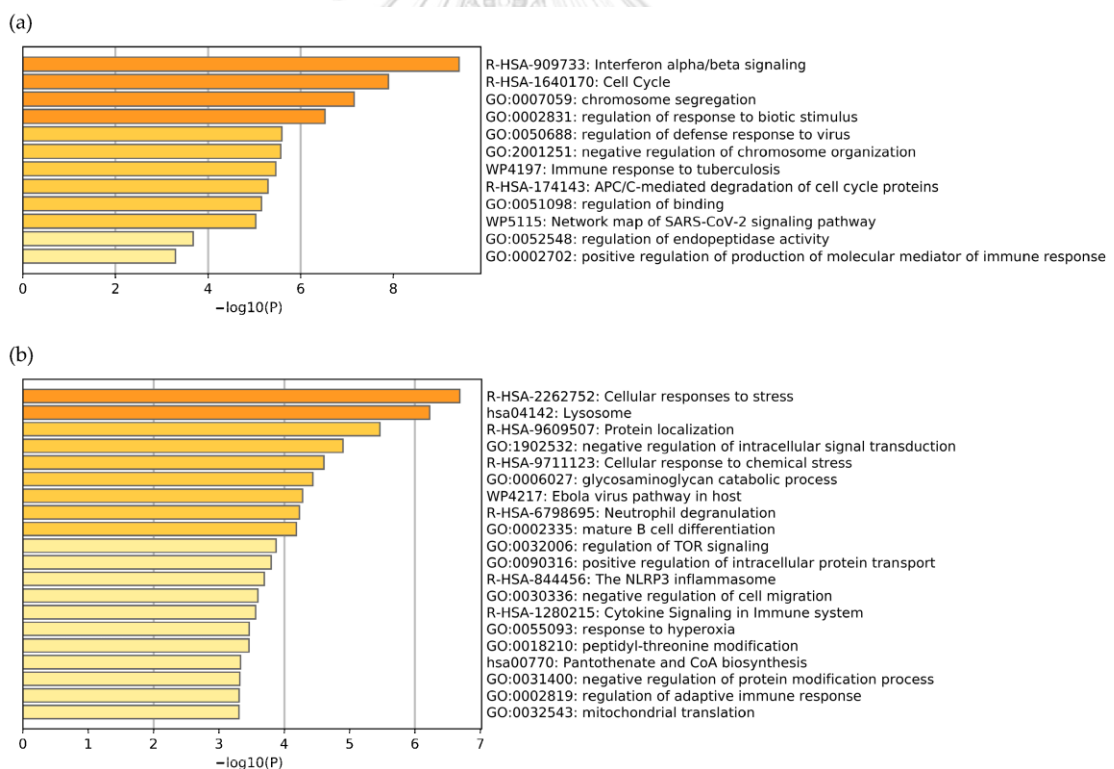
Figure 13. The bar graph represents the enrichment terms analyzed from (**a**) the upregulated DEGs and (**b**) the downregulated DEGs at a significant level (FDR < 0.01). Each enrichment term is colored based on the significance level.

2.2.3.3 PPI NETWORK CONSTRUCTION, TOPOLOGICAL ANALYSIS, AND CLUSTER DETECTION

From the PPI network construction without the neighboring node expansion via STRING v11.0, there were 85 components with 384 nodes and 861 edges. The largest component containing 288 nodes and 848 edges was extracted for topological analysis and identifying clusters and key genes. The edge list information for the component is also provided in Table S2 in Supplementary Materials. Global topological parameters calculated from the Network Analyzer plugin in Cytoscape are illustrated in Table 5. Moreover, local topological parameters in each node in the network are summarized in Table S3 in Supplementary Materials.

Table 5. Global Topological Parameters of the PPI network.

Symbol	Description	Value
N	Number of nodes	288
M	Number of edges	848
$<k>$	Average degree	5.89
d	Diameter	11
r	Radius	7
$mspl$	Mean shortest path length	4.33
D	Density	0.02
acc	Average clustering coefficient	0.28

The largest network visualized by STRING v11.0 is shown in Figure 14. The results analyzed by the STRING revealed that the average node degree, expected number of edges, and average local clustering coefficient were 5.89, 544, and 0.461, respectively. Additionally, a PPI enrichment p-value was less than 10^{-16}, indicating that the proteins have interactions with each other more than by chance.
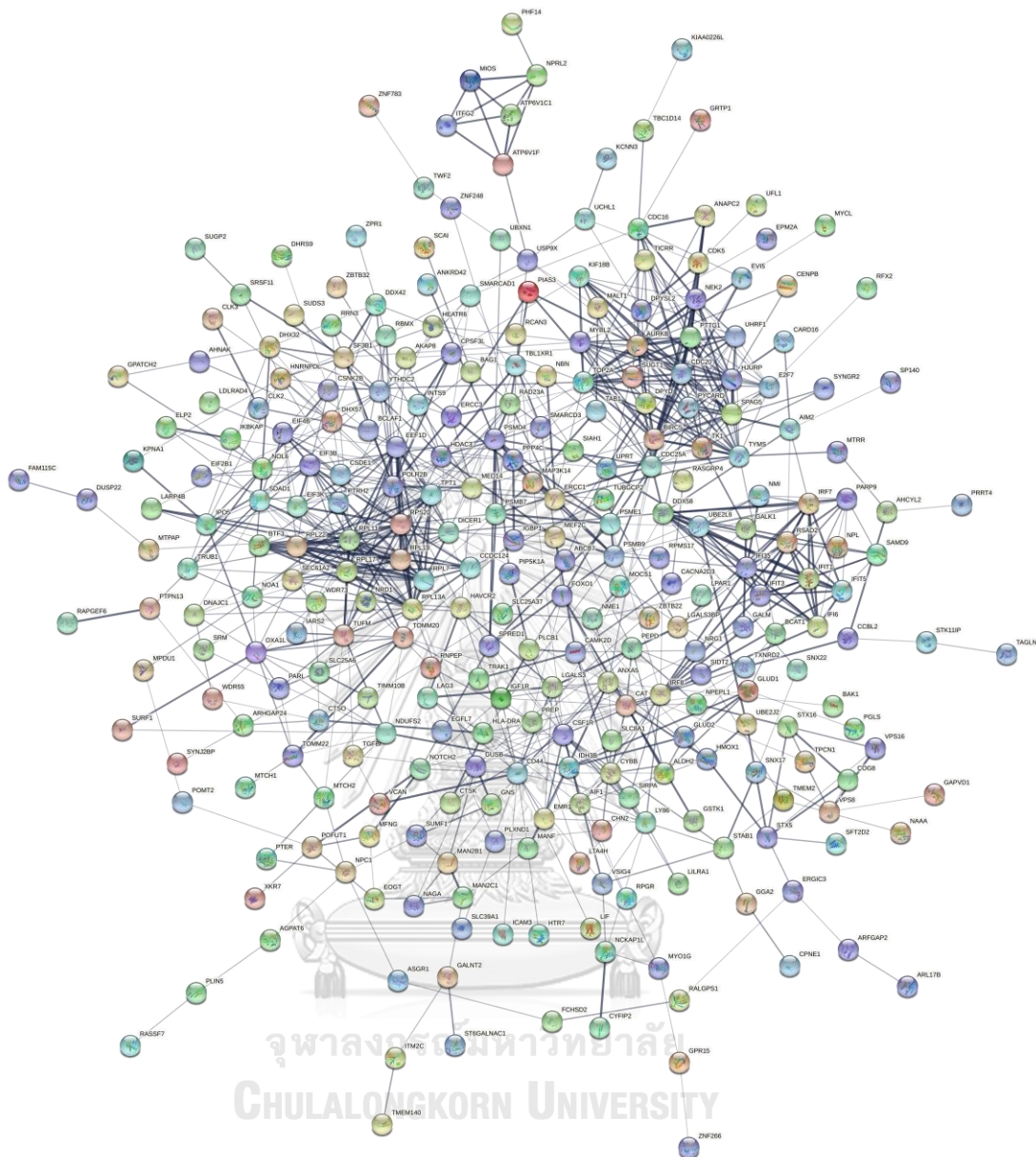
Figure 14. The largest component of the PPI network constructed from the common DEGs visualized by STRING v11.0 with the interaction confidence score > 0.400 (medium confidence). The network consists of 288 nodes and 848 interactions.

The network probably provided the small-world effect, such as several biological networks, because it had a low value of the mean shortest path length ($mspl$ = 4.33) even though there was a moderate average clustering coefficient (acc = 0.28). Furthermore, the degree distribution plot illustrated in Figure 15a shows the power-law property, indicating the strong negative association between logarithmic scales of degree and its probability (R^2 = 0.86). On the other hand, the clustering coefficient

versus degree plot (Figure 15b) shows no relationship between the clustering coefficient and degree (R^2 = 0.12). These behaviors suggested that the network had scale-free properties.

(a) (b)
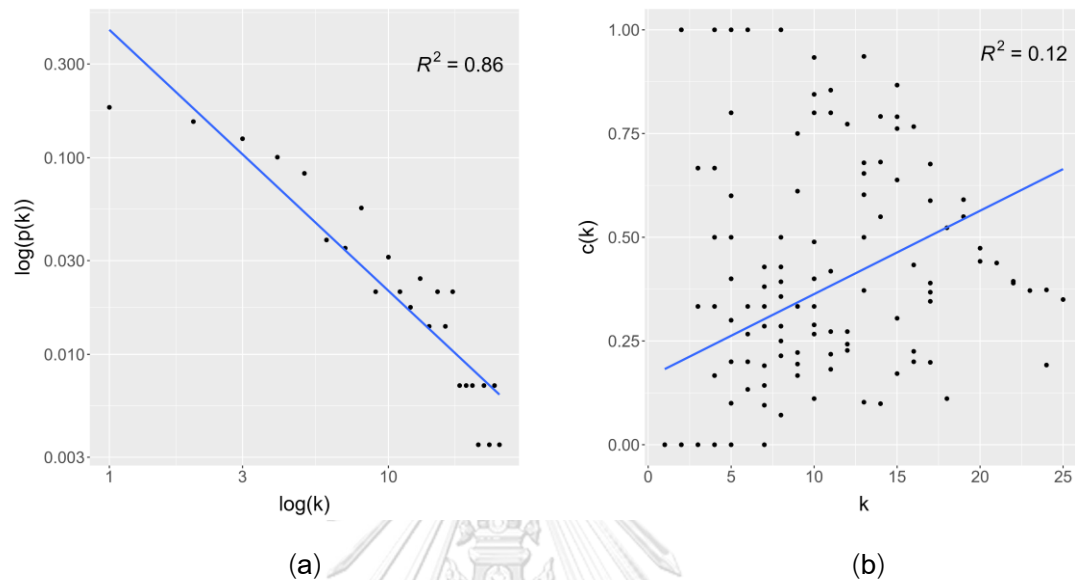
Figure 15. Topological analysis of the PPI network. (**a**) Degree distribution plot. (**b**) Clustering coefficient versus degree plot. k denotes the degree; $p(k)$ denotes the probability of degree k; $c(k)$ denotes the clustering coefficient of a node that has degree k.

There were three clusters identified from the MCODE plugin with the score of more than 5: MCODE 1, 2, and 3. Topological parameters of the clusters were described in Supplementary Table S4. Most MCODE 1 and 3 cluster members were upregulated DEGs, while MCODE2's cluster members were downregulated DEGs. Functional enrichment results of each cluster are illustrated in Table 6 and Supplementary Figure S1. For instance, MCODE 1 (Figure 16a) is enriched in the cell cycle and division regulation process, while MCODE 2 (Figure 16b) is concentrated in the translation process and transactivation response element RNA-binding protein (TRBP). Moreover, MCODE 3 (Figure 16c) is associated with an innate immune response.

(a)   (b)   (c)
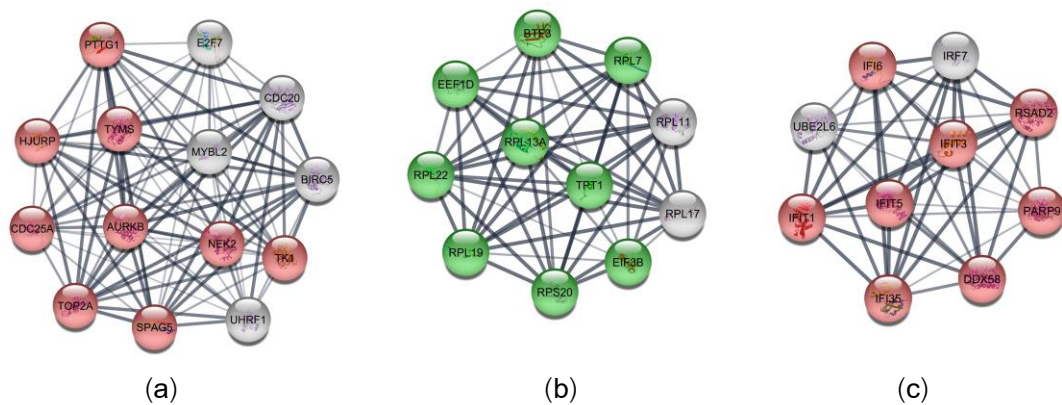
Figure 16. Cluster detection of the PPI network using MCODE plugin in Cytoscape 3.9.0.
(**a**) MCODE 1 had 14 nodes and 89 edges. (**b**) MCODE 2 had 11 nodes and 53 edges.
(**c**) MCODE 3 had 10 nodes and 45 edges. The red and green nodes represent
upregulated and downregulated DEGs. In contrast, gray nodes represent genes having
both upregulation and downregulation.

Table 6. Functional enrichment analysis of the MCODE clusters using Metascape.

Cluster	Cluster Score	Term ID	Biological Term	Count	Log10 (q-value)
MCODE1	13.692	R-HSA-1640170	Cell cycle	11	−11.20
		GO:0007059	Chromosome segregation	7	−6.85
		M40	PID E2F pathway	5	−6.28
		GO:1903047	Mitotic cell cycle process	7	−5.60
MCODE2	10.600	R-HSA-156842	Eukaryotic translation elongation	8	−13.67
		R-HSA-72766	Translation	9	−12.97
		CORUM:5380	TRBP containing complex (DICER, RPL7A, EIF6, MOV10, and subunits of the 60S ribosomal particle)	3	−4.38
MCODE3	10.000	R-HSA-913531	Interferon signaling	9	−14.37
		GO:0051607	Defense response to virus	8	−11.52
		WP4197	Immune response to tuberculosis	3	−3.91
		GO:0002831	Regulation of response to biotic stimulus	3	−3.91

2.2.3.4 FINDING POTENTIAL miRNAs AS NOVEL BIOMARKERS IN REGULATORY NETWORKS

Figure 17 illustrates miRNA–mRNA interaction networks constructed based on the three MCODE clusters. The interactions were statistically significant at FDR q-value < 0.05. There were five novel candidate biomarkers analyzed from the regulatory networks, for instance, hsa-miR-6792-5p, hsa-let-7b-5p, hsa-miR-34a-5p, hsa-miR-92a-3p, and hsa-miR-146a-5p. The further statistical and interaction data of regulatory networks in MCODE 1, 2, and 3 are explained in Figure S2 and Tables S5–S7 in Supplementary Materials. There were three miRNAs interacting with the mRNAs in MCODE 1 (Figure 17a): hsa-miR-6792-5p, hsa-let-7b-5p, and hsa-miR-34a-5p. In addition, hsa-miR-92a-3p and hsa-miR-146a-5p interacted with the mRNAs in MCODE 2 and 3, respectively. miRNA regulates gene expression via mRNA binding and increases mRNA degradation or activation [102,103]. A change in miRNA levels can indicate gene expression status; therefore, miRNA measurement can be applied to predict severe COVID-19 based on the effect on gene expression patterns.

(a)   (b)   (c)
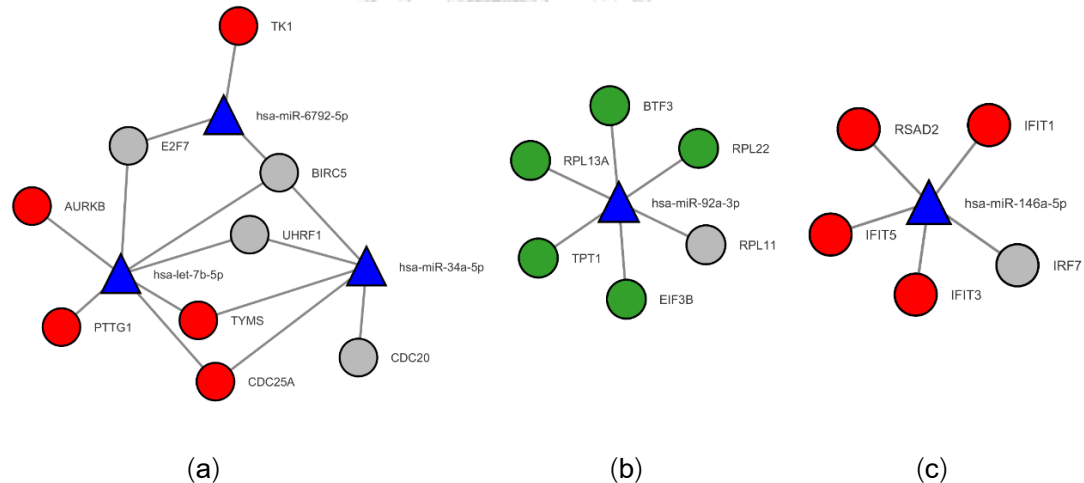
Figure 17. miRNA–mRNA interaction regulatory networks based on MCODE clusters from the PPI network. The networks were bipartite graphs. The regulatory network of (**a**) MCODE 1 had 12 nodes and 15 edges, (**b**) MCODE 2 had 7 nodes and 6 edges, and (**c**) MCODE 3 had 6 nodes and 5 edges. The blue triangular nodes are miRNAs. The red and green circular nodes represent upregulated and downregulated DEGs, respectively. In comparison, gray nodes represent genes having both upregulation and downregulation.

2.2.3.5 KEY GENES IDENTIFICATION AND SURVIVAL ANALYSIS

There were 19 and 15 genes being hub and bottleneck, respectively. Tables S8 and S9 in Supplementary Materials reveal topological parameters of the hub and bottleneck genes, such as degree, betweenness, closeness, and clustering coefficient. Furthermore, Figure S3 in Supplementary Materials shows a Venn diagram of nodes being the hub and bottleneck genes. Seven genes were both hub and bottleneck: *AURKB*, *CD44*, *CDC25A*, *DDX58*, *DICER1*, *POLR2B*, and *RPL7*. Table 7 displays the biological function of the hub and bottle genes. Most hub genes were involved in cell proliferation and differentiation, such as cell cycle regulation, hematopoiesis, antiapoptotic process, DNA replication and transcription, and ribosomal synthesis. Additionally, the bottleneck genes in the PPI network mainly play an essential role in inflammation, antiviral and innate immune activation, oxidative stress prevention, and biomolecule metabolisms, for instance, lymphocyte and macrophage activation, viral recognition, mitochondrial protein transportation, protein and glycosaminoglycan degradation, and heme catabolism.

Table 7. Summary of the biological functions of 27 genes which were hub or bottleneck.

Symbol	Description	High Centrality	Biological Function
ANXA5	Annexin A5	bottleneck	Inflammation, growth, and differentiation
AURKB	Aurora Kinase B	hub, bottleneck	Cell cycle regulation
BIRC5	Baculoviral IAP Repeat Containing 5	hub	Antiapoptotis
CAT	Catalase	bottleneck	Oxidative stress prevention
CD44	Cluster of Differentiation 44	hub, bottleneck	Hematopoiesis and lymphocyte activation
CDC20	Cell Division Cycle 20	hub	Cell cycle regulation
CDC25A	Cell Division Cycle 25A	hub, bottleneck	Cell cycle regulation

Table 7. *Cont.*

Symbol	Description	High Centrality	Biological Function
CSF1R	Colony Stimulating Factor 1 Receptor	bottleneck	Macrophage differentiation
DDX58	DExD/H-Box Helicase 58	hub, bottleneck	Viral dsRNA recognition
DICER1	Ribonuclease III	hub, bottleneck	Small RNA production and antiviral agent
EEF1D	Eukaryotic Translation Elongation Factor 1 Delta	hub	Transport tRNAs to ribosome
GUSB	Glucuronidase Beta	bottleneck	Glycosaminoglycan degradation
HMOX1	Heme Oxygenase 1	bottleneck	Heme catabolism
MYBL2	MYB Proto-Oncogene Like 2	hub	Cell cycle regulation
POLR2B	RNA Polymerase II Subunit B	hub, bottleneck	DNA transcription
PSMD4	Proteasome 26S Subunit Ubiquitin Receptor, Non-ATPase 4	bottleneck	Protein degradation
RPL7	Ribosomal Protein L7	hub, bottleneck	A protein component in ribosomes
RPL11	Ribosomal Protein L11	hub	A protein component in ribosomes
RPL13A	Ribosomal Protein L13a	hub	A protein component in ribosomes
RPL17	Ribosomal Protein L17	hub	A protein component in ribosomes
RPL19	Ribosomal Protein L19	hub	A protein component in ribosomes

Table 7. *Cont.*

Symbol	Description	High Centrality	Biological Function
RPS20	Ribosomal Protein S20	hub	A protein component in ribosomes
SDAD1	SDA1 Domain Containing 1	hub	Ribosomal production and transportation
TOMM20	Translocase Of Outer Mitochondrial Membrane 20	bottleneck	Mitochondrial protein transportation
TOP2A	DNA Topoisomerase II Alpha	hub	DNA replication and transcription
TYMS	Thymidylate Synthetase	hub	DNA replication and repair
USP9X	Ubiquitin Specific Peptidase 9 X-Linked	bottleneck	Similar to ubiquitin-specific proteases

IAP, inhibitor of apoptosis protein; dsRNA, double-strand RNA; tRNA; MYB, myeloblastosis; SDA1, severe depolymerization of actin protein 1

The survival analysis using GEPIA2 based on the LAML model in the TCGA database of the 27 hub and bottleneck genes revealed that only *MYBL2* provided significant overall survival (log-rank p-value < 0.05) and a high hazard ratio (HR = 1.7); however, there were three genes that were nearly significant overall survival and high hazard ratio, for example, *CDC25A* (log-rank p-value = 0.064 and HR = 1.7), *GUSB* (log-rank p-value = 0.057 and HR = 0.58), and *SDAD1* (log-rank p-value = 0.082 and HR = 1.6). Figure 18 displays Kaplan–Meier overall survival analysis of the significant and almost significant genes. The overall survival analysis of other hub and bottleneck genes is illustrated in Figure S4 in Supplementary and Materials.
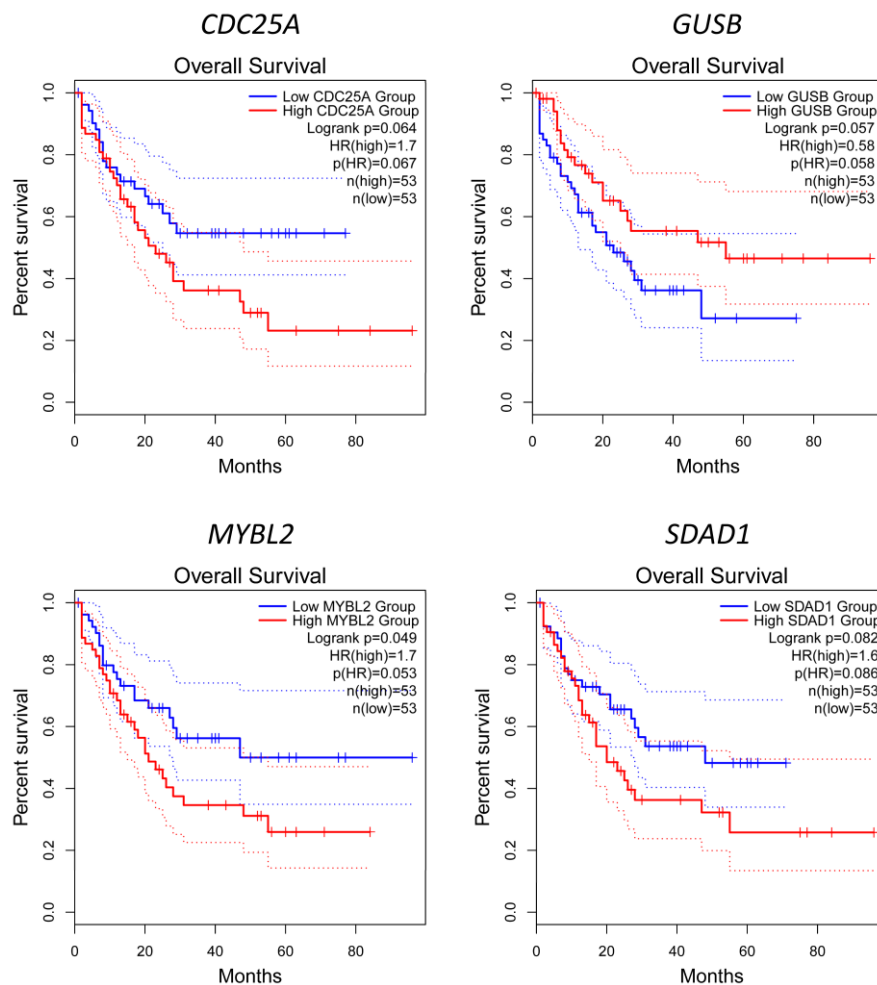
Figure 18. Kaplan–Meier overall survival analysis of the hub and bottleneck genes with significant or almost significant log-rank p-value: *CDC25A*, *GUSB*, *MYBL2*, and *SDAD1*. The curves were plotted using Gene Expression Profiling Interactive Analysis (GEPIA2). Acute myeloid leukemia (LAML) from The Cancer Genome Atlas (TCGA) database was used as a cell type model to find key survival genes in cytokine storm-related myeloid cells such as neutrophils, monocytes, and macrophages.

2.2.3.6 FINDING CANDIDATE TARGETED DRUGS

MYBL2, the significant key gene obtained from the survival analysis, was inputted to the drug–gene interaction databases: DrugBank database [82], TTD [83], CTD [84], and GeneCards [85]. The almost significant key genes, such as *CDC25A*, *GUSB*, and *SDAD1*, were also used to find drug–gene interactions. The result showed 35 FDA-approved drugs interacting with the key genes, as illustrated in Table S10 in Supplementary Materials. STITCH v5.0 database [86] was used to confirm the result

from the search. *MYBL2* was the only key gene having drug–protein interaction. The STITCH result revealed that doxorubicin and camptothecin interact with MYBL2, as shown in Figure 19.

Figure 20 displays the molecular docking results of the studied compounds binding to the LXXLL motif by the HDOCK webserver (Figure 20a) and AutoDock VinaXB (Figure 20b). The former program showed that either plumbagin or candidate drugs interacted with the three crucial residues associated with the motif, i.e., L685, R687, and L688. Through the interaction with the active site of B-Myb, doxorubicin and camptothecin produced an HDOCK score of -119.59 and -88.15 kcal mol^{-1}, relatively outperforming plumbagin's (-64.19 kcal mol^{-1}). The strong binding affinity of doxorubicin was supported by two hydrogen bonds formed with the two positively charged residues, R682 and R687. Conversely, only one hydrogen bond binding to residue R687 was detected in the reference ligand and camptothecin. The obtained data were in accordance with the AutoDock VinaXB results. All compounds can bind to the critical residues L685, R687, and L688 with binding affinities of -4.1, -5.6, and -5.5 kcal mol^{-1} for plumbagin, doxorubicin, and camptothecin, respectively. Again, there were hydrogen bonds between the candidate drugs and B-Myb through R682 and R687 residues. In contrast, no hydrogen bond formation was identified in the case of the reference ligand.
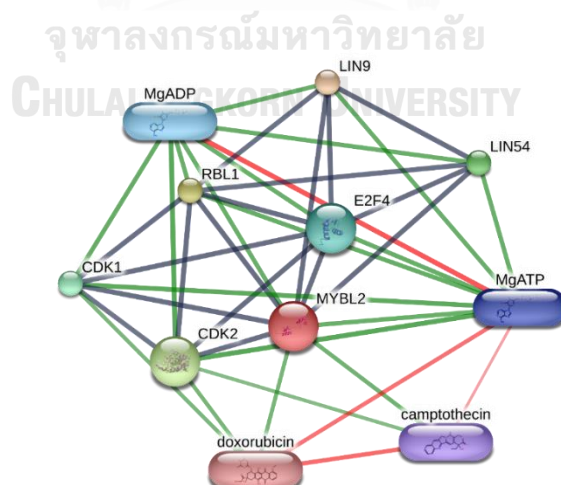
Figure 19. Drug–protein interaction network of the candidate drugs targeting MYBL2 resulted from STITCH v5.0. The black, green, and red edges represent protein–protein, drug–protein, and drug–drug interactions.
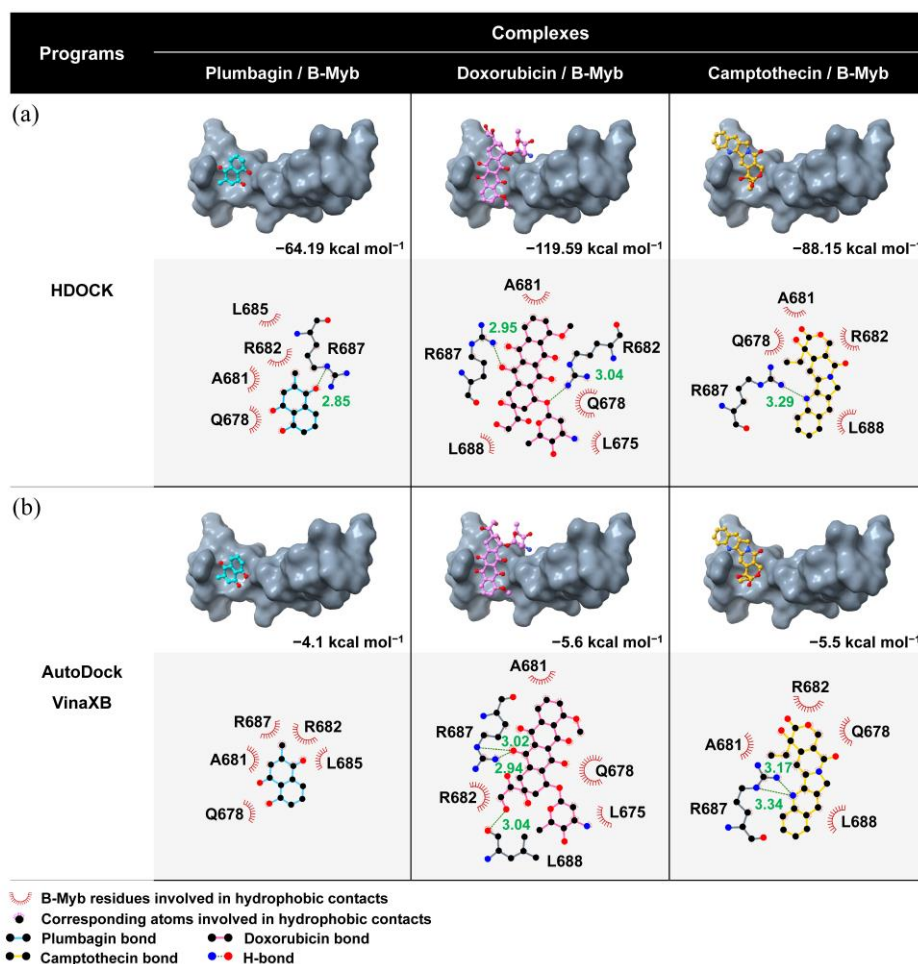
Figure 20. Binding orientation and interaction of the two focused drug candidates with the LXXLL motif of B-Myb compared to plumbagin/B-Myb complex via (**a**) HDOCK webserver and (**b**) AutoDock VinaXB. HDOCK scores and binding affinities of all complexes are also shown.

2.2.4 DISCUSSION

Finding novel biomarkers, key genes, and candidate targeted drugs is necessary to predict, treat, and follow severe COVID-19 patients. This study conducted various types of biological network analysis, such as regulatory and protein–protein interaction networks, based on common DEGs from microarray data and RNA-Seq data for the transcriptomics data of severe COVID-19 patients. The functional enrichment analysis of the upregulated and downregulated DEGs was operated to discover the disease's underlying molecular mechanisms. We also detected a network community in the PPI network. Novel biomarkers were discovered via miRNA identification in the

regulatory networks constructed based on the MCODE modules. In addition, the key genes in the PPI network were found by finding the hub and bottleneck nodes using degree and betweenness centrality measurement and were validated by the overall survival analysis of the LAML model. Finally, drug repurposing was performed by drug–gene and drug–protein interaction database searching, and molecular docking based on the key genes.

We identified 384 common DEGs that met the two datasets, and the number of upregulated and downregulated genes were 39 and 221, respectively. The remaining 124 DEGs had both upregulation and downregulation. The functional enrichment result of the upregulated DEGs revealed that the terms were generally involved in antiviral and innate immune response and cell cycle regulation. The processes and pathways were concordant with immune responses to infectious diseases. In host response to infections, immune-related, inflammatory-related, and leukocyte proliferation and differentiation genes are overexpressed to eradicate pathogens [104–107]; however, excessive immune and inflammatory responses can cause uncontrolled self-tissue injury, leading to severe complications and increased morbid and mortal cases. Furthermore, the enrichment analysis of the downregulated DEGs mainly concentrated in the cellular response to stress, lysosome, mature lymphocyte differentiation, negative regulation of protein modification, glycosaminoglycan catabolic pathway, response to hyperoxia, and adaptive immune response. Numerous studies have shown that impaired lymphocyte differentiation and adaptive immune activation are found in severe COVID-19, resulting in delayed viral clearance and persistent proinflammatory cytokine release [108–112]. ARDS and severe pneumonia are also found in severe COVID-19, causing hypoxia. Hence, genes related to the hyperoxia response were downregulated. In addition, negative protein modification regulation expression was reduced to increase the proinflammatory cytokine and antiviral protein production and release. Decreased glycosaminoglycan degradation can promote SAR-CoV, MERS-CoV, and SARS-CoV-2 to infect host cells. For example, some studies have revealed that the viruses use S protein binding with heparan sulfate proteoglycans (HSPGs) to enter the host cells in the disease's early stage [113–116].

The PPI network constructed by the STRING database based on the common DEGs, same as other biological networks, had the scale-free property. The scale-free property was proved by the strong relationship between degree and degree probability in degree distribution and the independence of the clustering coefficient and degree. Furthermore, the network likely provided the small-world effect because it had a low average shortest path length and moderate average clustering coefficient. The PPI network cluster detection using the MCODE algorithm showed three clusters with high MCODE scores: MCODE 1, 2, and 3. MCODE 1 was the upregulated gene cluster mainly enriched in cell proliferation and cell cycle. MCODE 2, the downregulated gene set, was primarily concentrated in ribosomal synthesis and protein translation regulation. Furthermore, MCODE 3 was centered on antiviral and innate immune responses; therefore, the enrichment terms of each cluster were according to the terms found in upregulated and downregulated DEGs.

The regulatory networks from the MCODE clusters showed that five miRNAs, hsa-miR-6792-5p, hsa-let-7b-5p, hsa-miR-34a-5p, hsa-miR-92a-3p, and hsa-miR-146a-5p, were the novel candidate biomarkers. hsa-miR-6792-5p, hsa-let-7b-5p, and hsa-miR-34a-5p interacted upregulated mRNAs related to cell proliferation and differentiation in MCODE 1 cluster. In MCODE 2, downregulated mRNAs involved in protein translation regulation were associated with hsa-miR-92a-3p. Moreover, hsa-miR-146a-5p interacted with upregulated antiviral and innate immune mRNAs in MCODE 3. miRNAs are small, non-coding RNAs that play an essential role in controlling gene expression via binding mRNA and then increase mRNA cleavage or translation dependent on their properties [103,117]. miRNAs also have a role in clinical applications such as diagnostic markers and therapeutic targets [118,119]. Because miRNAs are stable and detectable in serum and plasma, they are applied as biomarkers for diagnosis [120]. Several studies have revealed miRNA expression based on viral proteins, host membrane receptors, and proinflammatory cytokines [121–124]; however, no study has reported the relationship between the five miRNAs acquired from the regulatory network analysis and COVID-19. Thus, they could play a crucial role in novel diagnostic biomarkers and therapeutic agents in severe COVID-19 and further investigation of their roles should be needed.

There were 27 hub or bottleneck genes from high degree and betweenness value selection. The hub genes were mainly involved in cell proliferation and differentiation, while the bottleneck genes were focused on antiviral and innate immune responses. We also found the four key genes, such as *CDC25A*, *GUSB*, *MYBL2*, and *SDAD1*, from the overall survival analysis based on the LAML model. CDC25A is a cell cycle and apoptosis regulator that plays a vital role in many cancers' progression, for example, breast, esophageal, lung, colorectal, prostate, and ovarian cancer [125,126]. Furthermore, in viral infection, a study performing Sendai virus-infected cell line showed that upregulated *CDC25A* suppressed IFN-β activation while knockdown of *CDC25A* increased IFN-β stimulation [127]. The result suggested that CDC25A could participate in impaired viral innate immunity and increase viral survival. GUSB is a hydrolase enzyme for glycosaminoglycan degradation [128]. As described earlier, declined glycosaminoglycan degradation can promote the coronaviruses to enter the host cells. As a result, GUSB can play a central role in COVID-19 progression. B-Myb, encoded from *MYBL2*, is a transcription factor in the MYB family that plays an essential role in cell proliferation, differentiation, apoptosis, and tumorigenesis [129]. It is used as a prognostic marker in many cancer types, such as hepatocellular carcinoma, gallbladder, colorectal, and breast cancer [130–133]. Interestingly, a weighted gene co-expression network analysis in the COVID-19 study reported that *MYBL2* was one of 52 hub genes from the network analysis [134]. This result suggested the important role of *MYBL2* in numerous biological networks. There are a few studies on the role of SDAD1. It probably plays a role in ribosomal biogenesis and tumorigenesis [135]. There is no report about a relationship between its expression and COVID-19. Hence, further studies on the biological roles of SDAD1 are needed.

The candidate targeted drug discovery came from searching in the four drug–gene interaction databases and the drug–protein interaction database based on the four key genes. The result indicated that doxorubicin and camptothecin had interacted with MYBL2. The drug–protein interactions can be investigated by molecular docking. *No 3D structure of B-Myb in complex with known inhibitor is currently available.* The involvement between the key residues and binding site in B-Myb's LXXLL motif, a multifunctional binding sequence in transcriptional regulation [136], was reported [93–

95]. The B-Myb activity was inhibited by blocking the KIX domain of the B-Myb interaction partner, which was p300 [89], through natural [137–139] and small compounds [140]; however, identifying compounds that inhibit directly on B-Myb rather than p300 has not been revealed. In this work, the molecular docking results from the HDOCK webserver and AutoDock VinaXB showed that the two drug candidates, doxorubicin and camptothecin, had physical interactions with B-Myb. This evidence was supported by a reduction in cell proliferation in cancer cell lines having *MYBL2* overexpression without proving apparent mechanisms [141,142]. We then proposed the possible mechanism from our study that their direct interactions with B-Myb could be involved in the decreased cellular activity of upregulated *MYBL2* cells. Additionally, the candidate drugs demonstrated binding interaction and susceptibility with B-Myb significantly greater than plumbagin, the reference ligand; therefore, doxorubicin and camptothecin could be potential candidates to combat COVID-19.

There is other evidence to support that the candidate drugs could play an important role in severe COVID-19 treatment. Doxorubicin is a chemotherapeutic agent treating various types of cancer [143]. A study of structural bioinformatics revealed that doxorubicin proved the significant binding energy with SARS-CoV-2 main protease in the molecular docking [144]. This result suggested that doxorubicin could be a potential drug to treat severe COVID-19. Camptothecin is a natural product extracted from the Chinese happy tree (*Camptotheca acuminata*) [145]. It is used as a chemotherapeutic agent in cancer treatment by inhibiting DNA replication [146,147]. Camptothecin also has antiviral activity by inhibiting viral replication [148–150]. A study on transcriptomic profile in COVID-19 using bioinformatics showed that camptothecin could reverse the gene signature in COVID-19 [151]. In addition, the evidence from a molecular docking study uncovered that camptothecin formed hydrogen bonds with SARS-CoV-2 S protein to prevent the binding between S protein and ACE2 receptor [152]. The results indicated that camptothecin could play a vital role in COVID-19 treatment.

We studied the biological networks and structural biology to identify the key genes, novel biomarkers, and candidate targeted drugs based on leukocyte transcriptomic profiles; however, the immunopathology of severe COVID-19 is the interaction between immune cells and respiratory cells. Analysis of peripheral white

blood cell gene expression can lose some proinflammatory cytokine information. Performing lung transcriptomic profiles for biological network construction is our suggestion for future research. Single-cell methods should be conducted to identify key genes and targeted drugs in each cell type. Advanced computational chemical methods such as molecular mechanics and molecular dynamics should also be included to simulate drug–protein interactions. Moreover, machine learning approaches are needed to deal with the big data of transcriptomic profiles to find the important features and predict key genes, novel biomarkers, and candidate-targeted drugs more widely and precisely.

2.2.5 CONCLUSIONS

Our study performed the multi-level biological network analysis from peripheral white blood cell transcriptomic profiles in severe COVID-19 patients. We found that the upregulated genes were enriched in cell proliferation and innate immune responses while the downregulated genes were concentrated in lymphocyte differentiation, adaptive immune response, and glycosaminoglycan degradation. The regulatory network analysis of the PPI network clusters provided novel diagnostic biomarkers from miRNAs. The key genes in severe COVID-19 were also identified via topological and survival analysis. These key genes play a significant role in leukocyte proliferation, antiviral activity, and viral proliferation. Furthermore, the candidate drugs targeting the key genes were found from database searching and evaluated with molecular docking. Nonetheless, other biomarkers, key genes, and candidate-targeted drugs were not found and need further investigation; therefore, advanced experimental and computational tools should be integrated to find new biomarkers and target treatments more precisely and personally.

Supplementary Materials: The following supporting information can be found and downloaded at: https://www.mdpi.com/article/10.3390/jpm12071030/s1. Table S1: Common differentially expressed genes (DEGs) from the two GEO datasets; Table S2: Edgelist of the largest PPI network; Table S3: Local topological parameters in each node

in the PPI network; Table S4: Local topological parameters of the three MCODE clusters; Table S5: Statistical and interaction data of regulatory networks in MCODE 1; Table S6: Statistical and interaction data of regulatory networks in MCODE 2; Table S7: Statistical and interaction data of regulatory networks in MCODE 3; Table S8: Topological parameters of the 19 hub genes in the PPI network; Table S9: Topological parameters of the 15 bottleneck genes in the PPI network; Table S10: Drug-gene interaction data of the key genes; Figure S1: Functional enrichment analysis of genes in each MCODE module; Figure S2: Bar graph of the number of interactions of miRNAs in each gene in MCODE modules using MIENTURNET based on miRTarBase database; Figure S3: Venn diagram of the key genes in the degree and betweenness centrality; Figure S4: Kaplan-Meier overall survival analysis of the hub and bottleneck genes in severe COVID-19.

Conflicts of Interest: The authors declare no conflict of interest. The funders had no role in the design of the study; in the collection, analyses, or interpretation of data; in the writing of the manuscript, or in the decision to publish the results.

References

1.   Helmy, Y.A.; Fawzy, M.; Elaswad, A.; Sobieh, A.; Kenney, S.P.; Shehata, A.A. The COVID-19 Pandemic: A Comprehensive Review of Taxonomy, Genetics, Epidemiology, Diagnosis, Treatment, and Control. *J. Clin. Med.* **2020**, *9*, 1225–1253. [CrossRef] [PubMed]

2.   Fehr, A.R.; Perlman, S. Coronaviruses: An overview of their replication and pathogenesis. *Methods Mol. Biol.* **2015**, *1282*, 1–23. [PubMed]

3.   World Health Organization. WHO Coronavirus (COVID-19) Dashboard 2022. Available online: https://covid19.who.int/ (accessed on 22 June 2022).

4.   Hu, B.; Guo, H.; Zhou, P.; Shi, Z.L. Characteristics of SARS-CoV-2 and COVID-19. *Nat. Rev. Microbiol.* **2021**, *19*, 141–154. [CrossRef]

5.   Gebhard, C.; Regitz-Zagrosek, V.; Neuhauser, H.K.; Morgan, R.; Klein, S.L. Impact of sex and gender on COVID-19 outcomes in Europe. *Biol. Sex Differ.* **2020**, *11*, 29–41. [CrossRef]

6.   Lu, R.; Zhao, X.; Li, J.; Niu, P.; Yang, B.; Wu, H.; Wang, W.; Song, H.; Huang, B.; Zhu, N.; et al. Genomic characterisation and epidemiology of 2019 novel coronavirus: Implications for virus origins and receptor binding. *Lancet* **2020**, *395*, 565–574. [CrossRef]

7.   Lam TT, Jia N, Zhang YW, Shum MH, Jiang JF, Zhu HC; et al. Identifying SARS-CoV-2-related coronaviruses in Malayan pangolins. *Nature* **2020**, *583*, 282–285. [CrossRef]

8.   Tsang, H.F.; Chan, L.W.C.; Cho, W.C.S.; Yu, A.C.S.; Yim, A.K.Y.; Chan, A.K.C.; Ng, L.P.W.; Wong, Y.K.E.; Pei, X.M.; Li, M.J.W.; et al. An update on COVID-19 pandemic: The epidemiology, pathogenesis, prevention and treatment strategies. *Expert Rev. Anti-Infect. Ther.* **2021**, *19*, 877–888. [CrossRef]

9. Wiersinga, W.J.; Rhodes, A.; Cheng, A.C.; Peacock, S.J.; Prescott, H.C. Pathophysiology, Transmission, Diagnosis, and Treatment of Coronavirus Disease 2019 (COVID-19): A Review. *JAMA* 2020, *324*, 782–793. [CrossRef]

10. Lauer, S.A.; Grantz, K.H.; Bi, Q.; Jones, F.K.; Zheng, Q.; Meredith, H.R.; Azman, A.S.; Reich, N.G.; Lessler, J. The Incubation Period of Coronavirus Disease 2019 (COVID-19) from Publicly Reported Confirmed Cases: Estimation and Application. *Ann. Intern. Med.* 2020, *172*, 577–582. [CrossRef]

11. 11.Guan, W.-J.; Ni, Z.-Y.; Hu, Y.; Liang, W.-H.; Ou, C.-Q.; He, J.-X., Liu, L.; Shan, H.; Lei, C.L.; Hui, D.S.C.; et al. Clinical Characteristics of Coronavirus Disease 2019 in China. *N. Engl. J. Med.* 2020, *382*, 1708–1720. [CrossRef]

12. Gandhi, R.T.; Lynch, J.B.; del Rio, C. Mild or Moderate COVID-19. *New Engl. J. Med.* 2020, *383*, 1757–1766. [CrossRef] [PubMed]

13. Pan, L.; Mu, M.; Yang, P.; Sun, Y.; Wang, R.; Yan, J.; Li, P.; Hu, B.; Wang, J.; Hu, C.; et al. Clinical Characteristics of COVID-19 Patients with Digestive Symptoms in Hubei, China: A Descriptive, Cross-Sectional, Multicenter Study. *Am. J. Gastroenterol.* 2020, *115*, 766–773. [CrossRef] [PubMed]

14. Lechien, J.R.; Chiesa-Estomba, C.M.; De Siati, D.R.; Horoi, M.; Le Bon, S.D.; Rodriguez, A.; Dequanter, D.; Blecic, S.; El Afia, F.; Distinguin, L.; et al. Olfactory and gustatory dysfunctions as a clinical presentation of mild-to-moderate forms of the coronavirus disease (COVID-19): A multicenter European study. *Eur. Arch. Otorhinolaryngol.* 2020, 277, 2251-2261. [CrossRef] [PubMed]

15. Helms, J.; Kremer, S.; Merdji, H.; Clere-Jehl, R.; Schenck, M.; Kummerlen, C.; Collange, O.; Boulay, C.; Fafi-Kremer, S.; Ohana, M.; et al. Neurologic Features in Severe SARS-CoV-2 Infection. *N. Engl. J. Med.* 2020, *382*, 2268–2270. [CrossRef]

16. Spinato, G.; Fabbris, C.; Polesel, J.; Cazzador, D.; Borsetto, D.; Hopkins, C.; Boscolo-Rizzo, P. Alterations in Smell or Taste in Mildly Symptomatic Outpatients with SARS-CoV-2 Infection. *JAMA* 2020, *323*, 2089–2090. [CrossRef]

17. Huang, C.; Wang, Y.; Li, X.; Ren, L.; Zhao, J.; Hu, Y.; Zhang, L.; Fan, G.H.; Xu, J.Y.; Gu, X.; et al. Clinical features of patients infected with 2019 novel coronavirus in Wuhan, China. *Lancet* **2020**, 395, 497–506. [CrossRef]

18. Berlin, D.A.; Gulick, R.M.; Martinez, F.J. Severe Covid-19. *N. Engl. J. Med.* **2020**, *383*, 2451–2460. [CrossRef]

19. Grasselli, G.; Zangrillo, A.; Zanella, A.; Antonelli, M.; Cabrini, L.; Castelli, A.; Cereda, D.; Coluccello, A.; Foti, G.; Fumagalli, R.; et al. Baseline Characteristics and Outcomes of 1591 Patients Infected with SARS-CoV-2 Admitted to ICUs of the Lombardy Region, Italy. *JAMA* **2020**, *323*, 1574–1581. [CrossRef]

20. Docherty, A.B.; Harrison, E.M.; Green, C.A.; Hardwick, H.E.; Pius, R.; Norman, L.; Holden, K.A.; Read, J.M.; Dondelinger, F.; Carson, G.; et al. Features of 20,133 UK patients in hospital with COVID-19 using the ISARIC WHO Clinical Characterisation Protocol: Prospective observational cohort study. *BMJ* **2020**, *369*, m1985–m1996. [CrossRef]

21. Myers, L.C.; Parodi, S.M.; Escobar, G.J.; Liu, V.X. Characteristics of Hospitalized Adults with COVID-19 in an Integrated Health Care System in California. *JAMA* **2020**, *323*, 2195–2198. [CrossRef]

22. Yang, X.; Yu, Y.; Xu, J.; Shu, H.; Xia Ja Liu, H.; Wu, Y.; Zhang, L.; Yu, Z.; Fang, M.; et al. Clinical course and outcomes of critically ill patients with SARS-CoV-2 pneumonia in Wuhan, China: A single-centered, retrospective, observational study. *Lancet Respir. Med.* **2020**, *8*, 5475–5481. [CrossRef]

23. Boban, M. Novel coronavirus disease (COVID-19) update on epidemiology, pathogenicity, clinical course and treatments. *Int. J. Clin. Pract.* **2021**, *75*, e13868–e13874. [CrossRef] [PubMed]

24. Kumar, M.; Al Khodor, S. Pathophysiology and treatment strategies for COVID-19. *J. Transl. Med.* **2020**, *18*, 353–361. [CrossRef] [PubMed]

25. Kolarič, A.; Jukič, M.; Bren, U. Novel Small-Molecule Inhibitors of the SARS-CoV-2 Spike Protein Binding to Neuropilin 1. *Pharmaceuticals* **2022**, *15*, 165–178. [CrossRef]

26. Costela-Ruiz, V.J.; Illescas-Montes, R.; Puerta-Puerta, J.M.; Ruiz, C.; Melguizo-Rodríguez, L. SARS-CoV-2 infection: The role of cytokines in COVID-19 disease. *Cytokine Growth Factor Rev.* **2020**, *54*, 62–75. [CrossRef]

27. Fajgenbaum, D.C.; June, C.H. Cytokine Storm. *N. Engl. J. Med.* **2020**, *383*, 2255–2273. [CrossRef]

28. Bhaskar, S.; Sinha, A.; Banach, M.; Mittoo, S.; Weissert, R.; Kass, J.S.; Rajagopal, S.; Pai, A.R.; Kutty, S. Cytokine Storm in COVID-19-Immunopathological Mechanisms, Clinical Considerations, and Therapeutic Approaches: The REPROGRAM Consortium Position Paper. *Front. Immunol.* **2020**, *11*, 1648–1663. [CrossRef]

29. Yüce, M.; Filiztekin, E.; Özkaya, K.G. COVID-19 diagnosis—A review of current methods. *Biosens. Bioelectron.* **2020**, *172*, 112752–112752. [CrossRef]

30. Pascarella, G.; Strumia, A.; Piliego, C.; Bruno, F.; Del Buono, R.; Costa, F.; Scarlata, S.; Agrò, F.E. COVID-19 diagnosis and management: A comprehensive review. *J. Intern. Med.* **2020**, *288*, 192–206. [CrossRef]

31. Goudouris, E.S. Laboratory diagnosis of COVID-19. *J. de Pediatr.* **2020**, *97*, 7–12. [CrossRef]

32. 32. van Paassen, J.; Vos, J.S.; Hoekstra, E.M.; Neumann, K.M.I.; Boot, P.C.; Arbous, S.M. Corticosteroid use in COVID-19 patients: A systematic review and meta-analysis on clinical outcomes. *Cri. Care* **2020**, *24*, 696–717. [CrossRef] [PubMed]

33. Drożdżal, S.; Rosik, J.; Lechowicz, K.; Machaj, F.; Szostak, B.; Przybyciński, J.; Lorzadeh, S.; Kotfis, K;. Ghavami, S.; Łos, M.J.; et al. An update on drugs with therapeutic potential for SARS-CoV-2 (COVID-19) treatment. *Drug Resist. Updat.* **2021**, *59*, 100794–100820. [CrossRef] [PubMed]

34. Agrawal, U.; Raju, R.; Udwadia, Z.F. Favipiravir: A new and emerging antiviral option in COVID-19. *Med. J. Armed Forces India* **2020**, *76*, 370–376. [CrossRef] [PubMed]

35. Jinawath, N.; Bunbanjerdsuk, S.; Chayanupatkul, M.; Ngamphaiboon, N.; Asavapanumas, N.; Svasti, J.; Charoensawan, V. Bridging the gap between clinicians and systems biologists: From network biology to translational biomedical research. *J. Transl. Med.* **2016**, *14*, 324–336. [CrossRef] [PubMed]

36. Ranjbar, R.; Behzadi, P.; Najafi, A.; Roudi, R. DNA Microarray for Rapid Detection and Identification of Food and Water Borne Bacteria: From Dry to Wet Lab. *Open Microbiol. J.* **2017**, *11*, 330–338. [CrossRef] [PubMed]

37. Rivera-Sanchez, S.P.; Ocampo-Ibáñez, I.D.; Liscano, Y.; Martínez, N.; Muñoz, I.; Manrique-Moreno, M.; Martinez-Martinez, L.; Oñate-Garzon, J. Integrating In Vitro and In Silico Analysis of a Cationic Antimicrobial Peptide Interaction with Model Membranes of Colistin-Resistant *Pseudomonas aeruginosa* Strains. *Pharmaceutics* **2022**, *14*, 1248–1261. [CrossRef]

38. Puls, K.; Olivé-Marti, A.-L.; Pach, S.; Pinter, B.; Erli, F.; Wolber, G.; Spetea, M. In Vitro, In Vivo and In Silico Characterization of a Novel Kappa-Opioid Receptor Antagonist. *Pharmaceuticals* **2022**, *15*, 680–700. [CrossRef]

39. Behzadi, P.; Gajdács, M. Worldwide Protein Data Bank (wwPDB): A virtual treasure for research in biotechnology. *Eur. J. Microbiol. Immunol.* **2021**, *11*, 77–86. [CrossRef]

40. Wlodawer, A.; Dauter, Z.; Shabalin, I.G.; Gilski, M.; Brzezinski, D.; Kowiel, M.; Minor, W.; Rupp, B.; Jaskolski, M. Ligand-centered assessment of SARS-CoV-2 drug target models in the Protein Data Bank. *Febs. J.* **2020**, *287*, 3703–3718. [CrossRef]

41. Anand, K.; Ziebuhr, J.; Wadhwani, P.; Mesters, J.R.; Hilgenfeld, R. Coronavirus main proteinase (3CLpro) structure: Basis for design of anti-SARS drugs. *Science* **2003**, *300*, 1763–1767. [CrossRef]

42. Hilgenfeld, R. From SARS to MERS: Crystallographic studies on coronaviral proteases enable antiviral drug design. *FEBS J.* **2014**, *281*, 4085–4096. [CrossRef] [PubMed]

43. Baker, E.N. Visualizing an unseen enemy; mobilizing structural biology to counter COVID-19. *Acta Crystallogr. F Struct. Biol. Commun.* **2020**, *76 Pt 4*, 158–159. [CrossRef] [PubMed]

44. Yan, R.; Zhang, Y.; Li, Y.; Xia, L.; Guo, Y.; Zhou, Q. Structural basis for the recognition of SARS-CoV-2 by full-length human ACE2. *Science* **2020**, *367*, 1444–1448. [CrossRef]

45. Zhang, L.; Lin, D.; Sun, X.; Curth, U.; Drosten, C.; Sauerhering, L.; Becker, S.; Rox, K.; Hilgenfeld, R. Crystal structure of SARS-CoV-2 main protease provides a basis for design of improved α-ketoamide inhibitors. *Science* **2020**, *368*, 409–412. [CrossRef] [PubMed]

46. Barabási, A.-L.; Oltvai, Z.N. Network biology: Understanding the cell's functional organization. *Nat. Rev. Genet.* **2004**, *5*, 101–113. [CrossRef] [PubMed]

47. Zhang, B.; Tian, Y.; Zhang, Z. Network Biology in Medicine and Beyond. *Circ. Cardiovasc. Genet.* **2014**, *7*, 536–547. [CrossRef]

48. Hengphasatporn, K.; Plaimas, K.; Suratanee, A.; Wongsriphisant, P.; Yang, J.-M.; Shigeta, Y.; Chavasiri, W.; Boonyasuppayakorn, S.; Rungrotmongkol, T. Target Identification Using Homopharma and Network-Based Methods for Predicting Compounds Against Dengue Virus-Infected Cells. *Molecules* **2020**, *25*, 1883–1900. [CrossRef]

49. Janyasupab, P.; Suratanee, A.; Plaimas, K. Network diffusion with centrality measures to identify disease-related genes. *Math. Biosci. Eng.* **2021**, *18*, 2909–2929. [CrossRef]

50. Suratanee, A.; Buaboocha, T.; Plaimas, K. Prediction of Human-Plasmodium vivax Protein Associations from Heterogeneous Network Structures Based on Machine-Learning Approach. *Bioinfor. Biol. Insights* **2021**, *15*, 11779322211013350–11779322211013362. [CrossRef]

51. Suratanee, A.; Plaimas, K. Identification of inflammatory bowel disease-related proteins using a reverse k-nearest neighbor search. *J. Bioinform. Comput. Biol.* **2014**, *12*, 1450017–1450035. [CrossRef]

52. Suratanee, A.; Plaimas, K. DDA: A Novel Network-Based Scoring Method to Identify Disease-Disease Associations. *Bioinform. Biol. Insights* **2015**, *9*, 175–186. [CrossRef] [PubMed]

53. Suratanee, A.; Plaimas, K. Reverse Nearest Neighbor Search on a Protein-Protein Interaction Network to Infer Protein-Disease Associations. *Bioinform. Biol. Insights* **2017**, *11*, 1177932217720405–1177932217720415. [CrossRef] [PubMed]

54. Suratanee, A.; Plaimas, K. Network-based association analysis to infer new disease-gene relationships using large-scale protein interactions. *PLoS ONE* **2018**, *13*, e0199435–e0199454. [CrossRef] [PubMed]

55. Suratanee, A.; Plaimas, K. Heterogeneous Network Model to Identify Potential Associations between Plasmodium vivax and Human Proteins. *Int. J. Mol. Sci.* **2020**, *21*, 1310–1327. [CrossRef] [PubMed]

56. Suratanee, A.; Plaimas, K. Hybrid Deep Learning Based on a Heterogeneous Network Profile for Functional Annotations of *Plasmodium falciparum* Genes. *Int. J. Mol. Sci.* **2021**, *22*, 10019–10036. [CrossRef] [PubMed]

57. Kawichai, T.; Suratanee, A.; Plaimas, K. Meta-Path Based Gene Ontology Profiles for Predicting Drug-Disease Associations. *IEEE Access* **2021**, *9*, 41809–41820. [CrossRef]

58. Pushpakom, S.; Iorio, F.; Eyers, P.A.; Escott, K.J.; Hopper, S.; Wells, A.; Doig, A.; Guilliams, T.; Latimer, J.; McNamee, C.; et al. Drug repurposing: Progress, challenges and recommendations. *Nat. Rev. Drug Discov.* **2019**, *18*, 41–58. [CrossRef]

59. Chou, K.-C. Structural Bioinformatics and its Impact to Biomedical Science. *Curr. Med. Chem.* **2004**, *11*, 2105–2134. [CrossRef]

60. Muhammed, M.T.; Aki-Yalcin, E. Homology modeling in drug discovery: Overview, current applications, and future perspectives. *Chem. Biol. Drug Des.* **2018**, *93*, 12–20. [CrossRef]

61. Ferreira, L.G.; Dos Santos, R.N.; Oliva, G.; Andricopulo, A.D. Molecular Docking and Structure-Based Drug Design Strategies. *Molecules* **2015**, *20*, 13384–13421. [CrossRef]

62. Khan, A.; Rehman, Z.; Hashmi, H.F.; Khan, A.A.; Junaid, M.; Sayaf, A.M.; Ali, S.S.; Hassan, F.U.; Heng, W.; Wei, D.-Q. An Integrated Systems Biology and Network-Based Approaches to Identify Novel Biomarkers in Breast Cancer Cell Lines Using Gene Expression Data. *Interdiscip. Sci.* **2020**, *12*, 155–168. [CrossRef] [PubMed]

63. Zhou, Y.; Zhou, B.; Pache, L.; Chang, M.; Khodabakhshi, A.H.; Tanaseichuk, O.; Benner, C.; Chanda, S.K. Metascape provides a biologist-oriented resource for the analysis of systems-level datasets. *Nat. Commun.* **2019**, *10*, 1523–1532. [CrossRef] [PubMed]

64. Szklarczyk, D.; Gable, A.L.; Lyon, D.; Junge, A.; Wyder, S.; Huerta-Cepas, J.; Simonovic, M.; Doncheva, N.T.; Morris, J.H.; Bork, P.; et al. STRING v11: Protein-protein association networks with increased coverage, supporting functional discovery in genome-wide experimental datasets. *Nucleic Acids Res.* **2019**, *47*, D607–D613. [CrossRef] [PubMed]

65. Shannon, P.; Markiel, A.; Ozier, O.; Baliga, N.S.; Wang, J.T.; Ramage, D.; Amin, N.; Schwikowski, B.; Ideker, T. Cytoscape: A software environment for integrated models of Biomolecular Interaction Networks. *Genome Res.* **2003**, *13*, 2498–2504. [CrossRef] [PubMed]

66. Tang, Z.; Kang, B.; Li, C.; Chen, T.; Zhang, Z. GEPIA2: An enhanced web server for large-scale expression profiling and interactive analysis. *Nucleic Acids Res.* **2019**, *47*, W556–W560. [CrossRef] [PubMed]

67. Licursi, V.; Conte, F.; Fiscon, G.; Paci, P. MIENTURNET: An interactive web tool for microRNA-target enrichment and network-based analysis. *BMC Bioinform.* **2019**, *20*, 545–554. [CrossRef]

68. Huang, H.Y.; Lin, Y.C.; Cui, S.; Huang, Y.; Tang, Y.; Xu, J.; Bao, J.; Li, Y.; Wen, J.; Zuo, H.; et al. miRTarBase update 2022: An informative resource for

experimentally validated miRNA-target interactions. *Nucleic Acids Res.* **2022**, *50*, D222–D230. [CrossRef]

69. Barrett, T.; Wilhite, S.E.; Ledoux, P.; Evangelista, C.; Kim, I.F.; Tomashevsky, M.; Marshall, K.A.; Phillippy, K.H.; Sherman, P.M.; Holko, M.; et al. NCBI GEO: Archive for functional genomics data sets—Update. *Nucleic Acids Res.* **2012**, *41*, D991–D995. [CrossRef]

70. Zhang, Q.; Meng, Y.; Wang, K.; Zhang, X.; Chen, W.; Sheng, J.; Qiu, Y.; Diao, H.; Li, L. Inflammation and Antiviral Immune Response Associated with Severe Progression of COVID-19. *Front. Immunol.* **2021**, *12*, 631226–631237. [CrossRef]

71. Gill, S.E.; dos Santos, C.C.; O'Gorman, D.B.; Carter, D.E.; Patterson, E.K.; Slessarev, M.; Martin, C.; Daley, M.; Miller, M.R.; Cepinskas, G.; et al. Transcriptional profiling of leukocytes in critically ill COVID19 patients: Implications for interferon response and coagulation. *Intensiv. Care Med. Exp.* **2020**, *8*, 75–90. [CrossRef]

72. Wickham, H.; François, R.; Henry, L.; Müller, K. dplyr: A Grammar of Data Manipulation. 2022. Available online: https://dplyr.tidyverse.org. https://github.com/tidyverse/dplyr (accessed on 15 January 2022).

73. Harris, M.A.; Clark, J.; Ireland, A.; Lomax, J.; Ashburner, M.; Foulger, R.; Lewis, S.; Marshall, B.; Mungall, C.; Richter, J.; et al. The Gene Ontology (GO) database and informatics resource. *Nucleic Acids Res.* 2004, 32, D258–D261. [PubMed]

74. Kanehisa, M.; Furumichi, M.; Tanabe, M.; Sato, Y.; Morishima, K. KEGG: New perspectives on genomes, pathways, diseases and drugs. *Nucleic Acids Res.* **2017**, *45*, D353–D361. [CrossRef] [PubMed]

75. Jassal, B.; Matthews, L.; Viteri, G.; Gong, C.; Lorente, P.; Fabregat, A.; Sidiropoulos, K.; Cook, J.; Gillespie, M.; Haw, R.; et al. The reactome pathway knowledgebase. *Nucleic Acids Res.* **2020**, *48*, D498–D503. [CrossRef] [PubMed]

76. Martens, M.; Ammar, A.; Riutta, A.; Waagmeester, A.; Slenter, D.N.; Hanspers, K.; Miller, R.A.; Digles, D.; Lopes, E.N.; Ehrhart, F.; et al. WikiPathways: Connecting communities. *Nucleic Acids Res.* **2021**, *49*, D613–D621. [CrossRef]

77. Mvubu, N.E.; Pillay, B.; Gamieldien, J.; Bishai, W.; Pillay, M. Canonical pathways, networks and transcriptional factor regulation by clinical strains of *Mycobacterium tuberculosis* in pulmonary alveolar epithelial cells. *Tuberculosis* 2016, *97*, 73–85. [CrossRef]

78. Giurgiu, M.; Reinhard, J.; Brauner, B.; Dunger-Kaltenbach, I.; Fobo, G.; Frishman, G.; Montrone, C.; Ruepp, A. CORUM: The comprehensive resource of mammalian protein complexes-2019. *Nucleic Acids Res.* 2018, *47*, D559–D563. [CrossRef]

79. Bader, G.D.; Hogue, C.W.V. An automated method for finding molecular complexes in large protein interaction networks. *BMC Bioinform.* 2003, *4*, 2–27. [CrossRef]

80. Tomczak, K.; Czerwińska, P.; Wiznerowicz, M. Review The Cancer Genome Atlas (TCGA): An immeasurable source of knowledge. *Contem. Oncol.* 2015, *19*, 68–77. [CrossRef]

81. Lonsdale, J.; Thomas, J.; Salvatore, M.; Phillips, R.; Lo, E.; Shad, S.; Hasz, R.; Walters, G.; Garcia, F.; Young, N.; et al. The Genotype-Tissue Expression (GTEx) project. *Nat Genet.* 2013, *45*, 580-585. [CrossRef]

82. Wishart, D.S.; Feunang, Y.D.; Guo, A.C.; Lo, E.J.; Marcu, A.; Grant, J.R.; Sajed, T.; Johnson, D.; Li, C.; Sayeeda, Z.; et al. DrugBank 5.0: A Major Update to the DrugBank Database for 2018. *Nucleic Acids Res.* 2018, *46*, D1074–D1082. [CrossRef]

83. Wang, Y.; Zhang, S.; Li, F.; Zhou, Y.; Zhang, Y.; Wang, Z.; Zhang, R.; Zhu, J.; Ren, Y.; Tan, Y.; et al. Therapeutic target database 2020: Enriched resource for facilitating research and early development of targeted therapeutics. *Nucleic Acids Res.* 2020, *48*, D1031–D1041. [CrossRef] [PubMed]

84. Davis, A.P.; Grondin, C.J.; Johnson, R.J.; Sciaky, D.; Wiegers, J.; Wiegers, T.C.; Mattingly, C.J. Comparative Toxicogenomics Database (CTD): Update 2021. *Nucleic Acids Res.* 2021, *49*, D1138–D1143. [CrossRef] [PubMed]

85. Safran, M.; Dalah, I.; Alexander, J.; Rosen, N.; Stein, T.I.; Shmoish, M.; Nativ, N.; Bahir, I.; Doniger, T.; Krug, H.; et al. GeneCards Version 3: The human gene integrator. *Database* **2010**, *2010*, baq020– baq035. [CrossRef] [PubMed]

86. Szklarczyk, D.; Santos, A.; von Mering, C.; Jensen, L.J.; Bork, P.; Kuhn, M. STITCH 5: Augmenting protein–chemical interaction networks with tissue and affinity data. *Nucleic Acids Res.* **2016**, *44*, D380–D384. [CrossRef]

87. Burley, S.K.; Berman, H.M.; Bhikadiya, C.; Bi, C.; Chen, L.; Di Costanzo, L.; Christie, C.; Dalenberg, K.; Duarte, J.M.; Dutta, S.; et al. RCSB Protein Data Bank: Biological macromolecular structures enabling research and education in fundamental biology, biomedicine, biotechnology and energy. *Nucleic Acids Res.* **2019**, *47*, D464–D474. [CrossRef]

88. Guiley, K.Z.; Iness, A.N.; Saini, S.; Tripathi, S.; Lipsick, J.S.; Litovchick, L.; Rubin, A.M. Structural mechanism of Myb-MuvB assembly. *Proc. Natl. Acad. Sci. USA* **2018**, *115*, 10016–10021. [CrossRef] [PubMed]

89. Zor, T.; De Guzman, R.N.; Dyson, H.J.; Wright, P.E. Solution Structure of the KIX Domain of CBP Bound to the Transactivation Domain of c-Myb. *J. Mol. Biol.* **2004**, *337*, 521–534. [CrossRef]

90. Kasper, L.H.; Boussouar, F.; Ney, P.A.; Jackson, C.W.; Rehg, J.; Van Deursen, J.M.; Brindle, P. A transcription-factor-binding surface of coactivator p300 is required for haematopoiesis. *Nature* **2002**, *419*, 738–743. [CrossRef]

91. Pattabiraman, D.R.; Gonda, T.J. Role and potential for therapeutic targeting of MYB in leukemia. *Leukemia* **2012**, *27*, 269–277. [CrossRef]

92. Schmidt, T.J.; Klempnauer, K.-H. Natural Products with Antitumor Potential Targeting the MYB-C/EBPβ-p300 Transcription Module. *Molecules* **2022**, *27*, 2077–2099. [CrossRef]

93. Uttarkar, S.; Frampton, J.; Klempnauer, K.-H. Targeting the transcription factor Myb by small-molecule inhibitors. *Exp. Hematol.* **2017**, *47*, 31–35. [CrossRef] [PubMed]

94. Uttarkar, S.; Piontek, T.; Dukare, S.; Schomburg, C.; Schlenke, P.; Berdel, W.E.; Müller-Tidow, C.; Schmidt, T.J.; Klempnauer, K.-H. Small-Molecule Disruption of the Myb/p300 Cooperation Targets Acute Myeloid Leukemia Cells. *Mol. Cancer Ther.* **2016**, *15*, 2905–2915. [CrossRef] [PubMed]

95. Cicirò, Y.; Sala, A. MYB oncoproteins: Emerging players and potential therapeutic targets in human cancer. *Oncogenesis* **2021**, *10*, 19–33. [CrossRef] [PubMed]

96. Yan, Y.; Tao, H.; He, J.; Huang, S.-Y. The HDOCK server for integrated protein–protein docking. *Nat. Protoc.* **2020**, *15*, 1829–1852. [CrossRef]

97. Eberhardt, J.; Santos-Martins, D.; Tillack, A.F.; Forli, S. AutoDock Vina 1.2.0: New Docking Methods, Expanded Force Field, and Python Bindings. *J. Chem. Inf. Model.* **2021**, *61*, 3891–3898. [CrossRef]

98. Olsson, M.H.M.; Søndergaard, C.R.; Rostkowski, M.; Jensen, J.H. PROPKA3: Consistent Treatment of Internal and Surface Residues in Empirical pKa Predictions. *J. Chem. Theory Comput.* **2011**, *7*, 525–537. [CrossRef]

99. Pirok, G.; Máté, N.; Varga, J.; Vargyas, M.; Dóránt, S.; Csizmadia, F. Making Real Molecules in Virtual Space. *J. Chem. Inf. Model.* **2006**, *46*, 563–568. [CrossRef]

100. Pettersen, E.F.; Goddard, T.D.; Huang, C.C.; Couch, G.S.; Greenblatt, D.M.; Meng, E.C.; Ferrin, T.E. UCSF Chimera–A visualization system for exploratory research and analysis. *J. Comput. Chem.* **2004**, *25*, 1605–1612. [CrossRef]

101. Laskowski, R.A.; Swindells, M.B. LigPlot+: Multiple ligand–protein interaction diagrams for drug discovery. *J. Chem. Inf. Model.* **2011**, *51*, 2778–2786. [CrossRef]

102. Lu, T.X.; Rothenberg, M.E. MicroRNA. *J. Allergy Clin. Immunol.* **2018**, *141*, 1202–1207. [CrossRef]

103. O'Brien, J.; Hayder, H.; Zayed, Y.; Peng, C. Overview of MicroRNA Biogenesis, Mechanisms of Actions, and Circulation. *Front. Endocrinol.* **2018**, *9*, 402–413. [CrossRef] [PubMed]

104. Sherwood, E.R.; Burelbach, K.R.; McBride, M.A.; Stothers, C.L.; Owen, A.M.; Hernandez, A.; Patil, N.K.; Williams, D.L.; Bohannon, J.K. Innate Immune Memory and the Host Response to Infection. *J. Immunol.* **2022**, *208*, 785–792. [CrossRef] [PubMed]

105. McCormick, A.L.; Mocarski, Jr, E.S. Viral modulation of the host response to infection. In *Human Herpesviruses: Biology, Therapy, and Immunoprophylaxis*; Arvin, A., Campadelli-Fiume, G., Mocarski, E., Moore, P.S., Roizman, B., Whitley, R., Whitley, R., Yamanishi, K., Eds.; Cambridge University Press: Cambridge, UK, 2007.

106. Wang, J.; Blanchard, T.G.; Ernst, P.B. Host Inflammatory Response to Infection. In *Helicobacter pylori: Physiology and Genetics*; Mobley, H.L.T., Mendz, G.L., Hazell, S.L., Eds.; ASM Press: Washington, DC, USA, 2001.

107. Weston, D. The pathogenesis of infection and immune response. *Br. J. Nurs.* **2010**, *19*, S4–S11. [CrossRef] [PubMed]

108. Yang, L.; Xie, X.; Tu, Z.; Fu, J.; Xu, D.; Zhou, Y. The signal pathways and treatment of cytokine storm in COVID-19. *Signal Transduct. Target. Ther.* **2021**, *6*, 255–274. [CrossRef]

109. van Eijk, L.E.; Binkhorst, M.; Bourgonje, A.R.; Offringa, A.K.; Mulder, D.J.; Bos, E.M.; Kolundzic, N.; Abdulle, A.E.; van der Voort, P.H.J.; Olde Rikkert, M.G.M.; et al. COVID-19: Immunopathology, pathophysiological mechanisms, and treatment options. *J. Pathol.* **2021**, *254*, 307–331. [CrossRef]

110. Merad, M.; Blish, C.A.; Sallusto, F.; Iwasaki, A. The immunology and immunopathology of COVID-19. *Science* **2022**, *375*, 1122–1127. [CrossRef]

111. Shahgolzari, M.; Yavari, A.; Arjeini, Y.; Miri, S.M.; Darabi, A.; Nejad, A.S.M.; Keshavarz, M. Immunopathology and Immunopathogenesis of COVID-19, what we know and what we should learn. *Gene Rep.* **2021**, *25*, 101417–101434. [CrossRef]

112. Tascioglu, D.; Akkaya, E.; Genc, S. The understanding of the immunopathology in COVID-19 infection. *Scand. J. Clin. Lab. Investig.* **2021**, *81*, 255–263. [CrossRef]

113. Lang, J.; Yang, N.; Deng, J.; Liu, K.; Yang, P.; Zhang, G.; Jiang, C. Inhibition of SARS Pseudovirus Cell Entry by Lactoferrin Binding to Heparan Sulfate Proteoglycans. *PLoS ONE* **2011**, *6*, e23710– e23720. [CrossRef]

114. Milewska, A.; Zarebski, M.; Nowak, P.; Stozek, K.; Potempa, J.; Pyrc, K. Human Coronavirus NL63 Utilizes Heparan Sulfate Proteoglycans for Attachment to Target Cells. *J. Virol.* **2014**, *88*, 13221–13230. [CrossRef]

115. Clausen, T.M.; Sandoval, D.R.; Spliid, C.B.; Pihl, J.; Perrett, H.R.; Painter, C.D.; Narayanan, A.; Majowicz, S.A.; Kwong, E.M.; McVicar, R.N.; et al. SARS-CoV-2 Infection Depends on Cellular Heparan Sulfate and ACE2. *Cell* **2020**, *183*, 1043– 1057.e1015. [CrossRef] [PubMed]

116. Shi, D.; Sheng, A.; Chi, L. Glycosaminoglycan-Protein Interactions and Their Roles in Human Disease. *Front. Mol. Biosci.* **2021**, *8*, 639666–639680. [CrossRef] [PubMed]

117. Catalanotto, C.; Cogoni, C.; Zardo, G. MicroRNA in Control of Gene Expression: An Overview of Nuclear Functions. *Int. J. Mol. Sci.* **2016**, *17*, 1712–1728. [CrossRef] [PubMed]

118. Sayed, D.; Abdellatif, M. MicroRNAs in Development and Disease. *Physiol. Rev.* **2011**, *91*, 827–887. [CrossRef]

119. Hammond, S.M. An overview of microRNAs. *Adv. Drug Deliv. Rev.* **2015**, *87*, 3–14. [CrossRef]

120. Kroh, E.M.; Parkin, R.K.; Mitchell, P.S.; Tewari, M. Analysis of circulating microRNA biomarkers in plasma and serum using quantitative reverse transcription-PCR (qRT-PCR). *Methods* **2010**, *50*, 298–301. [CrossRef]

121. Zhang, S.; Amahong, K.; Sun, X.; Lian, X.; Liu, J.; Sun, H.; Lou, Y.; Zhu, F.; Qiu, Y. The miRNA: A small but powerful RNA for COVID-19. *Briefings Bioinform.* **2021**, *22*, 1137–1149. [CrossRef]

122. Ying, H.; Ebrahimi, M.; Keivan, M.; Khoshnam, S.E.; Salahi, S.; Farzaneh, M. miRNAs; a novel strategy for the treatment of COVID-19. *Cell Biol. Int.* **2021**, *45*, 2045–2053. [CrossRef]

123. Arghiani, N.; Nissan, T.; Matin, M.M. Role of microRNAs in COVID-19 with implications for therapeutics. *Biomed. Pharmacother.* **2021**, *144*, 112247–112256. [CrossRef]

124. Paul, S.; Bravo Vázquez, L.A.; Reyes-Pérez, P.R.; Estrada-Meza, C.; Aponte Alburquerque, R.A.; Pathak, S.; Banerjee, A.; Bandyopadhyay,. A.; Chakraborty, S.; Srivastava, A.; et al. The role of microRNAs in solving COVID-19 puzzle from infection to therapeutics: A mini-review. *Virus Res.* **2022**, *308*, 198631–198643. [CrossRef]

125. Boutros, R.; Lobjois, V.; Ducommun, B. CDC25 phosphatases in cancer cells: Key players? Good targets? *Nat. Rev. Cancer* **2007**, *7*, 495–507. [CrossRef] [PubMed]

126. Shen, T.; Huang, S. The role of Cdc25A in the regulation of cell proliferation and apoptosis. *Anticancer Agents Med. Chem.* **2012**, *12*, 631–639. [CrossRef] [PubMed]

127. Qi, D.; Hu, L.; Jiao, T.; Zhang, T.; Tong, X.; Ye, X. Phosphatase Cdc25A Negatively Regulates the Antiviral Immune Response by Inhibiting TBK1 Activity. *J. Virol.* **2018**, *92*, e01118-18. [CrossRef] [PubMed]

128. Tomatsu, S.; Montaño, A.M.; Dung, V.C.; Grubb, J.H.; Sly, W.S. Mutations and polymorphisms in GUSB gene in mucopolysaccharidosis VII (Sly Syndrome). *Hum. Mutat.* **2009**, *30*, 511–519. [CrossRef]

129. Musa, J.; Aynaud, M.-M.; Mirabeau, O.; Delattre, O.; Grünewald, T.G. MYBL2 (B-Myb): A central regulator of cell proliferation, cell survival and differentiation involved in tumorigenesis. *Cell Death Dis.* **2017**, *8*, e2895– e2903. [CrossRef]

130. Frau, M.; Ladu, S.; Calvisi, D.F.; Simile, M.M.; Bonelli, P.; Daino, L.; Tomasi, M.L.; Seddaiu, M.A.; Feo, F.; Pascale, R.M. Mybl2 expression is under genetic control and contributes to determine a hepatocellular carcinoma susceptible phenotype. *J. Hepatol.* **2011**, *55*, 111–119. [CrossRef]

131. Ren, F.; Wang, L.; Shen, X.; Xiao, X.; Liu, Z.; Wei, P.; Wang, Y.; Qi, P.; Shen, C.; Sheng, W.; et al. MYBL2 is an independent prognostic marker that has tumor-promoting functions in colorectal cancer. *Am. J. Cancer Res.* **2015**, *5*, 1542–1552.

132. Liang, H.-B.; Cao, Y.; Ma, Q.; Shu, Y.-J.; Wang, Z.; Zhang, F.; Ye, Y.-Y.; Li, H.-F.; Xiang, S.-S.; Song, X.-L.; et al. MYBL2 is a Potential Prognostic Marker that Promotes Cell Proliferation in Gallbladder Cancer. *Cell. Physiol. Biochem.* **2017**, *41*, 2117–2131. [CrossRef] [PubMed]

133. Bayley, R.; Ward, C.; Garcia, P. MYBL2 amplification in breast cancer: Molecular mechanisms and therapeutic potential. *Biochim. Biophys Acta Rev. Cancer* **2020**, *1874*, 188407–188416. [CrossRef]

134. Auwul, R.; Rahman, R.; Gov, E.; Shahjaman; Moni, M.A. Bioinformatics and machine learning approach identifies potential drug targets and pathways in COVID-19. *Briefings Bioinform.* **2021**, *22*, bbab120– bbab132. [CrossRef]

135. Babbio, F.; Farinacci, M.; Saracino, F.; Carbone, M.L.A.; Privitera, E. Expression and localization studies of hSDA, the human ortholog of the yeast SDA1 gene. *Cell Cycle* **2004**, *3*, 484–488. [CrossRef]

136. Plevin, M.; Mills, M.M.; Ikura, M. The LxxLL motif: A multifunctional binding sequence in transcriptional regulation. *Trends Biochem. Sci.* **2005**, *30*, 66–69. [CrossRef] [PubMed]

137. Bujnicki, T.; Wilczek, C.; Schomburg, C.; Feldmann, F.; Schlenke, P.; Müller-Tidow, C.; Schmidt, T.J.; Klempnauer, K.-H. Inhibition of Myb-dependent gene expression by the sesquiterpene lactone mexicanin-I. *Leukemia* **2012**, *26*, 615–622. [CrossRef] [PubMed]

138. Schomburg, C.; Schuehly, W.; Da Costa, F.B.; Klempnauer, K.-H.; Schmidt, T.J. Natural sesquiterpene lactones as inhibitors of Myb-dependent gene expression: Structure–activity relationships. *Eur. J. Med. Chem.* **2013**, *63*, 313–320. [CrossRef] [PubMed]

139. Uttarkar, S.; Dassé, E.; Coulibaly, A.; Steinmann, S.; Jakobs, A.; Schomburg, C.; Trentmann, A.; Jose, J.; Schlenke, P.; Berdel, W.E.; et al. Targeting acute myeloid

leukemia with a small molecule inhibitor of the Myb/p300 interaction. *Blood* **2016**, *127*, 1173–1182. [CrossRef]

140. Uttarkar, S.; Dukare, S.; Bopp, B.; Goblirsch, M.; Jose, J.; Klempnauer, K.-H. Naphthol AS-E Phosphate Inhibits the Activity of the Transcription Factor Myb by Blocking the Interaction with the KIX Domain of the Coactivator p300. *Mol. Cancer Ther.* **2015**, *14*, 1276–1285. [CrossRef]

141. Thorner, A.R.; A Hoadley, K.; Parker, J.S.; Winkel, S.; Millikan, R.C.; Perou, C.M. In vitro and in vivo analysis of B-Myb in basal-like breast cancer. *Oncogene* **2009**, *28*, 742–751. [CrossRef]

142. Sottile, F.; Gnemmi, I.; Cantilena, S.; D'Acunto, W.C.; Sala, A. A chemical screen identifies the chemotherapeutic drug topotecan as a specific inhibitor of the B-MYB/MYCN axis in neuroblastoma. *Oncotarget* **2012**, *3*, 535–545. [CrossRef]

143. Johnson-Arbor, K.; Dubey, R. *Doxorubicin. StatPearls*; StatPearls Publishing: Treasure Island, FL, USA, 2022.

144. Sajid Jamal, Q.M.; Alharbi, A.H.; Ahmad, V. Identification of doxorubicin as a potential therapeutic against SARS-CoV-2 (COVID-19) protease: A molecular docking and dynamics simulation studies. *J. Biomol. Struct. Dyn.* **2021**, 1–15. [CrossRef]

145. Sirikantaramas, S.; Asano, T.; Sudo, H.; Yamazaki, M.; Saito, K. Camptothecin: Therapeutic potential and biotechnology. *Curr. Pharm. Biotechnol.* **2007**, *8*, 196–202. [CrossRef]

146. Thomas, C.J.; Rahier, N.J.; Hecht, S.M. Camptothecin: Current perspectives. *Bioorg. Med. Chem.* **2004**, *12*, 1585–1604. [CrossRef] [PubMed]

147. Martino, E.; Della Volpe, S.; Terribile, E.; Benetti, E.; Sakaj, M.; Centamore, A.; Sala, A.; Collina, S. The long story of camptothecin: From traditional medicine to drugs. *Bioorg. Med. Chem. Lett.* **2017**, *27*, 701–707. [CrossRef] [PubMed]

148. Horwitz, S.B.; Chang, C.-K.; Grollman, A.P. Antiviral Action of Camptothecin. *Antimicrob. Agents Chemother.* **1972**, *2*, 395–401. [CrossRef] [PubMed]

149. Horwitz, M.S.; Brayton, C. Camptothecin: Mechanism of inhibition of adenovirus formation. *Virology* **1972**, *48*, 690–698. [CrossRef]

150. Kelly, D.C.; Avery, R.J.; Dimmock, N.J.; Ivánovics, G.; Gaál, V.; Pragai, B. Camptothecin: An Inhibitor of Influenza Virus Replication. *J. Gen. Virol.* **1974**, *25*, 427–432. [CrossRef]

151. Pushparaj, P.N.; Abdulkareem, A.A.; Naseer, M.I. Identification of Novel Gene Signatures using Next-Generation Sequencing Data from COVID-19 Infection Models: Focus on Neuro-COVID and Potential Therapeutics. *Front. Pharmacol.* **2021**, *12*, 688227–688245. [CrossRef]

152. Mamkulathil Devasia, R.; Altaf, M.; Fahad Alrefaei, A.; Manoharadas, S. Enhanced production of camptothecin by immobilized callus of Ophiorrhiza mungos and a bioinformatic insight into its potential antiviral effect against SARS-CoV-2. *J. King Saud. Univ. Sci.* **2021**, *33*, 101344–101350. [CrossRef]

PART III

CONCLUSIONS

3.1 DISCUSSIONS AND CONCLUSIONS

This thesis proposed the PPI network analysis based on leukocyte transcriptomic profiles of severe COVID-19 patients to identify the key genes, candidate targeted drugs, and novel biomarkers. The thesis composed the two research articles. The former constructed the IPIN using LHD algorithm and identified the key genes via several centrality measurement and ranking score calculation. The key genes were validated by reviewing computational, experimental, and clinical studies relevant to their effects on COVID-19 severity. Meanwhile, the latter combined the two different leukocyte transcriptomic datasets to construct the PPI network using the software tool in the STRING database. Moreover, the key genes were identified using the combination of degree and betweenness centrality. They were validated from the survival analysis using acute myeloid leukemia as the model in the second article. miRNA-mRNA regulatory networks were also established in the second article for discovering the novel biomarkers. Although both articles found the candidate targeted drugs using drug-gene or drug-protein interaction networks construction from searching drug-gene and drug-protein interaction databases, the second article also conducted the molecular docking to evaluate the physical interactions between the candidate drugs and the proteins encoded by the key genes, according to a reviewer's suggestion during the peer review process of the article.

In topological analysis, the PPI networks constructed by both articles were not ideal biological network because they were not fulfilled the small-world and scale-free criteria. The reason is explained by that the constructed networks were subnetworks extracted from the human interactome. Thus, they can lose some topological properties from the interactome network. Furthermore, the networks are real-world networks, then the small-world and scale-free criterion cannot be completely fulfilled. The functional

enrichment analysis from the DEGs, PPI network, and network clusters in the two articles revealed that antiviral and innate immune responses, apoptosis, and cell cycle regulation term were involved, indicating the leukocyte function in severe COVID-19.

There were 23 key genes found in the first article: *CCNA2*, *CCNE1*, *CDC20*, *CDC25A*, *CMPK2*, *DDX58*, *FOXM1*, *IFI6*, *IFI35*, *IFIH1*, *IFIT1*, *IFIT2*, *IFIT3*, *IRF7*, *ISG15*, *MX1*, *OAS1*, *OAS2*, *OASL*, *RRM2*, *RSAD2*, *STAT1*, and *XAF1*. These key genes were identified using several centrality measurements, for instance, degree, betweenness, closeness, and eigenvector. The combination of degree and betweenness centrality is a powerful tool for identifying the key genes and proteins in PPI networks because it could capture the highest number of the key genes (22 of 23 genes). On the other hand, while the ranking score calculation captured the key genes mainly found in degree centrality calculation, it found a low number of the key genes measured from the betweenness centrality and it could not discover other key genes different from degree and betweenness. The reason can be described by that the ranking score was mostly dependent on degree centrality and its variant (eigenvector centrality). Hence, the key genes identified by the ranking score were primarily found in the high degree centrality genes. There were 12 key genes identified by the combined degree and betweenness centrality, but the ranking score could not capture. These genes were interesting as well, and they should be needed to investigate their roles in severe COVID-19. In addition, there were 7 potential drugs identified from searching drug-gene and -protein interaction databases, for example, poly(I:C), mitomycin C, decitabine, gemcitabine, hydroxyurea, tamoxifen, and curcumin. The literature review proved these key genes and candidate drugs had a role in severe COVID-19.

It is interesting to discuss the methods used in the first article. First, the permutation test was done to filter out the false-positive high diffuse score nodes according to the z-score calculation. However, multiple z-score measurements in every gene in the interactome can cause false-positive significant scores, like a *p*-value from

gene expression measurement in transcriptomics. Therefore, to correct the z-score, adjustment techniques such as Bonferroni, Hommel, Holm, and Benjamini-Hochberg test should be performed. The second thing discussed in the first article's methods is the proposed gene prioritization technique in the PPI network, the ranking score. Although the score could not cover any gene apart from the combined degree and betweenness centrality, applying the proposed score to identify key genes in the network is suggested because the score provides many benefits. For example, it includes all involved centralities with normalization by using the product of their reciprocal rank instead of directly using the centralities' value. Geometric mean was applied in the ranking score instead of arithmetic mean because a maximal score will be 1 when using the former mean calculation. The latter mean need additional normalization to convert a maximal value to 1. However, the dependency among the considered parameters, such as degree and eigenvector centrality, providing the biased results, is a drawback of the score. Therefore, it is recommended to include independent potential factors in the score.

There were 4 key genes explored in the second article such as *CDC25A*, *GUSB*, *MYBL2*, and *SDAD1*. Three key genes, except *CDC25A*, were different from the key genes identified in the first article. Furthermore, two additional 2 candidate drugs were found in the article: camptothecin and doxorubicin. The structural analysis results from the two ligand-protein docking programs revealed that the candidate drugs provided the better binding affinity with the key protein than the reference ligand (plumbagin). These suggest that PPI network analysis based on different transcriptomic datasets combination can reveal further key genes and candidate drugs apart from the single transcriptomic profile. Additionally, there were 5 novel biomarkers identified from the miRNA-mRNA regulatory network analysis, for instance, hsa-miR-6792-5p, hsa-let-7b-5p, hsa-miR-34a-5p, hsa-miR-92a-3p, and hsa-miR-146a-5p. miRNAs have many applications in medicine. They play a role in therapeutic agents and predictive

biomarkers. Consequently, the identified miRNAs can be applied in biomarkers development. However, further investigation of biomarker roles in these predicted miRNAs is required.

Different materials and methods exist between the two articles, such as DEGs selection, PPI network construction, cut-point differences, and technique for key gene validation. First, the first article selected only the upregulated DEGs, while the second included the downregulated DEGs. The reasons for describing these issues are the first article hypothesized that genes having upregulation were associated with COVID-19 severity. However, more research articles about pathophysiology and disease mechanisms were reviewed during the second article. It was found that the downregulated genes also play an essential role in accelerated disease progression. Therefore, the downregulated DEGs were included in the study in the second article.

The second difference is that the first article constructed the PPI network using the network diffusion algorithm. On the other hand, the second research created the network based on the protein interaction data in the STRING for the common DEGs (including both upregulated and downregulated DEGs) without the node expansion. The second network was constructed differently from the first because the LHD algorithm consumed prolonged computational time and the DEGs' number in the second was enough to establish the PPI network without extending the network.

Furthermore, the articles' cut-point values, such as log2 FC and drug-protein interaction confidence score, were quite different. In the first article, DEGs were selected with log2 FC greater than 1.5 and the PPI network was built using the interaction confidence score of more than 0.9. Moreover, the chosen drugs had STTICH's drug-protein interaction confidence greater than 0.9. Compared with the second study, the cut-off values of |log2 FC| (including both upregulated and downregulated DEGs), protein interaction, and drug-protein interaction confidence scores were 1, 0.4, and 0.4, respectively. The values were changed because previously, the second article was

conducted according to the cut point from the first article. As a result, no significant key gene from the survival analysis and no drug met with interaction confidence criteria was identified. Thus, relieving the strict criteria was permitted to discover possible and further key genes and candidate drugs. Due to still no standard cut-point value in these parameters, it is suggested that gene expression's FDR q-value should not be greater than or equal to 0.05 because it is the highest cut-point for statistical significance as long as acceptable. The absolute of log2 FC (|log2 FC|) should be more than 1 because if it equals 1, there is no gene expression difference between the experiment and control group. The confidence score of protein-protein and drug-protein should not be less than 0.4 because this cut-point is the medium confidence. Using the low interaction confidence score can result in the research's reliability.

The other difference between the two methods is validating the key genes. The first article validated the key genes using the review of previous computational, experimental, and clinical studies, while the second evaluated the key genes using the survival analysis based on the cancer model. The reason for using the survival analysis in the second article comes from the experience in the first article. Validating the key genes using the literature review looks quite manual and laborious and takes a long time. The survival analysis then was operated in the second article to deal with the problem. Performing the survival analysis based on the cancer data on severe COVID-19's key gene identification can cause erroneous results although the same key cell type (myelocyte-lineage leukocytes) was operated. It is recommended to use key gene validation tools directly involved in COVID-19 or infectious diseases if they exist.

A comparison between the proposed methods and reviewed previous studies is also discussed. Prasad et al. (2020) [34] constructed a PPI network based on the SARS-CoV-2 infected lung adenocarcinoma cell line transcriptomic profiles. They identified 120 DEGs and used them to construct a PPI network without node expansion. Functional enrichment analysis based on the DEGs was performed using DAVID [45] by

considering GO-BP [46] and KEGG pathway [47] terms. The study identified key genes by a combination between degree and betweenness centrality measurement. The targeted drugs were discovered using drug-gene interaction database searching and confirmed with the STITCH database [48]. The methods from Prasad et al. were mainly used in the proposed methods in this thesis. However, the previous techniques were modified to provide more accurate and specific results. For instance, this thesis constructed the PPI network based on the patient transcriptomes instead of the cell line transcriptomes. The thesis also extended the PPI network by using the LHD algorithm to infer the disease-associated genes more than only DEGs consideration because DEGs provided a few nodes. Low node samples can detect a few key genes and candidate drugs. Metascape [49] was performed in this thesis rather than other enrichment programs because the software integrates the highest number of databases collecting biological enrichment terms such as GO-BP, KEGG, WikiPathways [50], Reactome [51], Canonical [52], and CORUM pathway [53]. Other enrichment software tools only focus on the biological terms in GO-BP and KEGG pathways. This thesis also included several network centralities, such as degree, betweenness, closeness, and eigenvector, and the proposed ranking score to identify the key genes and measure their performance compared to the traditional method using combined degree and betweenness centrality. Moreover, this thesis conducted several network clustering algorithms to detect the network community for finding more specific biological terms rarely seen in the whole network enrichment analysis. Prasad and colleagues also performed the DrugBank database [54] and CTD [55] to find drug-gene interaction information. This thesis incorporated more drug-gene interaction databases, such as TTD [56] and GeneCards [57], to cover more possible candidate drugs.

To compare with the study by Zhang et al. (2020) [58] and Messina et al. (2021) [59], both studies performed a network diffusion algorithm called random walk with restart (RWR) using human proteins interacting with viral proteins as seed nodes. The

previous studies used human proteins interacting with the virus as the seed nodes because they concerned with the key genes related to the infectivity. Conversely, this thesis performed the seed nodes based on the genes associated with COVID-19 severity instead of the disease susceptibility. Additionally, there is no proven evidence about the performance measurement between LHD used in this thesis and RWR conducted in the previous studies. Interestingly, Lu et al. (2018)'s study [60], using both LHD and RWR to infer uveitis-related genes, revealed that both algorithms provided markedly different inferred genes. Hence, comparisons between the two network diffusion algorithms' efficacy and goal are needed for further investigation. Moreover, Zhang and colleagues' study operated a permutation test to filter out false-positive nodes like this thesis. The permutation test used in the previous study, however, has a possibility to capture true-positive nodes with a low diffuse score because the test concerned the quality but not the quantity of the diffuse score. Therefore, we conducted the z-score for diffuse score level consideration by selecting the nodes having a true-positive high diffuse score.

It is recommended in the result part of both studies that the identified key genes should be analyzed about their expression statuses in individual patients. Because the studied patient transcriptome samples came from different countries, nationalities, ages, genders, and other factors, their different key gene expression pattern should be needed more investigation. Furthermore, in the second article, the unique DEGs in each leukocyte transcriptomic dataset should be additionally investigated that they play an important role in severe COVID-19 or are only noises. Due to the sample and dataset variant, some important DEGs can be found in each unique set instead of the common set. The proposed methods in this thesis can loss some invaluable data.

3.2 LIMITATIONS

There were three limitations found in this study. First, the study focused on the PPI network construction principally in leukocyte transcriptomic profiles, although the

immunopathology of COVID-19 is the interaction between white blood cells (leukocytes) and pulmonary cells and other organ tissues. As a result, the study can lose the information of complex mechanisms of severe COVID-19 in a whole body. This research only constructed the PPI networks indicating the host immune status in the severe COVID-19 but not considered organ systems. Second, performing LHD algorithm and permutation test for diffusion-based PPI network construction consumes a large computational time and needs HPC. Third, there are still no gold standard tools to validate the key genes related to immune-induced severe COVID-19 compared to other diseases such as genetic diseases, cancers, aging, and metabolic syndrome. The survival analysis based on the cancer model cannot provide the best appropriate key gene identification results. The identified key genes in severe COVID-19 are still needed for further investigation.

3.3 FUTURE WORKS

Machine and deep learning play an essential role in finding important features and classifying data in many expert areas such as business, medicine, and social science in the data science era. Combining machine and deep learning and biological network analysis will be included in the future works for finding the key genes that the conventional methods cannot identify. In addition, single-cell transcriptomic approaches are required to build specific biological networks in individual cells for more precise treatment, according to precision medicine concepts. Advanced network-based and structure-based drug repurposing are also needed to discover more accurate candidate existing drugs. Experimental and clinical procedure should be participated to confirm computational results

APPENDICES

In this section, the important and interesting supplementary materials, tables, and figures from the two research articles are shown.

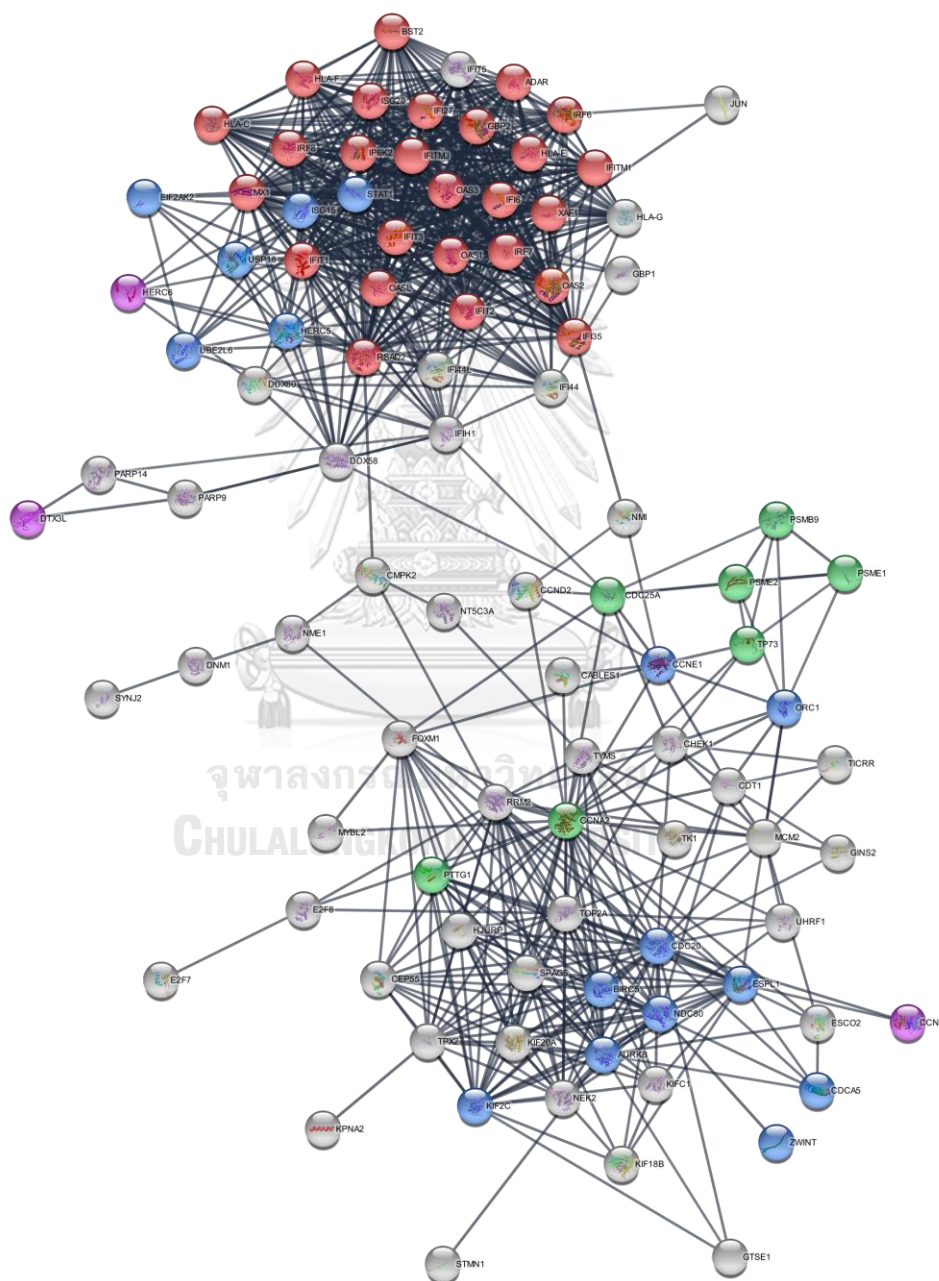## APPENDIX A: SUPPLEMENTARY DATA FOR RESEARCH ARTICLE 1

Figure 21. MCODE clusters shown in the whole network of IPIN. MCODE1, 2, 3, and 4 are marked as red, blue, green, and purple nodes, respectively.

Figure 22. IPIN clustered by MCL algorithm with an inflation parameter of 1.5. The red, yellow, green, and blue nodes are grouped in the 1st, 2nd, 3rd, and 4th cluster, respectively.

Table 8. List of nodes with high degree centrality.

Ensembl ID	Symbol	Degree Centrality
ENSP00000360869	IFIT1	39
ENSP00000368699	ISG15	38
ENSP00000371471	RSAD2	38
ENSP00000381601	MX1	38
ENSP00000360883	IFIT3	37
ENSP00000354394	STAT1	36
ENSP00000360891	IFIT2	34
ENSP00000380697	IRF7	33
ENSP00000257570	OASL	32
ENSP00000274026	CCNA2	31
ENSP00000342278	OAS2	31
ENSP00000342513	IFI6	31
ENSP00000354822	XAF1	31
ENSP00000388001	OAS1	31
ENSP00000395590	IFI35	31

Table 9. List of nodes with high betweenness centrality.

Ensembl ID	Symbol	Betweenness Centrality
ENSP00000303706	CDC25A	0.248509
ENSP00000371471	RSAD2	0.221581
ENSP00000256722	CMPK2	0.207767
ENSP00000353770	RRM2	0.205415
ENSP00000274026	CCNA2	0.186888
ENSP00000263642	IFIH1	0.149838
ENSP00000369213	DDX58	0.111075
ENSP00000361540	CDC20	0.051103
ENSP00000395590	IFI35	0.042906
ENSP00000342307	FOXM1	0.041747

Table 10. List of nodes with high closeness centrality.

Ensembl ID	Symbol	Closeness Centrality
ENSP00000371471	RSAD2	0.436364
ENSP00000303706	CDC25A	0.428571
ENSP00000256722	CMPK2	0.424779
ENSP00000353770	RRM2	0.422907
ENSP00000263642	IFIH1	0.419214
ENSP00000274026	CCNA2	0.417391
ENSP00000369213	DDX58	0.415584
ENSP00000262643	CCNE1	0.388664
ENSP00000360869	IFIT1	0.38247
ENSP00000368699	ISG15	0.380952
ENSP00000381601	MX1	0.380952

Table 11. List of nodes with high eigenvector centrality.

Ensembl ID	Symbol	Eigenvector Centrality
ENSP00000360869	IFIT1	1
ENSP00000381601	MX1	0.994698
ENSP00000368699	ISG15	0.994698
ENSP00000371471	RSAD2	0.989394
ENSP00000360883	IFIT3	0.985845
ENSP00000360891	IFIT2	0.968306
ENSP00000354394	STAT1	0.963544
ENSP00000354822	XAF1	0.93284
ENSP00000342513	IFI6	0.93284
ENSP00000380697	IRF7	0.927411

APPENDIX B: SUPPLEMENTARY DATA FOR RESEARCH ARTICLE 2

Table 12. Common differentially expressed genes (DEGs) from the two GEO datasets *.

DEGs	Gene Symbol
Upregulated	KIF18B, BTN3A1, NEK2, RSAD2, TMEM140, IFI6, SP140, PRRT4, KCNN3, HJURP, TYMS, LEFTY2, ZNF595, ITM2C, ZNF493, PTTG1, CDC25A, SPAG5, NBN, TOP2A, SAMD9, PARP9, IFIT3, AIM2, IFIT1, DDX58, AURKB, CCR10, TICRR, PSMB9, CARD16, GRTP1, MZB1, LGALS3BP, IFI35, PCP2, NMI, IFIT5, TK1
Downregulated	HLA-DRA, EPM2A, NAAA, CD44, MCUB, STARD7, TRIO, IDH3B, KYAT3, RPL13A, EIF4B, MYO1G, HAVCR2, RPL22, RASSF7, ATP6V1F, GLUD1, LPAR1, TAB1, NRG1, CYB561A3, LPXN, RBMX, CSNK2B, DMAC1, SCAI, RPL19, GOLGA8B, EOGT, UBXN1, RAD23A, ADCK5, LGALS3, ALDH2, RALGPS1, CAT, TWF2, PTER, PGLS, LDLRAD4, SDAD1, HDAC3, PTPN13, SUGP2, IRF8, ASB1, MIOS, AHNAK, CTSK, ERGIC3, PSMB7, PYCARD, ZBTB22, MAP3K4, TCAF2, PREP, EID1, NPEPL1, MFNG, CAMK2D, TBC1D9, SLC46A2, XKR7, CREBL2, TSPAN3, RPS20, RASGRP4, MYO9A, TUBGCP2, SRSF11, PLCB1, RRN3, YTHDC2, GLMP, MED14, NCKAP1L, CENPB, ICAM3, POMT2, MAP10, THAP12, GLUD2, MAN2C1, ADGRE1, RUBCNL, IPO5, USP9X, GNS, LY86, ASGR1, CERS5, ASB13, CPNE1, CEMIP2, MPDU1, UFL1, EIF2B1, PEPD, PARL, SNX22, CREBZF, ANXA5, MTCH2, FCN1, RAB34, GPAT4, DDX42, MTPAP, KPNA1, SNX17, NAGA, IARS2, GSTK1, MALT1, GUSB, HMOX1, SF3B1, CCDC124, TXNRD2, OXA1L, DOP1A, KLHL36, WDR55, OPN3, CYFIP2, KIAA1143, NEPRO, DYRK2, GHITM, PTRH2, AKAP8, STK11IP, RTL6, BTF3, ZNF783, EEF1D, ANKRD42, RNPEP, STAB1, DET1, SH3BGRL, SCYL1, EIF3B, TOMM20, COMMD10, UPRT, TGFBI, SURF1, TAGLN, SLC25A6, GIMAP6, BCAT1, CRYBG3, PHF14, ARFGAP2, RPL7, TRUB1, SUMF1, FOXO1, PIP5K1A, CLK2, VPS16, INTS11, NOL6, SLC25A13, MEF2C, NOA1, TOMM22, ZDHHC6, ZPR1, PLXND1, INTS9, SYNJ2BP, PSMD4, SYNGR2, BCLAF1, MRPS17, ERCC3, ZDHHC3, GAPVD1, KDM4C, MYCL, SLC25A37, CSDE1, UBE2J2, SUGT1, ARPIN, DHX57, TUFM, TEPSIN, CTSO, HNRNPDL, MAN2B1, CDC16, TPT1, SMARCAD1, NPC1, ITFG2, GPATCH2, ELP2, ANAPC2, MAP3K14, DUSP22, CDK5, THTPA, WDR73, HEATR6, LRRC58, ARHGAP24, DPYD, GALK1, FLII, NPRL2, LILRA1, NBPF8, LARP4B, MTCH1, PCID2, SMIM7, GGA2, SNTB2

Table 12. *Cont.*

DEGs	Gene Symbol
Both up- and downregulated	IGBP1, ZBTB14, ZNF248, DHX32, KIAA0825, BAG1, LTA4H, RPL11, HTR7, GPR15, POFUT1, PLIN5, ABCB7, VSIG4, PPP4C, SLC8A1, DOCK5, IRGQ, CIPC, ST6GALNAC1, CYBB, VPS8, DSC2, PNPLA8, SEC61A2, SPRED1, VCAN, SMARCD3, TBL1XR1, RPL17, FLOT2, RPGR, RFX2, TIMM10B, ATP6V1C1, NOTCH2, STX5, ZNF266, SUDS3, NRDC, WDR91, CHN2, WDR45, KIAA0753, FCHSD2, DICER1, SLC38A6, ZNF785, EIF3K, PIGG, ZDHHC20, BOD1, MDFIC, POLR2B, SLITRK4, MTRR, SIDT2, RCAN3, GDF7, AHCYL2, TBC1D14, FCGRT, COG8, SIAH1, EVI5, SLC39A1, GALNT2, FAM135A, AREL1, FAM168B, ZSWIM6, AIF1, CLK3, ZNF263, SOWAHC, SFT2D2, NPL, IGF1R, WDR37, TPCN1, TRAK1, DPYSL2, PIAS3, CSF1R, ERCC1, ELP1, NDUFS2, SASH1, FAM20A, FAM204A, STX16, SLC22A4, RALGAPA1, CACNA2D3, SPSB3, RAPGEF6, SIRPA, LAG3, INSYN2B, MOCS1, EGFL7, ZBTB32, MANF, BTN3A2, GALM, UHRF1, BAK1, IRF7, SRM, PCDHGA12, DNAJC1, PSME1, E2F7, CDC20, BTN3A3, UBE2L6, DHRS9, UCHL1, ARL17B, KY, BIRC5, MYBL2, LIF, NME1

* Leukocyte transcriptomic profiles came from GSE164805 and GSE154998 datasets. The criterion for being DEGs were FDR q-value < 0.05 and |log2 FC| > 1. A total of 384 common DEGs were found including 39 upregulated and 221 downregulated DEGs. The remaining 124 genes were found in both up- and downregulated expression.
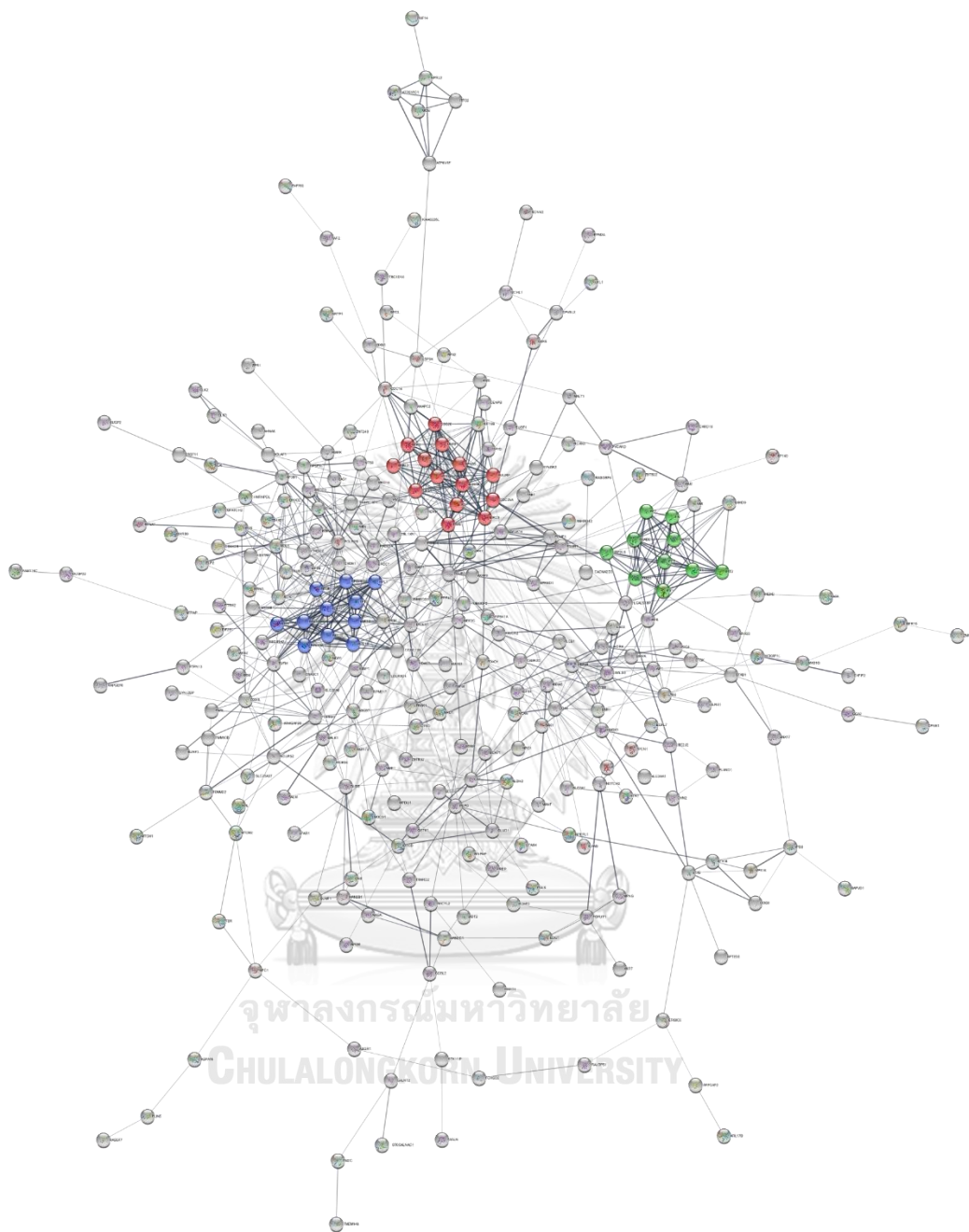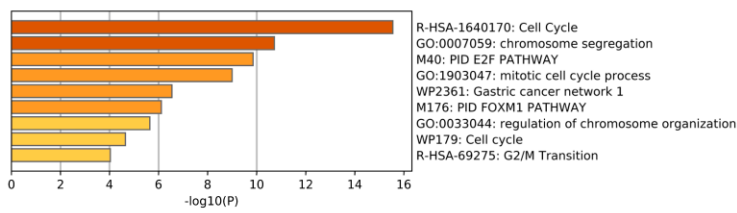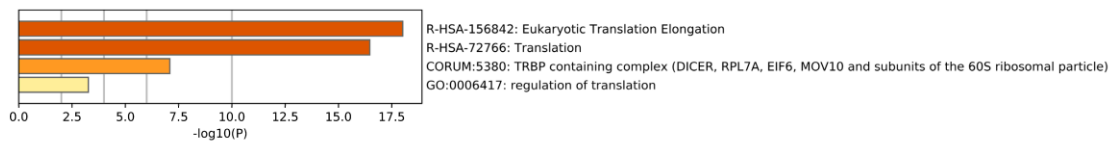
Figure 23. MCODE clusters shown in the whole network of the common PPI network. MCODE1, 2, and 3 are marked as red, blue, and green nodes, respectively.
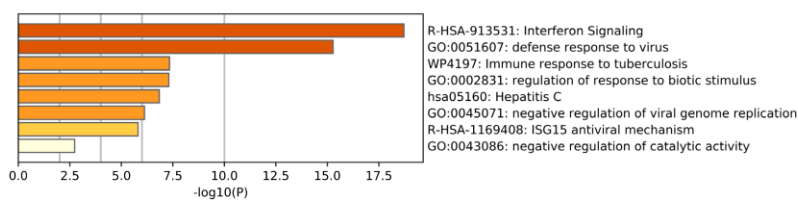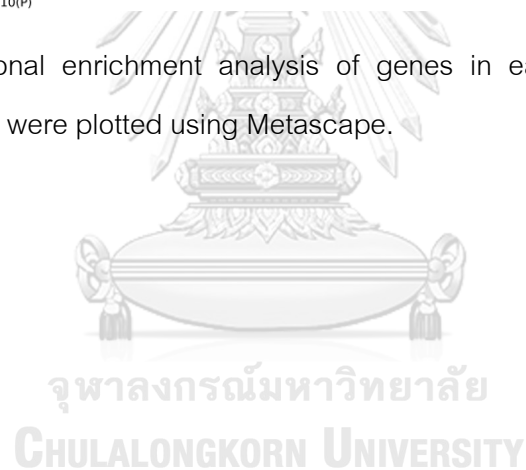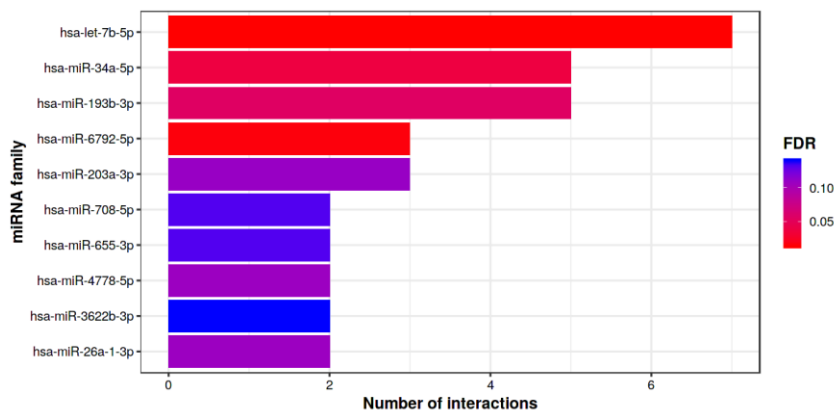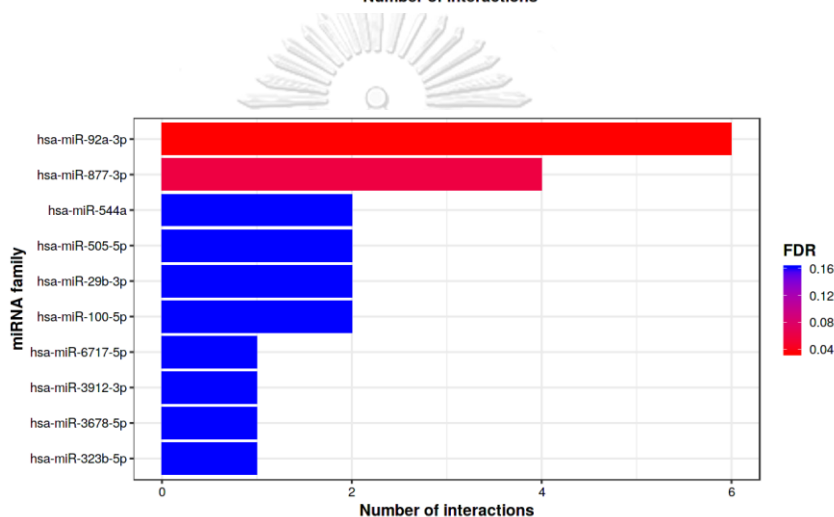
Figure 24. Functional enrichment analysis of genes in each MCODE module. The enrichment graphs were plotted using Metascape.
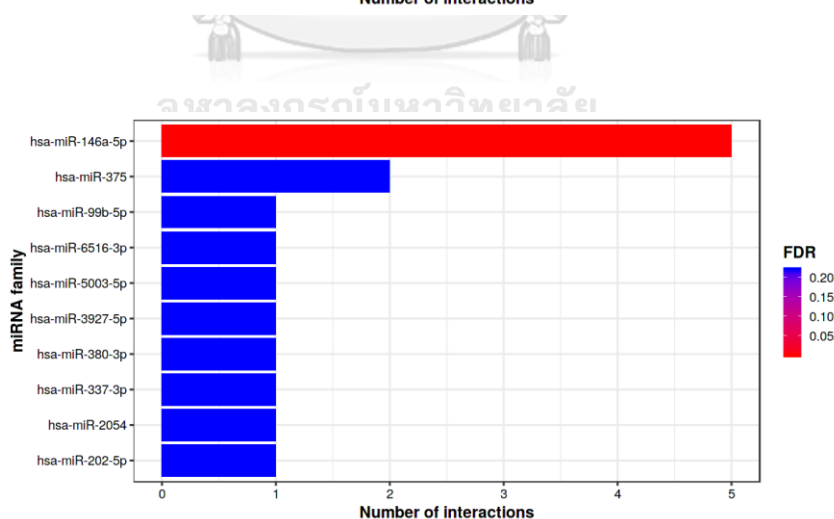
MCODE 1

MCODE 2

MCODE 3

Figure 25. Bar graph of the number of interactions of miRNAs in each gene in MCODE modules using MIENTURNET based on miRTarBase database. The bar graph color represents the interaction significance.
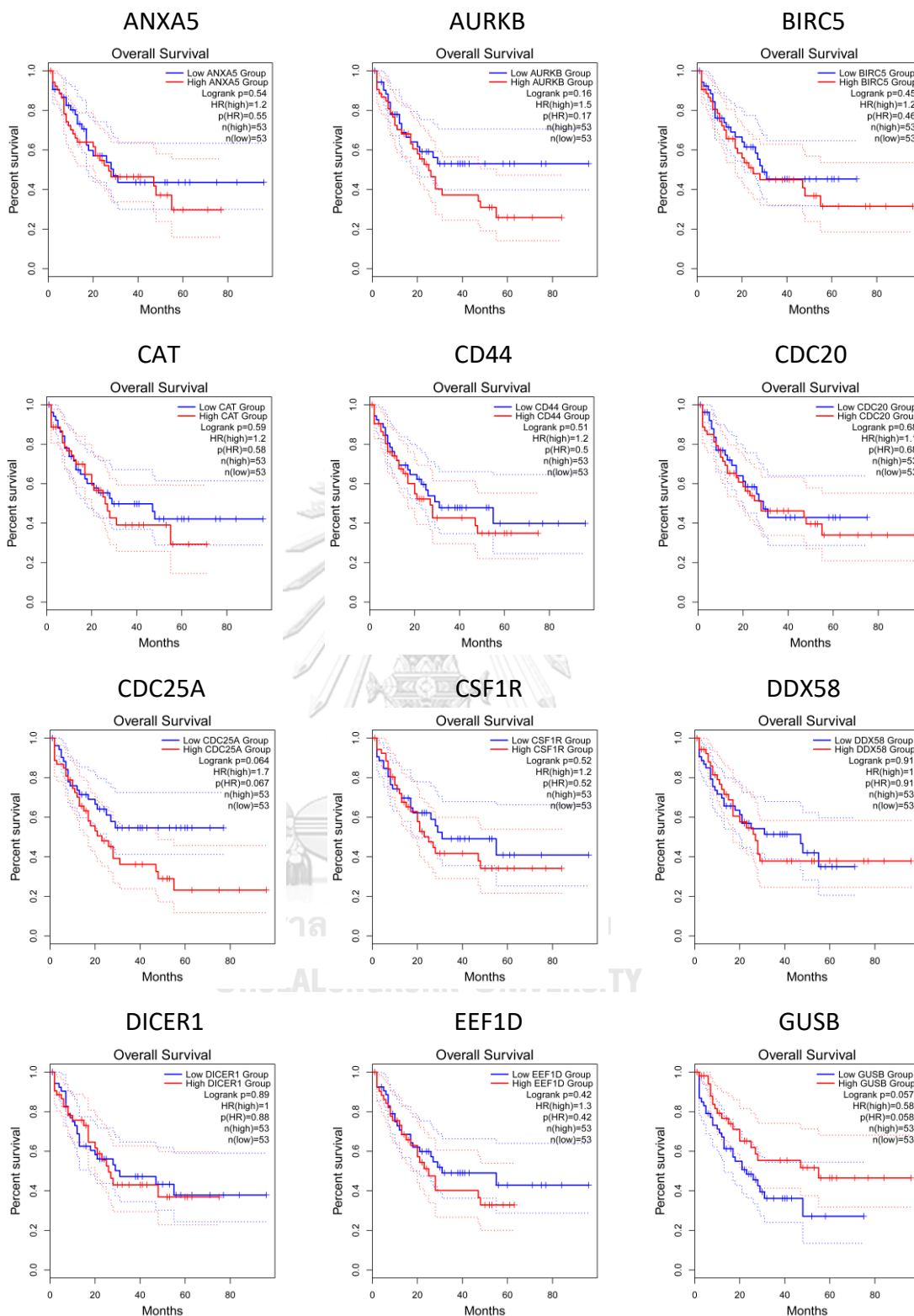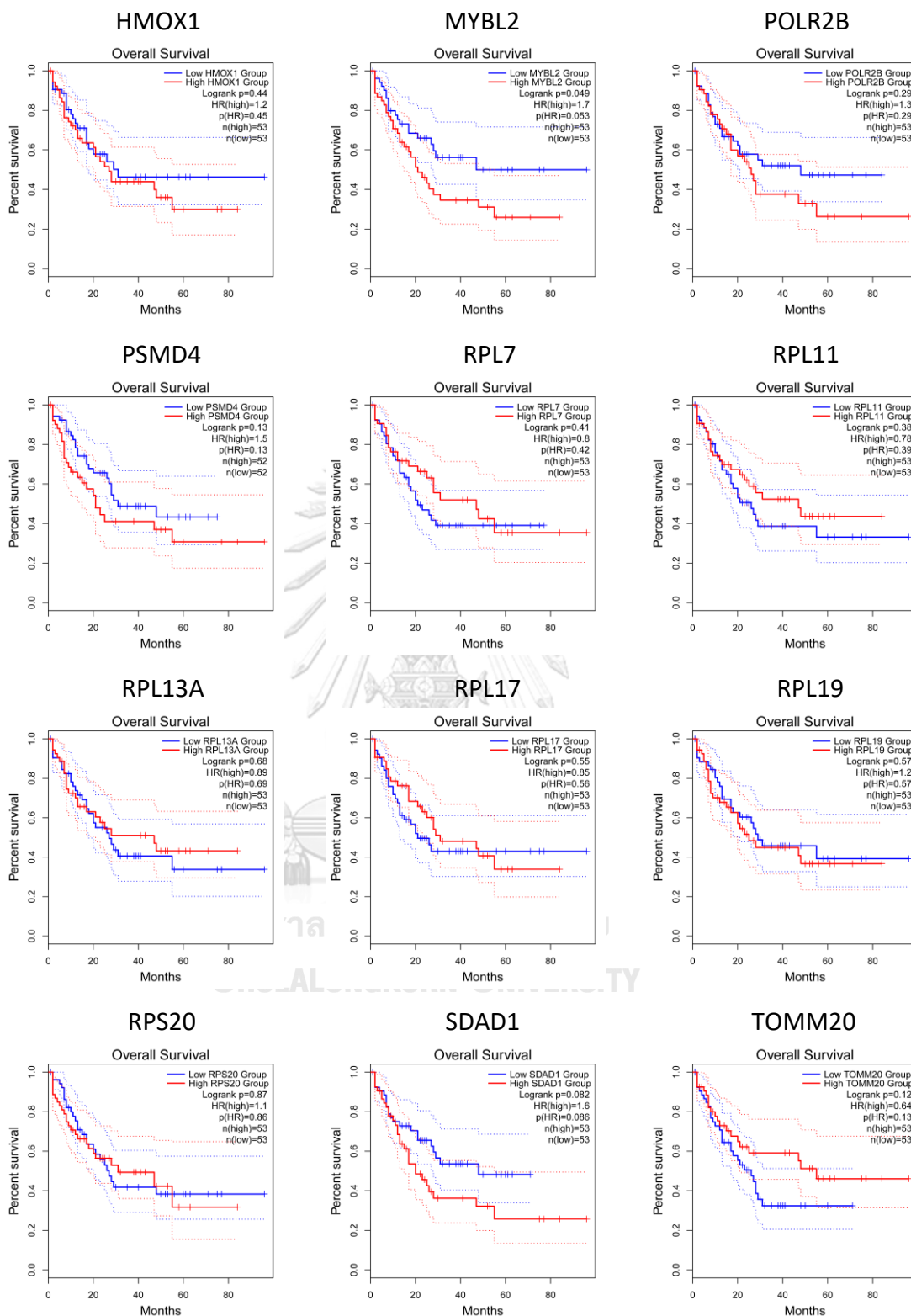
Figure 25. *Cont.*

Figure 25. *Cont.*

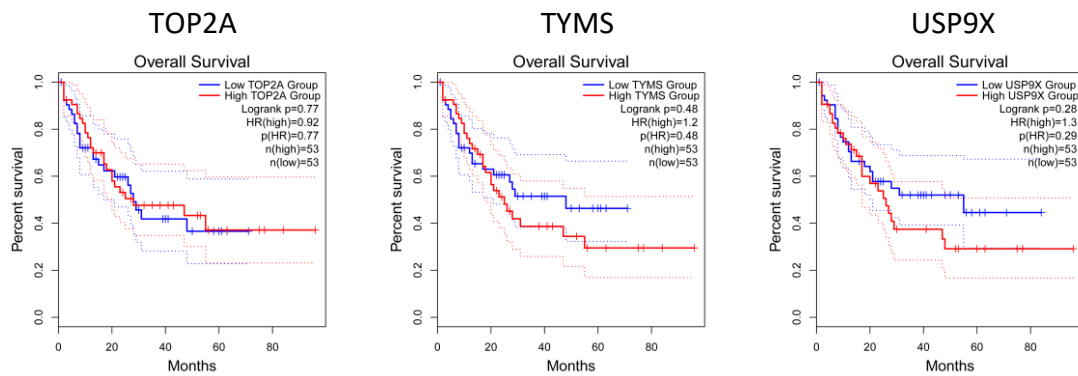**Figure 26.** Kaplan-Meier overall survival analysis of the hub and bottleneck genes in severe COVID-19. The curves were plotted using Gene Expression Profiling Interactive Analysis (GEPIA2). Acute myeloid leukemia (LAML) from The Cancer Genome Atlas (TCGA) database was used as a cell type model to find key survival genes in cytokine storm-related myeloid cells such as neutrophils, monocytes, and macrophages.

REFERENCES

[1] Zhou P, Yang XL, Wang XG, Hu B, Zhang L, Zhang W, et al. A pneumonia outbreak associated with a new coronavirus of probable bat origin. Nature. 2020;579(7798):270-273.

[2] Huang C, Wang Y, Li X, Ren L, Zhao J, Hu Y, et al. Clinical features of patients infected with 2019 novel coronavirus in Wuhan, China. Lancet. 2020;395(10223):497-506.

[3] Wu F, Zhao S, Yu B, Chen YM, Wang W, Song ZG, et al. A new coronavirus associated with human respiratory disease in China. Nature. 2020;579(7798):265-269.

[4] Gordon DE, Jang GM, Bouhaddou M, Xu J, Obernier K, White KM, et al. A SARS-CoV-2 protein interaction map reveals targets for drug repurposing. Nature. 2020;583(7816):459-468.

[5] World Health Organization. WHO Coronavirus (COVID-19) Dashboard 2022 [Available from: https://covid19.who.int/].

[6] Tsang HF, Chan LWC, Cho WCS, Yu ACS, Yim AKY, Chan AKC, et al. An update on COVID-19 pandemic: the epidemiology, pathogenesis, prevention and treatment strategies. Expert Rev Anti Infect Ther. 2021;19(7):877-888.

[7] Wiersinga WJ, Rhodes A, Cheng AC, Peacock SJ, Prescott HC. Pathophysiology, Transmission, Diagnosis, and Treatment of Coronavirus Disease 2019 (COVID-19): A Review. Jama. 2020;324(8):782-793.

[8] Lu R, Zhao X, Li J, Niu P, Yang B, Wu H, et al. Genomic characterisation and epidemiology of 2019 novel coronavirus: implications for virus origins and receptor binding. The Lancet. 2020;395(10224):565-574.

[9] Hu B, Guo H, Zhou P, Shi ZL. Characteristics of SARS-CoV-2 and COVID-19. Nat Rev Microbiol. 2021;19(3):141-154.

[10] Guan W-j, Ni Z-y, Hu Y, Liang W-h, Ou C-q, He J-x, et al. Clinical Characteristics of Coronavirus Disease 2019 in China. New England Journal of Medicine. 2020;382(18):1708-1720.

[11] Gandhi RT, Lynch JB, del Rio C. Mild or Moderate Covid-19. New England Journal of Medicine. 2020;383(18):1757-1766.

[12] Pan L, Mu M, Yang P, Sun Y, Wang R, Yan J, et al. Clinical Characteristics of COVID-19 Patients With Digestive Symptoms in Hubei, China: A Descriptive, Cross-Sectional, Multicenter Study. Am J Gastroenterol. 2020;115(5):766-773.

[13] Lechien JR, Chiesa-Estomba CM, De Siati DR, Horoi M, Le Bon SD, Rodriguez A, et al. Olfactory and gustatory dysfunctions as a clinical presentation of mild-to-moderate forms of the coronavirus disease (COVID-19): a multicenter European study. Eur Arch Otorhinolaryngol. 2020;277(8):2251-2261.

[14] Helms J, Kremer S, Merdji H, Clere-Jehl R, Schenck M, Kummerlen C, et al. Neurologic Features in Severe SARS-CoV-2 Infection. New England Journal of Medicine. 2020;382(23):2268-2270.

[15] Spinato G, Fabbris C, Polesel J, Cazzador D, Borsetto D, Hopkins C, et al. Alterations in Smell or Taste in Mildly Symptomatic Outpatients With SARS-CoV-2 Infection. Jama. 2020;323(20):2089-2090.

[16] Berlin DA, Gulick RM, Martinez FJ. Severe Covid-19. New England Journal of Medicine. 2020;383(25):2451-2460.

[17] Centers for Disease Control and Prevention. Coronavirus disease 2019 (COVID-19): people with certain medical conditions 2020 [Available from: https://www.cdc.gov/coronavirus/2019-ncov/need-extra-precautions/people-with-medical -conditions.html].

[18] Gebhard C, Regitz-Zagrosek V, Neuhauser HK, Morgan R, Klein SL. Impact of sex and gender on COVID-19 outcomes in Europe. Biol Sex Differ. 2020;11(1):29-41.

[19] Boban M. Novel coronavirus disease (COVID-19) update on epidemiology,

pathogenicity, clinical course and treatments. Int J Clin Pract. 2021;75(4):e13868-e13874.

[20] Kumar M, Al Khodor S. Pathophysiology and treatment strategies for COVID-19. J Transl Med. 2020;18(1):353-362.

[21] Kolarič A, Jukič M, Bren U. Novel Small-Molecule Inhibitors of the SARS-CoV-2 Spike Protein Binding to Neuropilin 1. Pharmaceuticals. 2022;15(2):165-178.

[22] Fajgenbaum DC, June CH. Cytokine Storm. New England Journal of Medicine. 2020;383(23):2255-2273.

[23] Hassanipour S, Arab-Zozani M, Amani B, Heidarzad F, Fathalipour M, Martinez-de-Hoyo R. The efficacy and safety of Favipiravir in treatment of COVID-19: a systematic review and meta-analysis of clinical trials. Sci Rep. 2021;11(1):11022-11032.

[24] Jinawath N, Bunbanjerdsuk S, Chayanupatkul M, Ngamphaiboon N, Asavapanumas N, Svasti J, et al. Bridging the gap between clinicians and systems biologists: from network biology to translational biomedical research. J Transl Med. 2016;14(1):324-336.

[25] Barabási AL, Oltvai ZN. Network biology: understanding the cell's functional organization. Nat Rev Genet. 2004;5(2):101-113.

[26] Bihari A, Pandia MK. Eigenvector centrality and its application in research professionals' relationship network. 2015 International Conference on Futuristic Trends on Computational Analysis and Knowledge Management (ABLAZE). 2015:510-514.

[27] Raman K. Construction and analysis of protein-protein interaction networks. Autom Exp. 2010;2(1):2-10.

[28] Zhang B, Tian Y, Zhang Z. Network biology in medicine and beyond. Circ Cardiovasc Genet. 2014;7(4):536-547.

[29] Harun S, Zulkifle N. Construction and Analysis of Protein-Protein Interaction Network to Identify the Molecular Mechanism in Laryngeal Cancer. Sains Malaysiana.

2018;47:2933-2940.

[30] Chen C, Shen H, Zhang LG, Liu J, Cao XG, Yao AL, et al. Construction and analysis of protein-protein interaction networks based on proteomics data of prostate cancer. Int J Mol Med. 2016;37(6):1576-1586.

[31] Hao T, Zhao L, Wu D, Wang B, Feng X, Wang E, et al. The Protein–Protein Interaction Network of Litopenaeus vannamei Haemocytes. Frontiers in Physiology. 2019;10:156-165.

[32] Ran J, Li H, Fu J, Liu L, Xing Y, Li X, et al. Construction and analysis of the protein-protein interaction network related to essential hypertension. BMC Systems Biology. 2013;7(1):32-43.

[33] Chen S-J, Liao D-L, Chen C-H, Wang T-Y, Chen K-C. Construction and Analysis of Protein-Protein Interaction Network of Heroin Use Disorder. Scientific Reports. 2019;9(1):4980-4988.

[34] Prasad K, Khatoon F, Rashid S, Ali N, AlAsmari AF, Ahmed MZ, et al. Targeting hub genes and pathways of innate immune response in COVID-19: A network biology perspective. Int J Biol Macromol. 2020;163:1-8.

[35] Zhou Y, Hou Y, Shen J, Huang Y, Martin W, Cheng F. Network-based drug repurposing for novel coronavirus 2019-nCoV/SARS-CoV-2. Cell Discovery. 2020;6(1):14-31.

[36] Messina F, Giombini E, Agrati C, Vairo F, Ascoli Bartoli T, Al Moghazi S, et al. COVID-19: viral-host interactome analyzed by network based-approach model to study pathogenesis of SARS-CoV-2 infection. J Transl Med. 2020;18(1):233-242.

[37] Adhami M, Sadeghi B, Rezapour A, Haghdoost AA, MotieGhader H. Repurposing novel therapeutic candidate drugs for coronavirus disease-19 based on protein-protein interaction network analysis. BMC Biotechnology. 2021;21(1):22-32.

[38] More SA, Patil AS, Sakle NS, Mokale SN. Network analysis and molecular mapping for SARS-CoV-2 to reveal drug targets and repurposing of clinically developed

drugs. Virology. 2021;555:10-18.

[39] Barrett T, Wilhite SE, Ledoux P, Evangelista C, Kim IF, Tomashevsky M, et al. NCBI GEO: archive for functional genomics data sets--update. Nucleic Acids Res. 2013;41(Database issue):D991-D995.

[40] Szklarczyk D, Gable AL, Lyon D, Junge A, Wyder S, Huerta-Cepas J, et al. STRING v11: protein-protein association networks with increased coverage, supporting functional discovery in genome-wide experimental datasets. Nucleic Acids Res. 2019;47(D1):D607-D613.

[41] Biron CA. Interferons alpha and beta as immune regulators--a new look. Immunity. 2001;14(6):661-664.

[42] Davidson S, Crotta S, McCabe TM, Wack A. Pathogenic potential of interferon αβ in acute influenza infection. Nature Communications. 2014;5(1):3864-3878.

[43] Le Saout C, Hasley RB, Imamichi H, Tcheung L, Hu Z, Luckey MA, et al. Chronic exposure to type-I IFN under lymphopenic conditions alters CD4 T cell homeostasis. PLoS Pathog. 2014;10(3):e1003976-e1003990.

[44] Herold S, Steinmueller M, von Wulffen W, Cakarova L, Pinto R, Pleschka S, et al. Lung epithelial apoptosis in influenza virus pneumonia: the role of macrophage-expressed TNF-related apoptosis-inducing ligand. J Exp Med. 2008;205(13):3065-3077.

[45] Sherman BT, Hao M, Qiu J, Jiao X, Baseler MW, Lane HC, et al. DAVID: a web server for functional enrichment analysis and functional annotation of gene lists (2021 update). Nucleic Acids Res. 2022;194:1-6.

[46] Harris MA, Clark J, Ireland A, Lomax J, Ashburner M, Foulger R, et al. The Gene Ontology (GO) database and informatics resource. Nucleic Acids Res. 2004;32(Database issue):D258-D261.

[47] Kanehisa M, Furumichi M, Tanabe M, Sato Y, Morishima K. KEGG: new perspectives on genomes, pathways, diseases and drugs. Nucleic Acids Res. 2017;45(D1):D353-

D361.

[48] Szklarczyk D, Santos A, von Mering C, Jensen LJ, Bork P, Kuhn M. STITCH 5: augmenting protein-chemical interaction networks with tissue and affinity data. Nucleic Acids Res. 2016;44(D1):D380-D384.

[49] Zhou Y, Zhou B, Pache L, Chang M, Khodabakhshi AH, Tanaseichuk O, et al. Metascape provides a biologist-oriented resource for the analysis of systems-level datasets. Nat Commun. 2019;10(1):1523-1542.

[50] Martens M, Ammar A, Riutta A, Waagmeester A, Slenter DN, Hanspers K, et al. WikiPathways: connecting communities. Nucleic Acids Res. 2021;49(D1):D613-D621.

[51] Jassal B, Matthews L, Viteri G, Gong C, Lorente P, Fabregat A, et al. The reactome pathway knowledgebase. Nucleic Acids Res. 2020;48(D1):D498-D503.

[52] Mvubu NE, Pillay B, Gamieldien J, Bishai W, Pillay M. Canonical pathways, networks and transcriptional factor regulation by clinical strains of Mycobacterium tuberculosis in pulmonary alveolar epithelial cells. Tuberculosis (Edinb). 2016;97:73-85.

[53] Giurgiu M, Reinhard J, Brauner B, Dunger-Kaltenbach I, Fobo G, Frishman G, et al. CORUM: the comprehensive resource of mammalian protein complexes-2019. Nucleic Acids Res. 2019;47(D1):D559-D563.

[54] Wishart DS, Feunang YD, Guo AC, Lo EJ, Marcu A, Grant JR, et al. DrugBank 5.0: a major update to the DrugBank database for 2018. Nucleic Acids Res. 2018;46(D1):D1074-D1082.

[55] Davis AP, Grondin CJ, Johnson RJ, Sciaky D, Wiegers J, Wiegers TC, et al. Comparative Toxicogenomics Database (CTD): update 2021. Nucleic Acids Res. 2021;49(D1):D1138-D1143.

[56] Wang Y, Zhang S, Li F, Zhou Y, Zhang Y, Wang Z, et al. Therapeutic target database 2020: enriched resource for facilitating research and early development of targeted

therapeutics. Nucleic Acids Res. 2020;48(D1):D1031-D1041.

[57] Stelzer G, Rosen N, Plaschkes I, Zimmerman S, Twik M, Fishilevich S, et al. The GeneCards Suite: From Gene Data Mining to Disease Genome Sequence Analyses. Curr Protoc Bioinformatics. 2016;54:1.30.1-1..3.

[58] Zhang Y, Zeng T, Chen L, Ding S, Huang T, Cai YD. Identification of COVID-19 Infection-Related Human Genes Based on a Random Walk Model in a Virus-Human Protein Interaction Network. Biomed Res Int. 2020;2020:4256301-4256307.

[59] Messina F, Giombini E, Montaldo C, Sharma AA, Zoccoli A, Sekaly RP, et al. Looking for pathways related to COVID-19: confirmation of pathogenic mechanisms by SARS-CoV-2-host interactome. Cell Death Dis. 2021;12(8):788-797.

[60] Lu S, Zhao K, Wang X, Liu H, Ainiwaer X, Xu Y, et al. Use of Laplacian Heat Diffusion Algorithm to Infer Novel Genes With Functions Related to Uveitis. Frontiers in Genetics. 2018;9:425-434.

จุฬาลงกรณ์มหาวิทยาลัย
CHULALONGKORN UNIVERSITY

VITA

NAME	Pakorn Sagulkoo
DATE OF BIRTH	11 June 1992
PLACE OF BIRTH	Chiang Mai, Thailand
INSTITUTIONS ATTENDED	M.D. (second class honor), Chiang Mai University, 2017
HOME ADDRESS	49/7 M.2 T. Yang Noeng A. Saraphi, Chiang Mai, 50140

PUBLICATION

[1] Buawangpong N, Pinyopornpanish K, Jiraporncharoen W, Dejkriengkraikul N, Sagulkoo P, Pateekhum C, et al. Incorporating the patient-centered approach into clinical practice helps improve quality of care in cases of hypertension: a retrospective cohort study. BMC Fam Pract. 2020;21(1):108-115.

[2] Sagulkoo P, Suratanee A, Plaimas K. Immune-Related Protein Interaction Network in Severe COVID-19 Patients toward the Identification of Key Proteins and Drug Repurposing. Biomolecules. 2022;12(5):690-721.

[3] Sagulkoo P, Chuntakaruk H, Rungrotmongkol T, Suratanee A, Plaimas K. Multi-Level Biological Network Analysis and Drug Repurposing Based on Leukocyte Transcriptomics in Severe COVID-19: In Silico Systems Biology to Precision Medicine. Journal of Personalized Medicine. 2022;12(7):1030-1053.

[4] Sagulkoo P, Plaimas K, Suratanee A, Colado Simão AN, Vissoci Reiche EM, Maes M. Immunopathogenesis and Immunogenetic Variants in COVID-19. Current Pharmaceutical Design. 2022;28:1-17.

AWARD RECEIVED

Human resource development fund from Faculty of Medicine, Chiang Mai University